# The spatial-temporal geomorphology of meandering river channels in distributive fluvial systems

May Britt Kjærevik Zachariah


Master thesis in
Petroleum Geoscience

University of Bergen

June 2019

# Abstract

*Braided river systems are thought to dominate thick sandy successions in the rock record, however, recent work show that amalgamated sandy meander-belts are common in modern rivers and are likely under-represented in sedimentary successions. To investigate the controls and recognition of meandering river channels and their deposits in the rock record, a global analysis of 32 years of satellite imagery is used to investigate the spatial-temporal geomorphology of modern meandering river channels from proximal to distal portions. Based on the global analysis, a selection of eight representative examples in modern sedimentary basins across a range of climatic and tectonic settings are investigated further for trends and relationships between point-bar migration rate, water discharge, sediment load, channel and sandbar geometry. The results show the architecture of meandering river systems in distributive fluvial systems show similar temporal and geometrical trends from apex to toe but the magnitude and scale significantly differs by climatic and tectonic regime.*

# Acknowledgments

I would sincerely like to thank:

- University of Bergen for letting me pursue a degree in science, which I should have done from the start.
- My mentor Bjørn Nyberg, for practical help and patient encouragement. Without him this would not have happened.
- My mentor William Helland-Hansen for believing in me all five years.
- My employer Equinor ASA for allowing me to pursue this long-term goal.
- My children Thorbjørn, Mina, Hannah and Avran, for being supportive and independent.
- Last, but not least, I would like to thank my husband John, for looking after everything else so I could do this. This would not have happened without him either.

# Contents

# 1 Introduction

## 1.1 Rationale

Sedimentary basins have long-term preservation potential of sedimentary depo as tectonics create subsidence in which fluvial structures can accumulate (Jervey, 1988; Blum and Törnqvist, 2000). Hence in studying modern sedimentary systems as analogues for the rock record it is vital to only study those systems that have preservation potential (Nyberg and Howell, 2015). Weissman et al., (2015) found in a global study of fluvial systems that distributive fluvial systems (DFS) dominate modern sedimentary basins and likely the stratigraphic record. Yet our quantitative understanding about system wide temporal and morphological trends along DFS systems is lacking.

Meandering fluvial rivers of DFS systems are of particular interest considering their prevalence in modern sedimentary basins yet lack of recognition in the stratigraphic record. Recently, (Hartley et al., 2015) showed that thick amalgamated sand bodies often associated as braided river systems may in many circumstances represent amalgamated meandering sandbodies (AMS). However, our knowledge of the meandering portion of modern DFS systems is relatively poor, limited by an ability to study large scale systems in a quantitative, objective and efficient methodology. Such information may help to constrain the size, geometry and nature of the sedimentary systems, likely facies distributions (i.e. arrangement) that are preserved in the subsurface.

Encouraged by the release of new tools for analysing the geometry and topology of modern depositional elements by (Nyberg et al., 2015) and the access to global freely available remotely sensed information, this provides an opportunity to study the large scale spatial-temporal geomorphology of meandering river channels in distributive fluvial systems. In addition, the quantitative and numerical results would provide a valuable contribution for analogy repositories such as the Fluvial Architecture Knowledge Transfer System (FAKTS) or the Sedimentary Architecture of Field Analogues for Reservoir Information (SAFARI). These databases were designed to incorporate geospatial information of modern depositional elements as analogues to reservoir modelling and simulation but lacked proper methodology to gather quantitative geometrical information on modern sedimentary systems. The purpose of this work is to develop new methodology to analyse modern meandering fluvial systems at a quantitative and objective approach to revisit trends of DFS systems from proximal to distal portions.

## 1.2 Objectives

This study specifically aims to address current challenges by:

- Develop a workflow for a quantitative analysis of the temporal and spatial evolution of fluvial systems, so that similar work can be carried out for other systems.

- Studying the spatial and temporal variability and controls on modern meandering fluvial systems. through a high-level global analysis of the worlds fluvial systems, determining the rate of change between source and sink, in different climatic and tectonic settings. A more detailed analysis 8 modern, meandering fluvial systems, placed in sedimentary basins in different climatic and tectonic settings. Trends and changes for each climate zone will be determined and quantified. Each will be analysed with regard to trends and changes within each system and compared to each other based on climatic and tectonic setting. Satellite images will be used, and changes will be quantified using recently developed arithmetic methods
- Contribute to improving the fluvial facies models for subsurface models, by providing numerical trends for spatial and temporal variability in meandering systems in relation to climatic and tectonic setting.

## 1.3 Thesis outline

This thesis is structured into seven chapters. Chapter 1 highlights the rationale and objectives of the project. Chapter 2 will provide an overview of the theoretical background and state of the art. Chapter 3 gives a geological description of the 8 fluvial systems that were analysed. Chapter 4 contains an overview of the datasets and methods used in the global and regional analysis of fluvial systems. Chapter 5 presents the results and findings of the research. Chapter 6 gives interpretations and discussion of findings in chapter 5. Chapter 7 offers conclusions and suggestions for further studies. An appendix includes further detailed descriptions of workflows for reproducibility of the results for analyses.

# 2 Theoretical Background

The purpose of this chapter is to provide short theoretical background for the terms used in subsequent chapters.

## 2.1 Source-to-sink System

The source to sink model encompass the complete sedimentary system, linking the erosional catchment which is the source of the sediment flow, the transport route, as well as the depositional area in the sink.

Using the analogue "Earths big hourglass", the catchment area represents the upper part of the hourglass. It is delineated by the water divide and have a dendritic system of rivers draining the whole area. It is commonly larger than the adjoining depositional sink, at ratios between 30:1 to 10:1. Water and sediments are routed through an axial river or an apex point, into the lower part of the hourglass, the basins or sinks (Helland-Hansen et al., 2016).

Modern terrestric sinks make up 16% of the earth's surface and can be defined as an area where subsidence provides accommodation space for sediments to be deposited and preserved in a geological timescale (Jervey, 1988; Blum and Törnqvist, 2000). Sinks are characterised by low topographical gradient, as sediments accumulates in and fills topographic lows (Nyberg and Howell, 2015).

## 2.2 Sedimentary basins

A sedimentary basin is formed over a geological timescale (c. > 106 ma) as subsidence creates accommodation to preserve sediments (Jervey, 1988; Van Wagoner et al., 1990; Blum and Törnqvist, 2000). Subsidence is controlled by a number of factors including crustal thinning, mantle-lithosphere thickening, sedimentary and volcanic loading, tectonic loading, subcrustal loading, asthenosphere flow and crustal densification (Ingersoll, 2012). As subsidence rate differ by subsidence control related to specific basin types (Xie and Heller, 2009) it is important to differentiate those basin types to understand its potential to create accommodation. The capacity for a sedimentary basin to fill will depend on sediment supply

## 2.3 Geomorphology in fluvial systems

The relationship between the different elements in the fluvial system is shown in Figure 2-1. In the source region sediments are eroded and transported away, and river channels are typically cutting into confined valleys. Sediments are then transported to the depositional region, where channels become unconfined. The apex marks the transition from source to sink/basin. As the distance from

apex increases, more of the fan consists of floodplains, and the sediment deposits consist of finer grain material. The channels are for some time held in place by levees and vegetation, until the channel gets blocked by sediments or a flooding event breaks through the levees, and a partial or complete avulsion occur.

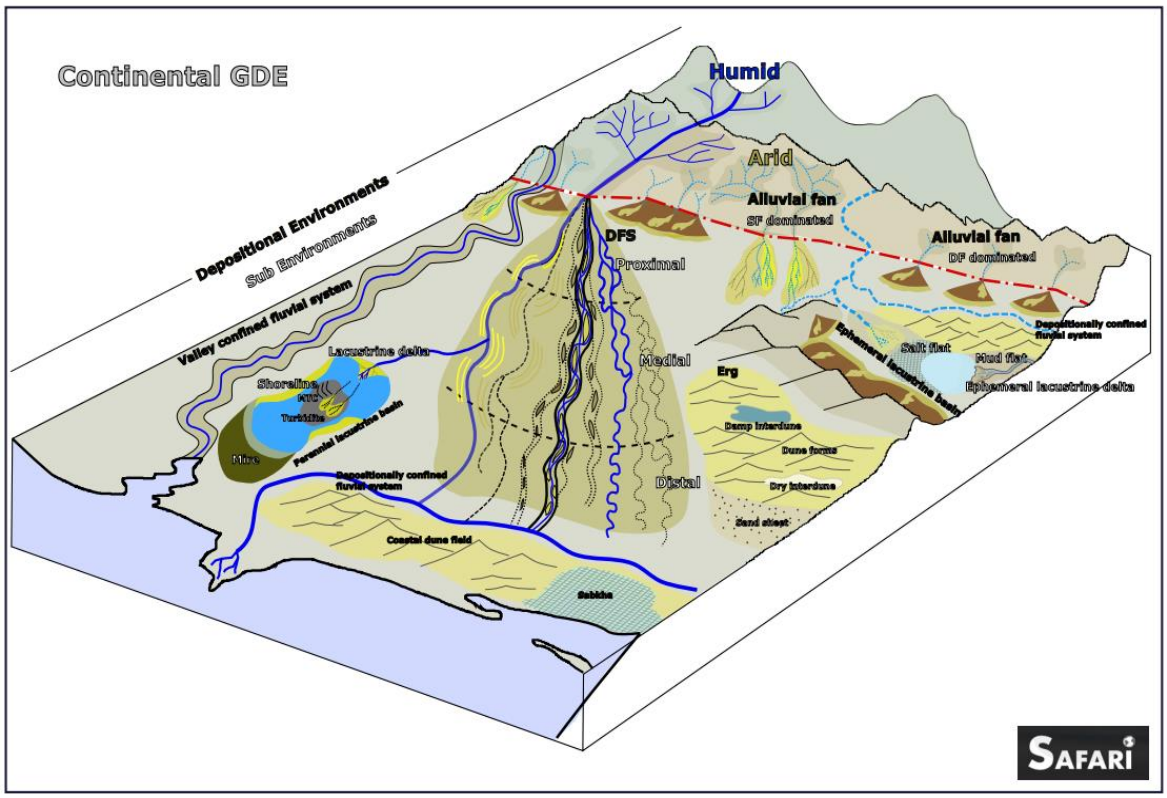


*Figure 2-1.The elements in a fluvial system and the relationship between them. Credit: Safari Database, NORCE Norwegian Research Centre and University of Aberdeen*

### 2.3.1 Types of fluvial channels

#### *2.3.1.1 Braided*

Braided rivers have more than three active channels and are laterally unstable. They have multiple mid channel bars that are constantly re-worked. They are high energy systems, with steep slopes and large sediment content (Fryirs and Brierley, 2013).

#### *2.3.1.2 Bifurcated*

Bifurcated rivers split into several stable channels, that all are active (Fryirs and Brierley, 2013).

#### *2.3.1.3 Anabranching*

Anabranching rivers are characterised by channels that bifurcate and re-join multiple times (Fryirs and Brierley, 2013).

They are found in a variety of climatic settings, from very arid (for example Australia), to humid, such as the Amazon. Channel stability is influenced by vegetation. The largest river systems in the world, also in terms of discharge, are anabranching. They tend to have wide and complex floodplains, wider than those of individual meandering channels (Latrubesse, 2015).

#### *2.3.1.4 Meandering rivers*

A meandering river migrates laterally by eroding the outer banks, while depositing sediments in point bars on the inner banks, a process that gradually changes the shape of the channel and increases the rivers sinuosity (Fryirs and Brierley, 2013).

The channel of meandering rivers can also change more abruptly by cut-offs and avulsions. Neck cut-offs occur when a bend gets sufficiently tightened and the channel shorten its course by cutting through the narrow neck of the point bar. This causes the meander to be abandoned and become an ox-bow lake, which may gradually be filled with fine grained, suspense load materials. Chute cut-offs occur through a point bar, at first only at high water levels, but gradually taking more of the flow, until it becomes the main channel of the river. The old meander is gradually filled with bedload deposits (Fryirs and Brierley, 2013).

Nodal avulsion occurs when the channel suddenly shifts its position and completely or partially abandons the entire channel below this point. The old channel may gradually fill in with suspense load materials and will retain the shape the river had at the time of avulsion. When compared to the contemporary channel, it can give indications of changes in sediment load and discharge (Fryirs and Brierley, 2013). Avulsions are an integral part of aggrading river systems, as they enable deposition of extensive fluvial deposits by diverting the flow to a lower part of the fan. The new channel will follow the steepest slope away from the old channel, and the deposition will move to the area surrounding the new channel (Smith et al., 1997). Channel avulsions typically occur during or after floods, downstream obstruction of the channel or periods of sediment aggradation near apex. This leads to the existing channel being completely or partially abandoned, and a new channel being incised into the fan sediments (Bridge, 2003).

### 2.3.2 Controls on development of river geomorphology

#### *2.3.2.1 Allogenic*

**Climate – Classification and effect**

Köppen-Geiger climate classification is based on temperature and seasonality of precipitation. It is based on three orders, of which the first consists of equatorial, arid, warm temperate, snow and polar. The second order is based on precipitation, and the third temperature (Nyberg et al., 2018a).

Rivers are directly influenced by climate in form of precipitation and thermal condition. Climate also has an indirect effect through vegetation. Tropical humid regions with consistent high temperatures and high rainfall, give little variation in the rivers flow, and vegetation often consists of rainforest. Rivers in tropical regions with monsoonal seasons have much higher variability in flow through the year, and vegetation is savannah. Vegetation stabilises channel banks. In cold humid climates have rivers freeze during winter and there may be permafrost in the ground. Extensive re-work of the channel may occur in spring when the ice thaws. Vegetation is taiga or tundra. Arid and semi-arid climates have little vegetation cover, and flow activity is highly variable. The lack of vegetation and high flow variability results in rapidly shifting channels, and high width/depth ratio. Vegetation contribute to channel stability by stabilising the rivers banks, and slowing down runoff after rainfalls (Fryirs and Brierley, 2013).

#### *2.3.2.2 Autogenic*

**Gradient**

Long rivers commonly have a concave upwards elevation profile, but there are exceptions, especially in tectonically active areas. Variations in the rivers gradient will affect the sinuosity of the channel. In areas with uplift and incision of the channel, the river will typically deposit sediments above the uplift, then erode through the uplifted area, and again deposit below it. For meandering river, this may result in increased sinuosity just below the uplift (Bridge, 2003).

### 2.3.3 Distributive Fluvial Systems (DFS)

Several recent studies (Hartley et al., 2010; Weissmann et al., 2011, 2013; Davidson et al., 2013; Fernandes et al., 2016) have highlighted the importance of large distributive fluvial systems (DFS) and their preservation potential in the rock record. An analysis of more than 700 modern sedimentary basins have shown that in all terrestrial basins, distributive fans are the dominating deposition forms (Weissmann et al., 2010).

A distributive fluvial system (DFS) can be defined a as “the deposit of a fluvial system which in planform displays a radial, distributive channel pattern”. They develop downstream from the point where a river that has been confined in a valley reaches an unconfined basin, and the horizontal flow expansion reduces velocity and allows deposition of sediments (Hartley et al., 2010). This change occurs at the river’s apex, the point above which the river is erosive or reworking sediments without leaving large deposits. Above the apex the rivers discharge is added to by tributaries, and the channel typically becomes wider downstream, whereas below the apex no more tributaries are added, and on the contrary, the river tends to bifurcate into several channels as it spreads out, each becoming narrower. In addition to bifurcation, the river also loses water due to evaporation and infiltration,

and commonly reduces in size as it flows over the fan. This affects sediment deposition, and larger grain sizes are deposited closer to the apex, whereas finer sediments are carried further towards the tow of the fan. As the river is no longer confined, over time it is able to avulse and shift laterally across the fan (Weissmann et al., 2010).

This implies that in many cases, the entire fan will not have active channels simultaneously, large areas can be dry and deprived of sediment influx until the channel again shifts (Davidson et al., 2013)

Hartley et al. (2010) identified and mapped 415 DFS, all in continental sedimentary basins, with the intention to create a descriptive database of modern fans. In doing so they identified and classified six different planform types, classified by number of channels, sinuosity, braiding and downstream bifurcation. These are (quote):

1) A single bifurcated channel that bifurcates downstream into braided and/or straight channels
2) A single dominant braided channel
3) A single dominant braided channel which becomes sinuous downstream often bifurcating
4) A single dominant sinuous channel
5) A single sinuous channel that bifurcates downstream into smaller sinuous channels
6) Multiple sinuous channels (end quote)

DFS included in the study were all more than 30km from apex to toe, and were found in all climate zones, and in all tectonic regimes. The largest DFS were found in foreland basins in compressional settings, 16 measuring more than 300 km, and one above 700 km. This size is enabled by the large size of foreland basins, providing sufficient accommodation space in which large fans can aggrade. Other types of basins, such as piggy back, extension, strike slip and cratonic basins are smaller geological features, and can only accommodate smaller fans. This model was further developed by Davidson et al. (2013), as shown in Figure 2-2.

Shuttle Radar Topography Mission (SRTM) data, show that most of the fans have low gradients, 66% of them below 0.17$^{o}$, and the relationship between size and gradient, is that the largest fans have the lowest gradients (Hartley et al., 2010).

Hartley et al (2010) defines apex as the point where the single trunk of the river bifurcates and starts to form the fan morphology. For the rivers in this study, apex is selected where they enter the sedimentary basin (Mamorecillo), or where they no longer receive discharge from tributaries (Koyukuk), whichever comes first.

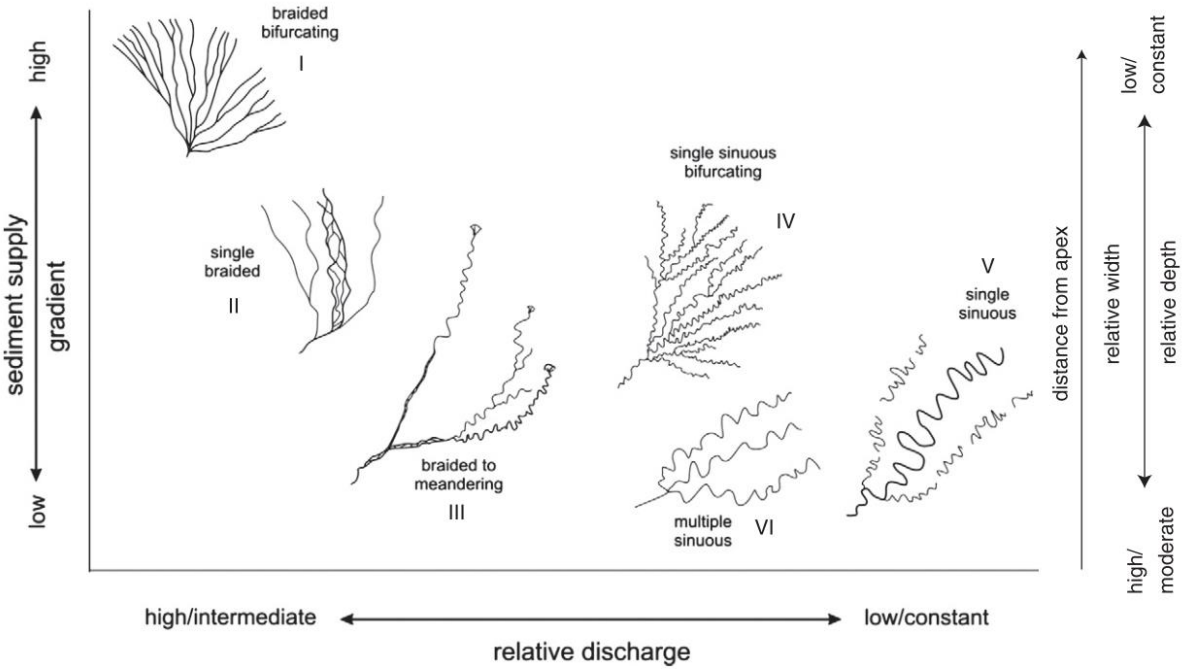


*Figure 2-2 Different plan form types of DFS* (Davidson et al., 2013)

They can terminate in wetlands, sand dunes/arid land, axial rivers or sea, in extensional settings they commonly terminate at axial rivers, lakes or playas (Weissmann et al., 2010).

DFSs are markedly different from tributary systems in that they:

1) Display a radial pattern of channels diverging from the fan's apex
2) Channel sizes decrease with distance from apex
3) Grain sizes decrease with distance from apex
4) Display laterally unconfined channels below apex (Weissmann et al., 2010)

### 2.3.4 Floodplains

Floodplains contain a number of sedimentary elements that can be more or less obscured by vegetation. These include levees, oxbow lakes, paleo channels, scroll bars and mud plains. Some landforms on the floodplain can be mapped by utilising the sediments grain sizes varying ability to contain moisture. Hollow topographic features such as paleo channels have been shown to have the highest moisture content on the floodplain (Gilvear and Bryant, 2016). This variation will be visible in a NDWI image.

Variances in vegetation also indicates different sediments and topographic features, this can be seen as different colours in a true colour image, and as different shades in a near IR image. Combined in a NDVI image, different types of vegetation can be identified.

### 2.3.5 Anthropogenic influence

From the dawn of man, humans have settled near rivers and deltas. As numbers and technology increased, the alterations of the river systems have become considerable. Such efforts include bank protection to reduce erosion on the outer banks and protect properties and man-made structures. Artificial levees and floodways have been built to contain and limit effects of seasonal flooding (Bridge, 2003).

Rivers are also utilised for irrigation, and water is often diverted into complex networks of manmade canals and ponds to provide irrigation for agriculture and even fish farming. Large dams are constructed to provide hydroelectric power and fresh water reservoirs, as well as controlling downstream discharge (Tandon and Sinha, 2008). This contributes to reducing discharge and sediment transportation, leading to sedimentation upstream of the constriction. Below the dam, the water surface slope will increase, which can lead to erosion and coarsening of sediments, as well as reduced sinuosity of the channel (Bridge, 2003).

Rivers have been and still are important for transportation, and efforts are made to deepen, straighten and widen channels. These alterations increase channel slope and width, as well as sediment transport rate, which can lead to upstream degradation, and downstream aggradation. Successful efforts to change a rivers natural flow may result in more devastating floods if the dams or levees breach, increased flooding further downstream, and sediment and nutrient deprivation on the surrounding floodplain (Bridge, 2003).

## 2.4 Remote sensing & Geographic Information Systems

### 2.4.1 Geographical Information Systems

Geographical information systems (GIS) are a set of IT tools that enables the user to gather, process and display spatial georeferenced data. It consists of both software, of which there are several suppliers, hardware with sufficient memory and processing capacity, and workflows. A GIS provides easy and quick access to data, and both local and global datasets are available. It also handles non-spatial (attribute) data in connection with spatial data. Different datasets can be combined to analyse spatial characteristics, and the output can be displayed as maps or tables, depending on the purpose. In addition to the software, necessary elements are a global positioning system and remote sensing (Heywood et al., 2011).

### 2.4.2 Remote sensing technologies

Remote sensing includes data from several platforms, such as satellites and planes, as well as hand-held devices. It includes passive recordings, such as photogrammetry and gravimetry, and active interrogation by radar, electromagnetism. Among the advantages are area coverage, Spatial and

temporal resolution, as well as recording of electromagnetic radiation otherwise invisible to the human eye. Digital storing of the data enables processing and analysis of large datasets (Gilvear and Bryant, 2016).

Satellite data offers spatial coverage and temporal resolution that is otherwise difficult to obtain and is a valuable addition to fieldwork or other survey methods. It gives access to a lot of data about large areas such as river basins, which would otherwise be very costly and time consuming to map. This especially applies to very remote or unsafe locations that otherwise would be very difficult to reach, where remote sensing makes data accessible in a fast, safe and economical manner. As the satellite revisits the same area at a set time interval (ranging from 12 hours to 44 days) over several years and decades, temporal changes are also possible to map and analyse (Gilvear and Bryant, 2016).

For surveying large river systems, capturing images from the air or from space gives an easy and accurate picture of the rivers morphology. Geomorphology, fluvial processes, hydrology and land use in the catchment area and the floodplain can be mapped, taking advantage of the different reflectance properties of the features (Gilvear and Bryant, 2016).

The stability of the satellite platforms gives georeferenced images with high geometric accuracy. Spatial resolutions range from 10-60m .

The scale and resolution of satellite images fills the gap between seismic resolution and the finer details found in outcrops and cores, as illustrated in Figure 2-3 (Nyberg et al., 2015). While logs and cores give very detailed information about small areas, seismic and outcrop give less detailed 3D information about larger areas, satellite images offer a unique opportunity to collect data from large modern systems.

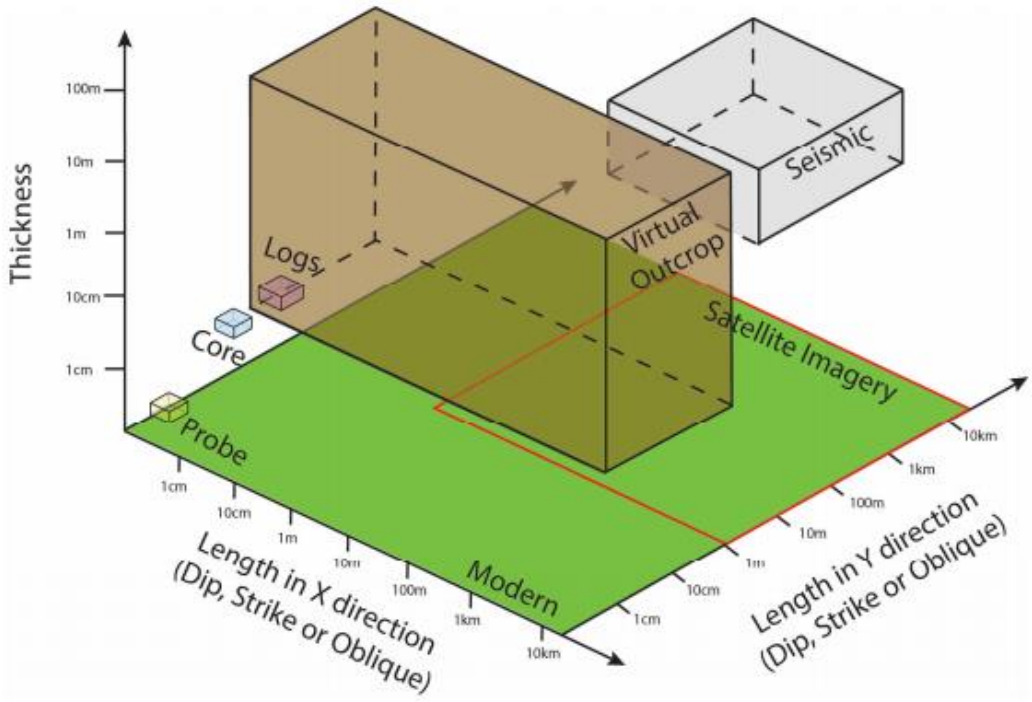


*Figure 2-3 Satellite imagery complements other geological methods for gathering information by providing a laterally very extensive dataset. Figure from Nyberg (2015)*

*Table 2-1 Satellites carry a range of sensors, which can record a range of spectral wavelengths at different spatial and temporal resolutions. Table from Nyberg (2015).*

| Satellite Sensor | Spectral (µm) | Spatial (m) | Radiometric (bits) | Temporal (days) | Bands | Operational |
|---|---|---|---|---|---|---|
| Landsat TM | 0.45 -1.75*, 10.4 - 12.5, 2.08 - 2.35 | 30 - 120 | 8 | 16 | 7 | 1982 - 2012 |
| Landsat ETM+ | 0.45 -1.75*, 10.4 - 12.5, 2.08 - 2.36, 0.5 - 0.9† | 15 - 60 | 8 | 16 | 8 | 1999 - |
| IKONOS | 0.45 - 0.9 0.45 - 0.9† | 0.8 - 4 | 11 | 3 | 5 | 1999 - |
| QuickBird | 0.45 - 0.9 0.45 - 0.9† | 0.61 - 2.44 | 11 | 1 - 3.5 | 5 | 2001 - |
| MODIS | 0.405 - 14.385 | 250 - 1000 | 12 | 1 - 2 | 36 | 1999 - |
| ASTER | 0.52 - 0.86, 1.6 - 2.43, 8.12 - 11.65 | 15 - 90 | 8 - 12 | 16 | 14 | 2000 - |
| WorldView-1 | 0.4 - 0.9† | 0.46 | 11 | 1.7 - 5.7 | 1 | 2007 - |
| WorldView-2 | 0.4 - 1.04*, 0.45 - 0.8† | 0.46 | 11 | 1.1 - 3.7 | 9 | 2009 - |

NASA's Landsite satellite program has been running since the launch of Landsat 1 in 1972 and is the world's longest continuous collection of remote sensing data. Landsat 5 is currently the longest

operating satellite, it completed 150 000 orbits and took 2,5 million images of the Earth between the launch in1984 and its decommissioning in 2013. Most of the bands have a resolution of 30 metres.

Sentinel – when, who, resolution (sentinel 2 gives best resolution)

Most satellite sensors have several bands, each catching a range of different wavelengths. Multispectral satellites typically have between 1-10 bands, ranging from 50-100nm, as opposed to hyperspectral satellites that can have up to 250 bands, each ranging from 1-10nm. Both Landsat and Sentinel are multispectral satellites. They have bands in the visible spectre (red, green and blue), in addition to near infra-red, several infra-reds and a thermal band, all capturing different and increasing wavelengths (Gilvear and Bryant, 2016).

| Sentinel 2 Bands | Name | Wave length captured | Spatial resolution, m | Used in this study for: |
|---|---|---|---|---|
| B01 | Coastal aerosol | 334 nm | 60 | |
| B02 | Blue | 490 nm | 10 | True colour |
| B03 | Green | 560 nm | 10 | True colour<br>False colour |
| B04 | Red | 665 nm | 10 | True colour<br>False colour |
| B05 | Vegetation Red Edge | 705 nm | 20 | |
| B06 | Vegetation Red Edge | 740 nm | 20 | |
| B07 | Vegetation Red Edge | 783 nm | 20 | |
| B08 | NIR (Near infra-red) | 842 nm | 10 | False colour |
| B08A | Vegetation Red Edge | 865 nm | 20 | Moisture index |
| B09 | Water vapour | 945 nm | 60 | |
| B10 | SWIR (Short wave infra-red) - Cirrus | 1375 nm | 60 | |
| B11 | SWIR | 1610 nm | 20 | Moisture index |
| B12 | SWIR | 2190 nm | 20 | |

*Table 2-2 Wave lengths as given in Sentinel-Hub which was used for downloading images*

*Table 2-3 Landsat bands and resolution, used in the temporal dataset.*

| Landsat 5 Bands | Name | Wave length captured | Spatial resolution, m | Used in this study for: |
|---|---|---|---|---|
| Band 1 | Blue | 450-520 | 30 | Temp. analysis |

| | | | | |
|---|---|---|---|---|
| Band 2 | Green | 520-600 | 30 | Temp. analysis |
| Band 3 | Red | 630-690 | 30 | Temp. analysis |
| Band 4 | NIR (Near infra-red) | 760-900 | 30 | Temp. analysis |
| Band 5 | SWIR 1 (Short wave infra-red) | 1 550-1 750 | 30 | Temp. analysis |
| Band 6 | Thermal | 10 4000-12 500 | 120 | Temp. analysis |
| Band 7 | SWIR 2 | 2 080- 2 350 | 30 | Temp. analysis |

#### *2.4.2.1 Considerations and limitations*

When acquiring images from a fluvial system, certain limitations must be considered. One of the most important is the size of the features that should be mapped, such as the width of the river channels and bars. Satellite imagery is suitable for rivers that are more than 200m wide, while for smaller rivers (20-200m), aerial imagery captured by planes might be better (Gilvear and Bryant, 2016). Narrow channels, especially if obscured by vegetation, can be difficult to detect.

The satellite collects information from rectangles of land based on the sensor resolution. Features within these squares will be blended together to give one value for each pixel. Details within these are lost. These square pixels will most often not be aligned perfectly with the edge of the river, resulting in a jagged riverbank. If the channel is too narrow for the resolution available, this jaggedness can affect the continuity of the channel in the image and make the delineation of the river unprecise. The pixels on the edge of the river will be influenced by the different reflective properties of the water, vegetation and sand, and this may impair the classification of the pixel (Gilvear and Bryant, 2016).

Spatial variability of reflectance within the image will affect the rendering of the features, and images that partly overlap can have the same features shown in slightly different colours. This is often necessary when mapping rivers, as they are long and narrow features, and in order to produce an image that covers a sufficient part of the river, many smaller pictures must be mosaiced together in a string.

When comparing images captured over time to map change, it must be considered that the geomorphology of bars and other features will change appearance depending on varying water level. It must be ensured that water level is the same if pictures are to be compared with each other (Gilvear and Bryant, 2016).

Some sensors, including Sentinel2 and Landsat cannot see through cloud cover, and are dependent on clear weather to obtain a good image.

Grain size cannot be directly determined from satellite images, but its effect on the river morphology can give an indication. For example, tend rivers with primarily bedload and course sediments to have un-cohesive channel banks, whereas rivers with mostly fine-grained suspended load to have cohesive channel banks. It may in some cases be possible to differentiate this in satellite images.

### 2.4.3 Image processing

Different features in the landscape show up as different colour in each band, and combinations of bands are chosen to compile an image that highlights the features of interest.

A natural colour image is composed of red, green and blue bands, all in the visible range, and create an image with colours similar to what our eyes see in nature.

A false colour image is made up of the near infrared (IR), red and green bands, and most commonly produces an image where vegetation is shown as red.

Spectral responses from fluvial environments can be categorised in three distinct classes based on their distinct signatures ; water, green vegetation and exposed sediment (Gilvear and Bryant, 2016).

- Water bodies appears clearly delineated and nearly black in near and mid IR bands, as these wavelengths are almost completely absorbed or transmitted by water. These bands show the greatest contrast between water and land. In the visible spectre as well, little light is reflected from water. Variability in deep water reflectance is caused by surface roughness, suspended vegetation, plankton or sediments. In shallow water, the substrate will influence the spectral signature as the sediments at the bottom will give a different reflectance signature.
- Chlorophyll in healthy vegetation reflects wavelengths in near IR bands, and the vegetation appears light. Different vegetation types can be deciphered, which is of interest as vegetation patterns on floodplains can relate to topography and moisture content (grain size) and thereby channel mobility.
- The spectral signature of exposed sediments depends primarily on moisture content, as well as organic content, texture, structure and iron oxide content (Gilvear and Bryant, 2016). As the moisture content increases, reflectance decreases in the visible range, and the feature will appear darker in the image. The effect is greater in fine sediments as clay, and less in sand.

Normalised Difference Water Index (NDWI) includes the bands B3 and B8 used in the formula (B3-B8)/B3+B8) and shows the moisture content, typically increased moisture is shown as yellow, and less moisture is shown as blue.

Normalised Difference Vegetation Index (NDVI) includes the bands B8 and B4 used in the formula (B-B4)/B4+B4) which in SentinelHub shows vegetated areas as green, unvegetated as light yellow, and water as grey

Unsupervised classification is available as a standard tool in ArcMap. It assigns values to pixels based on their spectral values, and groups similar values into a predetermined number of groups (Gilvear and Bryant, 2016).

### 2.4.4 Mapping Temporal variability

The study “High-resolution mapping of global surface water and its long-term changes” (Pekel et al., 2016) has used data from Landsat 5, 7 and 8 to make a worldwide high resolution map (30m x 30m ) of surface water, and changes to this between 1984 and 2015. The results were validated and found to include less than 1% false water detections.

# 3 Geological settings/Study areas

## 3.1 Global fluvial systems

Fluvial systems are found on all continents, and in all climate zones. Some areas have however none or very few active systems at the present, such as Antarctica, Greenland and some very arid desert regions. Global datasets are available for analysis, both with regard to whether they are located in source regions or sedimentary basins, and with regard to climate zones.

## 3.2 Eight DFS systems

In addition to a global analysis, eight DFS systems were chosen for further analysis and comparison. They are situated in different climatic and tectonic settings, as summarised in Figure 3-1 below. All the rivers chosen are perennial rivers, that have water in the canals throughout the year, even though the level varies between the seasons. Further all rivers are in terrestric settings, none terminate in the ocean, although two (Ili and Uvs) terminate in lakes. Okavango and Taquari terminates at the toe of the fan, while the rest join larger or axial rivers. River systems with extensive anthropogenic influence were excluded, as it was difficult to identify the original, natural channel.

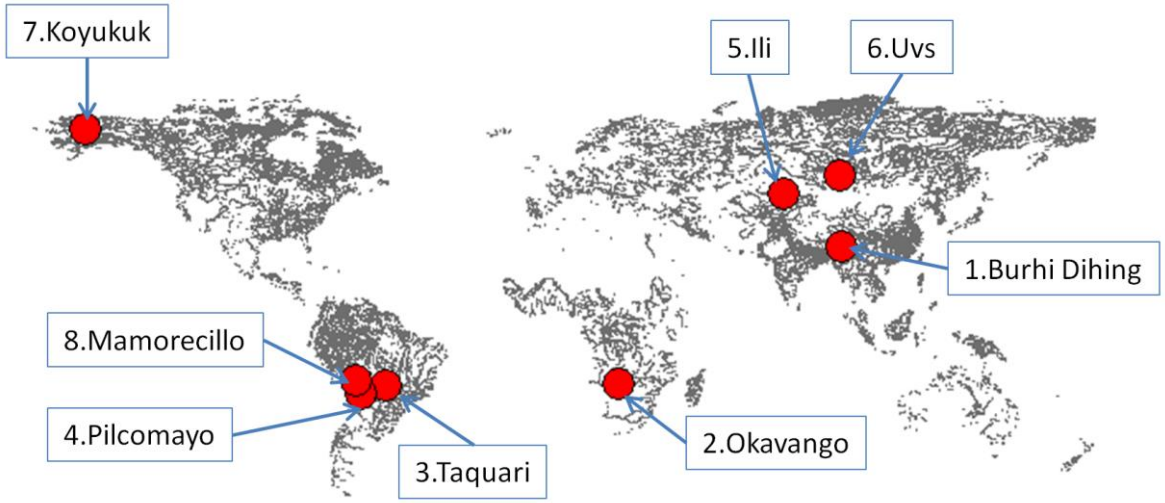


*Figure 3-1 The geographic location of all eight systems, on a map of the worlds fluvial systems*

## 3.3 Burhi Dihing, India

**Tectonic setting**

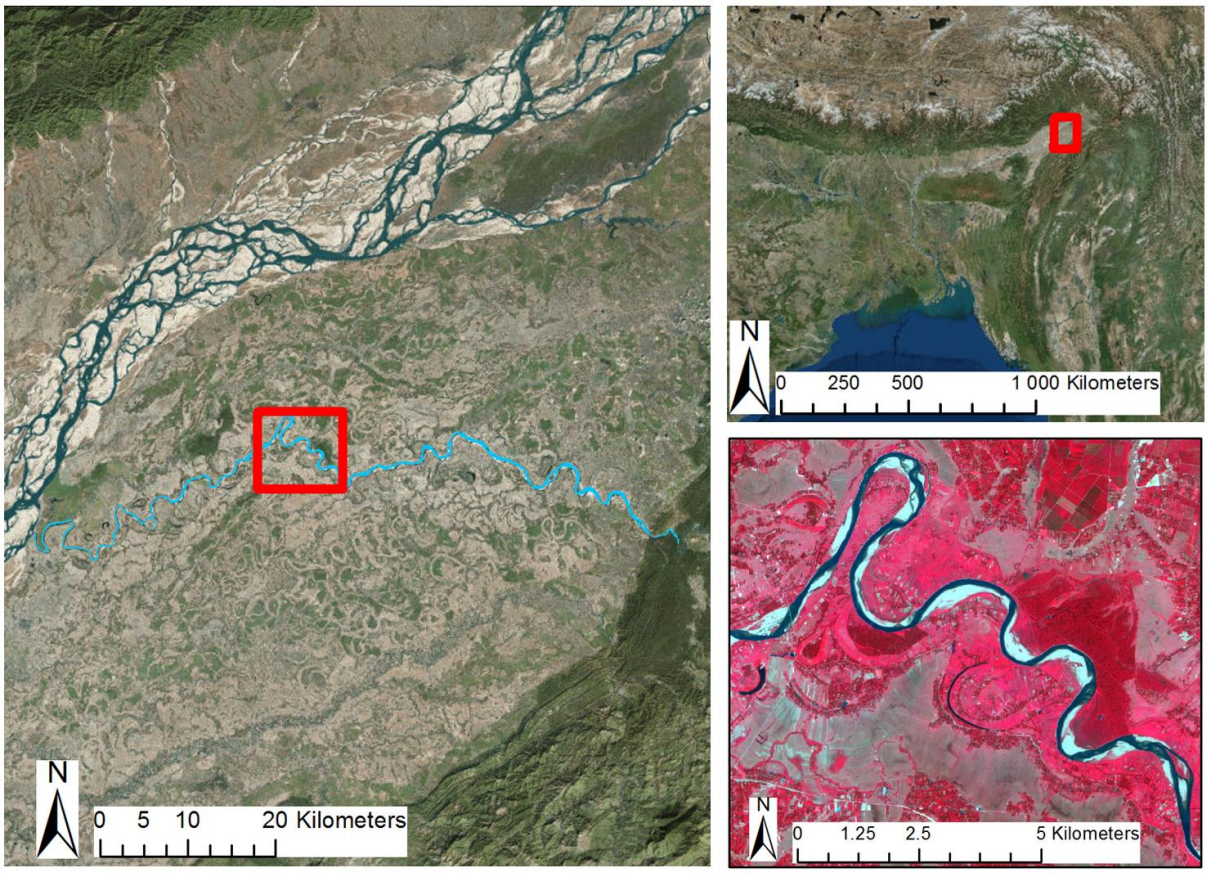


*Figure 3-2 Burhi Dihing, India*

The Burhi Dihing is located north-east in the Assam basin, in North India (Figure 3-2)

This is a tectonically active area with a compressional stress regime, as the Indian subcontinent is converging into the Eurasian plate and being subducted under it (Das Gupta and Biswas, 2000) The eastern part of the Assam basin is subducting on three sides (Mandal and Dasgupta, 2011)

The Assam basin is part of the Himalayan foreland basin, and this area is confined by the SSW-NNE trending, SE thrusting Eastern Himalaya Thrust Belt to the NE, and the similar trending, but NW thrusting Assam – Arakan Thrust Belt to the SW (Sahoo and Gogoi, 2009). The Arakan Thrust belt consists of two SSW-NNW trending thrust faults, Naga and Disang faults (Das Gupta and Biswas, 2000). The northern part of Brahmaputra is the axial river running through this basin.

As the river enters the basin from the east at Jaipur, it becomes unconfined and meanders westwards, joining the Brahmaputra after an aerial distance of approximately 70km. The river consists of a single, sinuous channel, where recent and ongoing neck cut-offs and the resulting ox-bow lakes.

This is the largest of several south bank tributaries to the Brahmaputra river, creating an alluvial plain where several paleo ox-bow lakes as well as previous river channels can be observed.

**Climatic controls**

The climate in Assam is monsoon driven, the wet season lasting from June to September. The total catchment area of Burhi Dihing is approximately 6000 km2, and receives on average 3000mm precipitation (J.N. Sarma, 1986) The catchment area is in the eastern part of the Assam basin, and is predominantly rain fed, meaning that runoff is generated by rainfall, with less input from snow and glacial melting (Singh and Bengtsson, 2005). Temperatures range between approximately 17oC in winter to 27oC in summer (Immerzeel, 2008).

**Water discharge & sediment supply**

Due to the seasonal monsoon rains, the rivers discharge is highly variable throughout the year. Flash floods are common in the beginning of the rainy season, and water discharge can increase from 100 at the end of the dry season to 1000m3/s in a matter of days. In high flood conditions, water discharge can be as high as 2200m3/s, although 1100 to 1900m3/s are considered normal flooding magnitude (J.N. Sarma, 1986)

The highest measured suspended sediment load is 1,19 g/l, measured in June at the hydrological station at Khowang. This corresponds to a discharge of 2024m3/s, carrying a sediment load of 2415kg/s (J.N. Sarma, 1986)

Total annual sediment transport is 3 620 000 t/yr, 33% of which is transported in the monsoon month of July alone. Negligible amounts of sediments are transported during the dry January to March months (J.N. Sarma, 1986)

The current alluvial sediments (Siwalik/Dhekiajuli formation) are 500m, although the oldest sediments in this area are from the Eocene (Sylhet group), and total sediment depth is 3000m (Mandal and Dasgupta, 2011).

**Anthropogenic influence**

The study area is largely agricultural land, which means anthropogenic influence with regards to land use, farming, damming and irrigation is present. Rice paddies are common along the river, which diverts water from the channel at time of planting.

In addition, there has been large scale mining and dumping of mining debris near the river channel in the Margherita-Ledo region (27° 16′ 48″ N, 95° 40′ 48″ E), which is upstream from the study area. This has greatly increased the sediment influx in the river since 1985 (Sarma et al., 2007).

## 3.4 Okavango

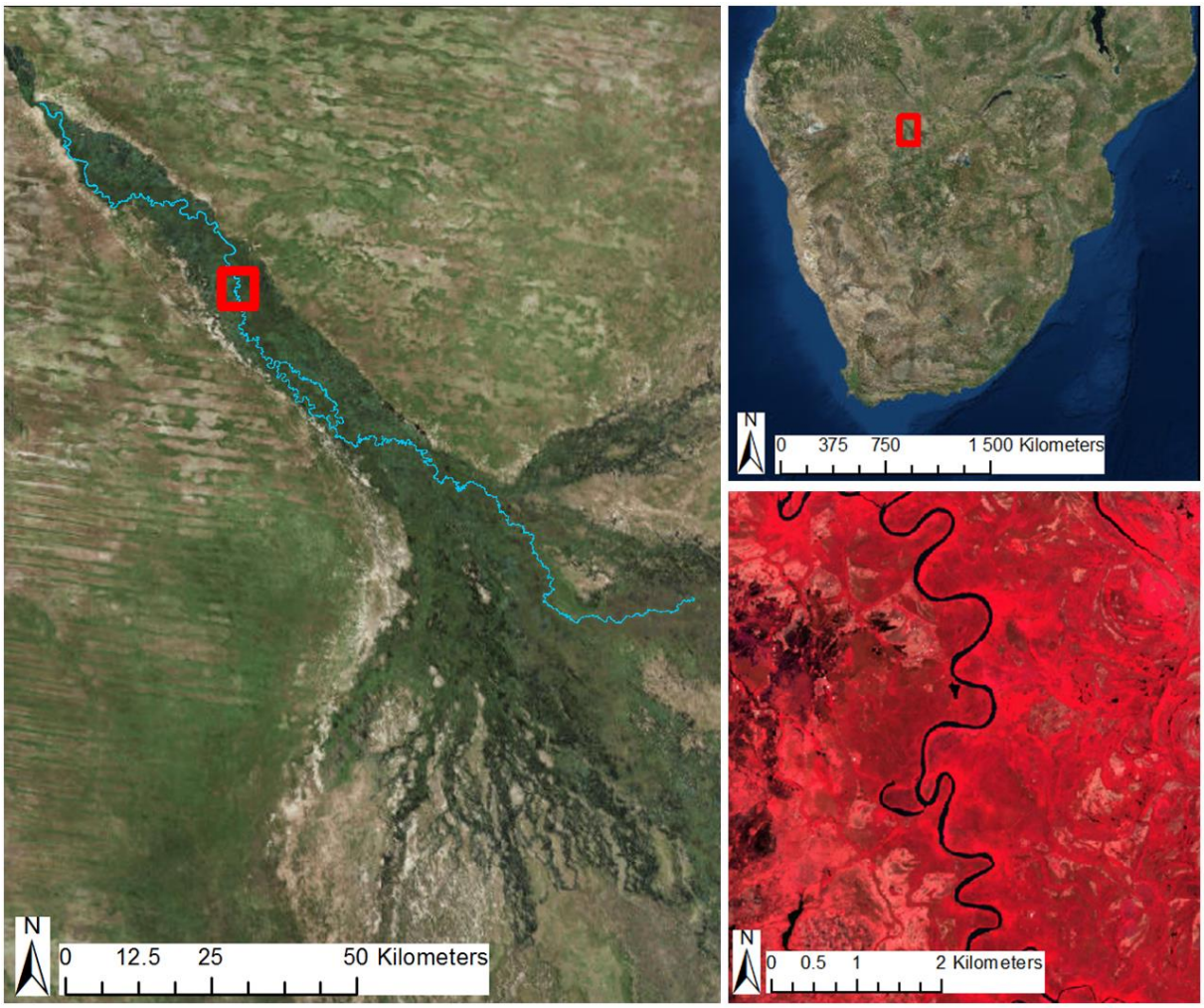


*Figure 3-3 Okavango fan, Botswana*

**Geological setting**

The Okavango fan is located in Botswana, in the intracratonic Kalahari Basin, which is an extensional stress regime connected to the East Africa rift (Figure 3-3). It is a large conical alluvial fan covering 18 000m$^2$ of an incipient rift basin, bound by the Gomare-Thamalakane fault system. This system consists of several northeast striking normal faults creating a graben-like structure confining the lower part of the bifurcated channels (Mccarthy and Cairncross, 2000).

The fan is fed by the Okavango river, and can be divided into three sections. The upper most "panhandle" section is confined by a small north westerly graben running perpendicular to the faults confining the lower parts. The panhandle is approximately 10 x 100 km, and the waterflow in this

section is confined by faults and vegetation (Mccarthy and Cairncross, 2000). At the basin bounding fault the channels bifurcates several times, each becoming more narrow downstream (Weissmann et al., 2010).

This area consists of perennial swamps, where the channels are confined by vegetation and peat banks. Water leaks through the permeable peat edges and causes channel aggradation. This, together with peat fires and subsequent collapse of river banks, causes frequent avulsions (McCarthy and Ellery, 1998).

The third and most distal part has only seasonal swamps, no peat, and the waterflow is largely unconfined (Mccarthy and Cairncross, 2000).

**Climatic controls**

The catchment area of the Okavango fan is in a sub-tropical climate, with a rainfall of 1000mm/year. The climate of the fan itself is semi-arid, with an annual rainfall of 513 mm/year. Evaporation and evapotranspiration exceed rainfall every month of the year (McCarthy and Ellery, 1998).

**Tectonic controls**

The most striking feature of this fan is the cross valley down-fault at the end of the panhandle, after which the channels spread out almost perpendicular to the channel above the fault.

**Water discharge and sediment supply**

Water discharge in the Okavango river, measured at Mohembo at the top of the panhandle, averages approximately 9 200 mill $m^3$/year. There is seasonal flooding from May to August, varying from a low of 400 mill $m^3$ in November, to maximum of 1 500 mill $m^3$ in May (McCarthy and Ellery, 1998). This equates to approximately 152 – 570 m3/s.

The flood wave takes four months to reach the toe of the fan, and the end, only 1,5% leaves the fan as outflow, which means that the entire sediment load is deposited on the fan. In the panhandle, the sediments are deposited as point bars in the meandering river, and in the lower area as channel bed aggradation. The most distal parts receive little clastic sediments, but transpiration causes precipitation of solutes (McCarthy and Ellery, 1998). Channel banks in the panhandle are held together by vegetation (Smith et al., 1997).

The sediments are largely of aeolian provenance from the Kalahari Desert, and thus have very low silt and mud content. Thus, most of the sediment-load is fine sand transported as bedload. The concentration of solubles is also low (40 ppm), as little chemical weathering takes place in the

catchment area. Bedload is 1 700 000t, Suspended load 39 000t, and total solute load 381 000t. In addition aerosol fall out contributes 250 000t (McCarthy and Ellery, 1998).

In addition to sediments carried by the river, is wind-blown sand a major source of sediments on the fan, especially in dryer climates than the current.

The total sediment accumulation in the thickest part of the fan is approximately 300m and has been deposited since the Cenozoic.

**Anthropogenic influence**

A large part of the middle and lower fan is a nature reserve, which combined with the swampy environment makes it virtually unpopulated. This means there are no artificial constructions that hinder the natural water flow. The panhandle section has a denser human population (McCarthy and Ellery, 1998)

## 3.5 Taquari fan, Pantanal Basin, Brazil

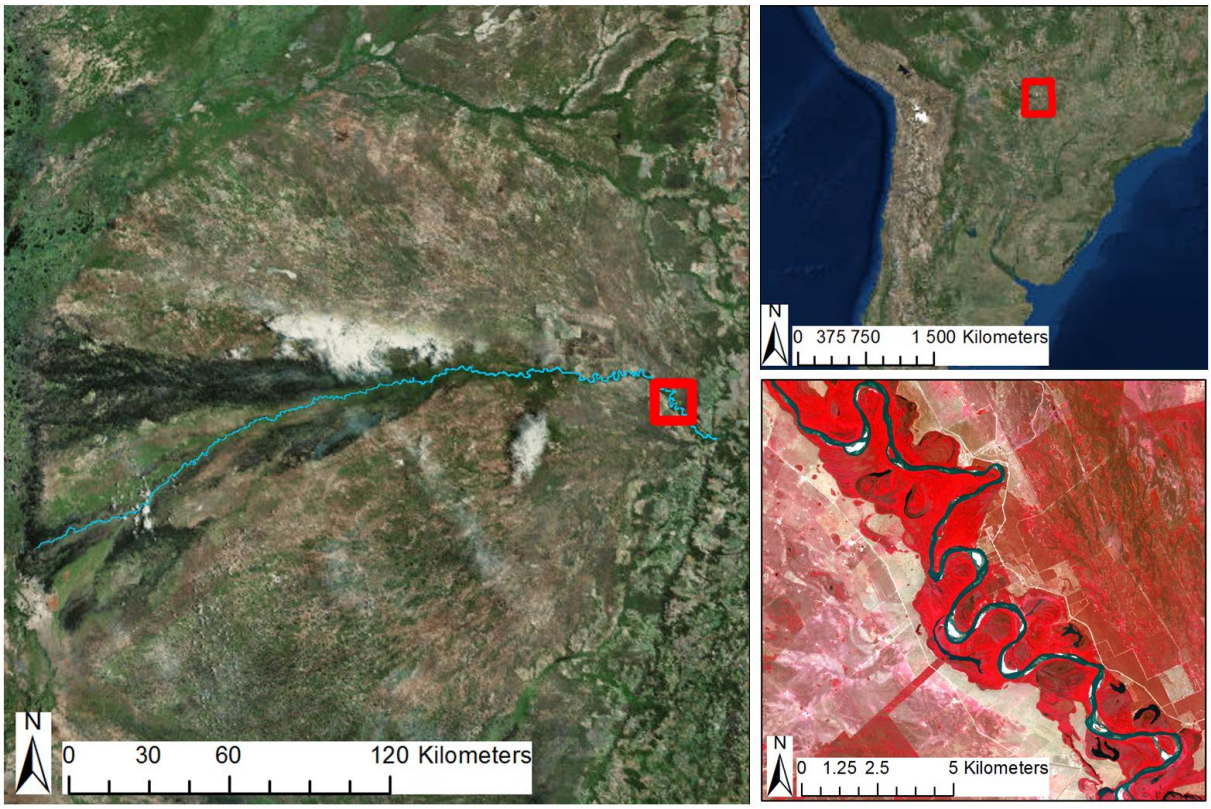


*Figure 3-4 Taquari fan, Brazil*

**Geological setting**

The Taquari fan (Figure 3-4) is one of several megafans in the Pantanal basin, a seismically active area which originated from the development of the Andes mountains to the west and has been filling with sediments since the Pliocene (Zani et al., 2012). The Taquari river crosses a steep escarpment from the Brazilian Plateau at 800m.a.s.l, enters the basin from the east and spreads out creating a semi-circular megafan covering 49 000 $km^2$. The apex to toe length for the entire fan is approximately 253km, elevation dropping from 190m.a.s.l to 85m.a.s.l along the way, giving a low gradient of 0,36m km-1 (Zani et al., 2012). As suggested by Stanistreet and McCarthys model (1993), this results in meandering channels with low sinuosity. The upper part of the active channel, a 3-5km wide channel belt is incising and confined by Pleistocene fan lobes. Chute and neck cut offs are common in this section of the river (Buehler et al., 2011) At approximately 56°W, the channel becomes unconfined and spreads out to form the active lobe where deposition takes place today. This is where the channel comes out of the Transbrasiliane Lineament, an active fault trend which crosses the fan with a NE-SW orientation, and from here it acquires a distributary pattern. These faults are of Neoproterozoic origin, but have been reactivated by Phanerozoic tectonic activity, and there is evidence of syn-sedimentary tectonic activity which may have created additional accommodation in

the basin (Zani et al., 2012). At this current apex, the gradient of the channel changes from 0,38m/km (confined) 0,44m/km (unconfined), and the sinuosity reduces from 1,6 to 1,3 (Assine, 2005) (Pott and Pott, 2005).

In the active lobe, neck and chute cut-offs are less common, but the channel moves by frequent avulsions (Buehler et al., 2011). The abandoned lobes display a well-preserved pattern of paleo channels, which indicate frequent avulsions. Recent avulsions have been documented using satellite data only (Buehler et al., 2011), as well as remote sensing combined with field work (Makaske et al., 2012).

**Climatic controls**

The Pantanal basin is poorly drained, and prone to annual flooding. Located at the approximate latitude of 18°S, and influenced by the Intertropical Convergence Zone (ITCZ), the Taquari fan has two seasons based on varying rainfall. The dry winter from May to September has a mean rainfall of 180mm, and the wet summer from October to April with 850mm mean precipitation. The vegetation on the fan consist of savanna-like grassland, semi-deciduous forest (which seasonally drops leaves), and seasonal dry forests (Zani et al., 2012). The climate is tropical sub-humid savannah climate, with temperatures ranging from 21° – 32°C (Assine, 2005)

**Water discharge and sediment supply**

In the dry season, monthly water discharge is approximately 150 $m^3/s$, increasing to approximately 950 $m^3/s$ (Assine, 2005)

The sediments of the fan are up to 550m deep (Assine, 2003).

**Anthropogenic influence**

The human impact on the Pantanal is largely agriculture and cattle grazing, which has led to deforestation and change in vegetation. This, together with diamond and gold mining, has led to land degradation and increased erosion. Several engineering projects in form of damming and dredging for ports have been implemented, but no large scale projects (Ioris, 2016).

## 3.6 Pilcomayo, Argentina/Paraguay

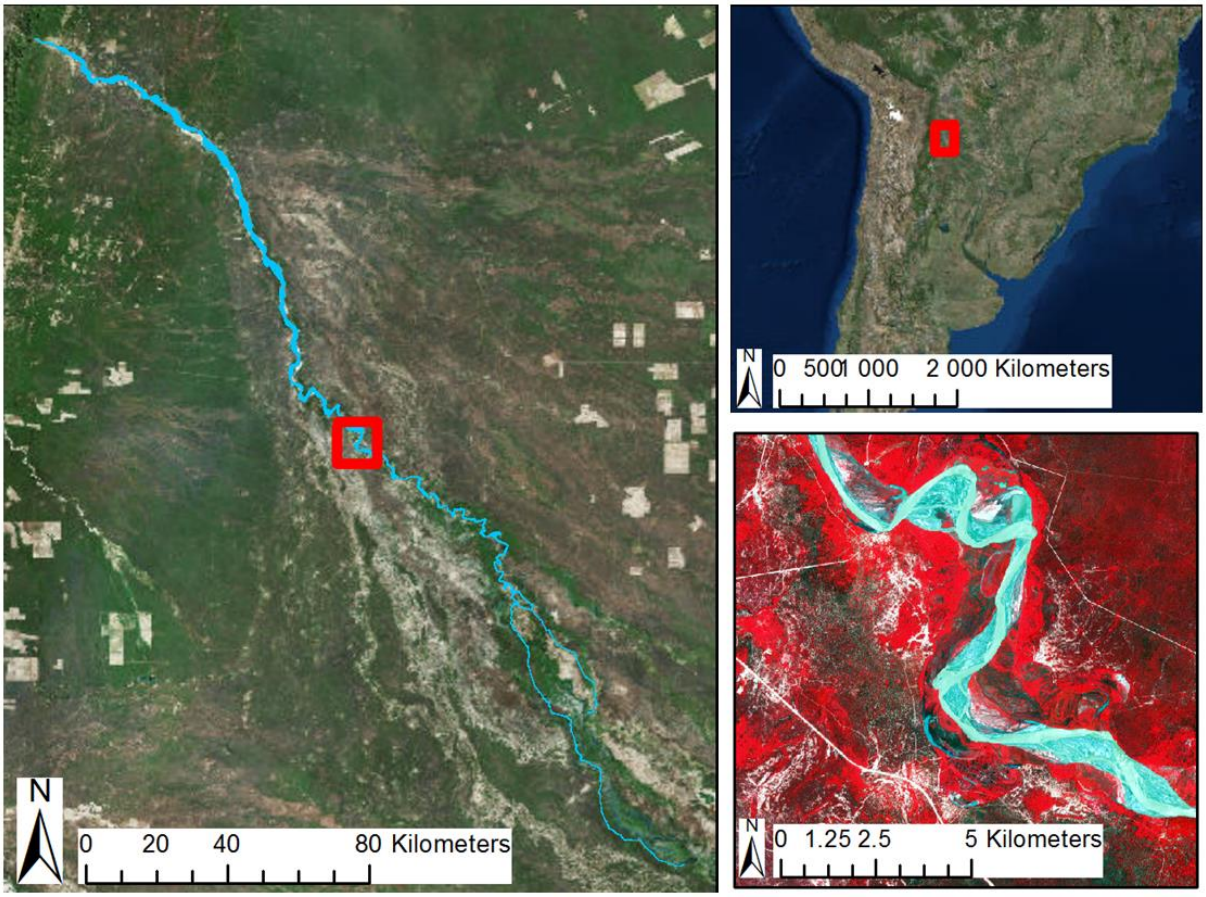


*Figure 3-5 Pilcomayo fan, Argentina/Paraguay*

**Geological setting**

The Pilcomayo River (Figure 3-5) originates in the Andes and flows in south-eastly direction into the Andean foreland basin. It is antecedent to the mountain range, as shown by incised meanders, and the age is estimated to early Pliocene (Iriondo, 1993). The entire river is over 700km long, and the depositional system covers more than 210 000km$^2$ (Weissmann et al., 2011)(Iriondo, 1993). It is one of five rivers running into the Chacko plain, located in along the eastern side of the Andes through Argentina, Paraguay and Bolivia. These rivers terminate in the axial Paraguay river when the discharge is sufficient.

**Climatic controls**

The climate in the western part of the Chacko plain is semi-arid (Iriondo, 1993) Rainfall is seasonal, with a dry period from May to October, and rainy season November to April. The discharge is very variable through the year, and highest discharge occurs in February, at approximately 700m$^3$/s.

During the dry season, the discharge can be less than 25 $m^3/s$ (Smolders et al., 2002). Iriondo (1993) operates with even higher variability, between 800$m^3/s$ to below 20 $m^3/s$.

**Water discharge and sediment supply**

The soil in the Andean mountains are susceptible to erosion and provide an ample influx of sediments, averaging 23,6 g/l during the rainy season (Smolders et al., 2002). The sediments carried are well sorted, very fine quarts sand, with no courser sediments. There are several abandoned channels in the western part of the fan, these are filled with fine, silty sand, but no clay or courser sediments. These paleochannels are frequently filled with water during the wet season. The lower part of the current channel is currently filling with sediments as part of an avulsion process that started in 1980, and hence gets blocked by sediments and vegetation, causing overflowing and upstream migrating collapse of the channel at a rate of 10-35 km/year (Iriondo, 1993).

**Anthropogenic influence**

The upper parts of the river is largely unregulated, and it follows the natural hydrological cycle (Smolders et al., 2002). There is however influx of mining sludge (approximately 360 000 tons) from the Potosi area, which settles in the upper part of the river (Smolders et al., 2002) The lowest part is led into numerous canals and dams for irrigation and fish farming, and thus not included in the study area.

## 3.7 Ili (Bakanas), Kazakhstan

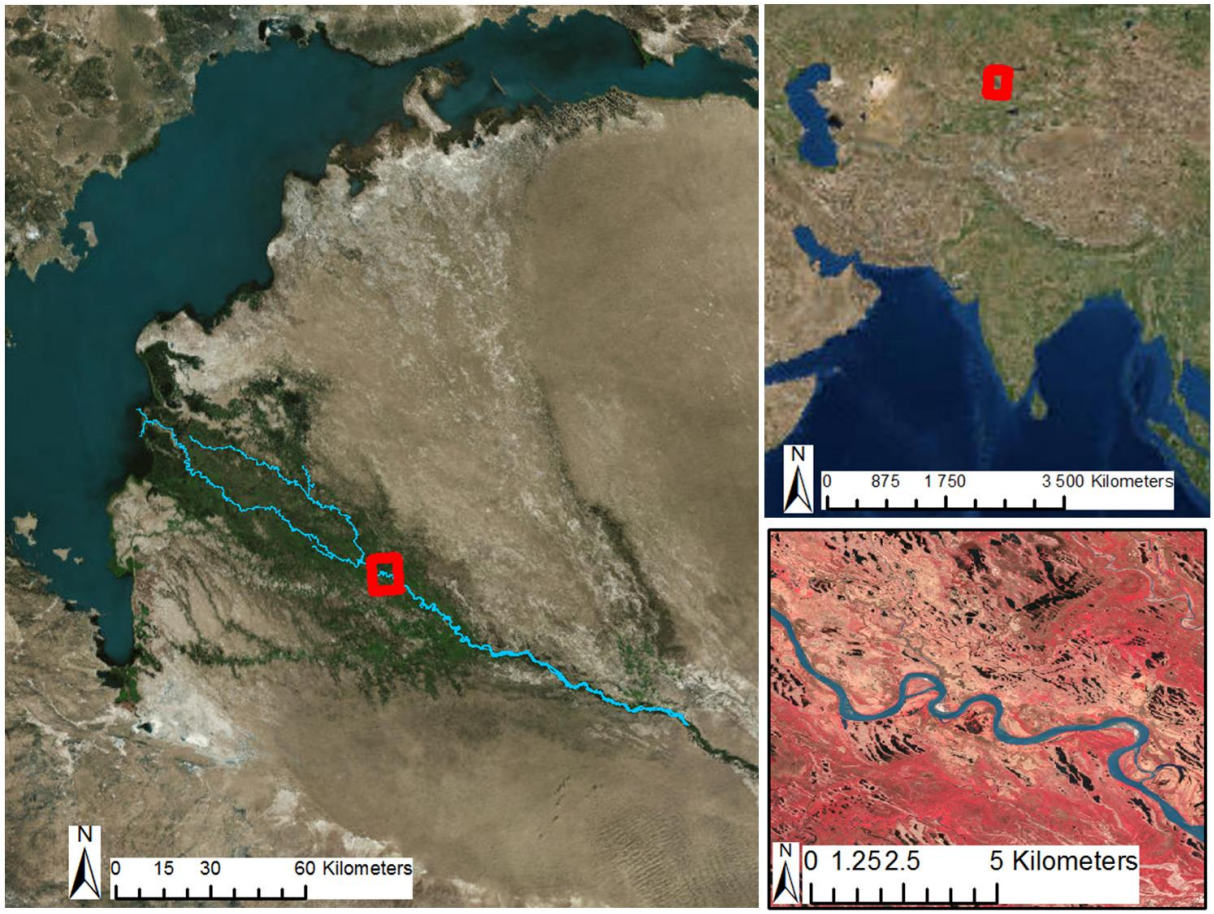


*Figure 3-6 Ili river, Kazhakstan*

**Geological setting**

The Ili river (Figure 3-6) flows westwards and splits into three separate channels near the city of Ushzharma. The eastern Zhidelinskaya, the central Ileyskaya and the western Toparskaya all drain into Lake Balkhash, although the Toparskaya is currently less active. The Ile branch consist of a winding channel and is the section that was mapped for this study. Previously, this was the mail watercourse, but it has been filled with sediments, and currently only contributes 4% of the runoff. Currently (since early 1900s) most of the discharge passes through the Zhidelinskaya section, which has a complicated morphology, consisting of multiple channels, lakes and spills.

Together they create an 8 $km^2$ large delta and form a large intracontinental estuary. The delta is made up of hilly ridged sand, complex waterways, floodplains and lakes, but also hilly ridged sand, desert grassland and scrub land (Dostay et al., 2013).

**Climatic controls**

Kazakhstan is an arid region, with typical inland climate characterized by frequent droughts and large temperature ranges. Humidity comes from the North Atlantic, but must travel far, and most is lost on the way. Air masses from Siberia gives very cold winters, with temperatures down to -40°C in winter. Summers can reach 40°C. Annual precipitation in the northern region is 250-350mm.

**Water discharge and sediment supply**

Average annual discharge has been measured at 472 m3/s just above apex, and less than 20 m3/s below (Dostay et al., 2013).

**Anthropogenic influence**

Kapchagay reservoir was constructed upstream from the river's apex, and subsequently reduced fluctuations in water inflow to the delta. Discharge measured by gauge stations along the river channel is affected by this, while calculated estimates based on catchment area and climatic zone are not.

## 3.9 Uvs (Tes), Mongolia/Russia

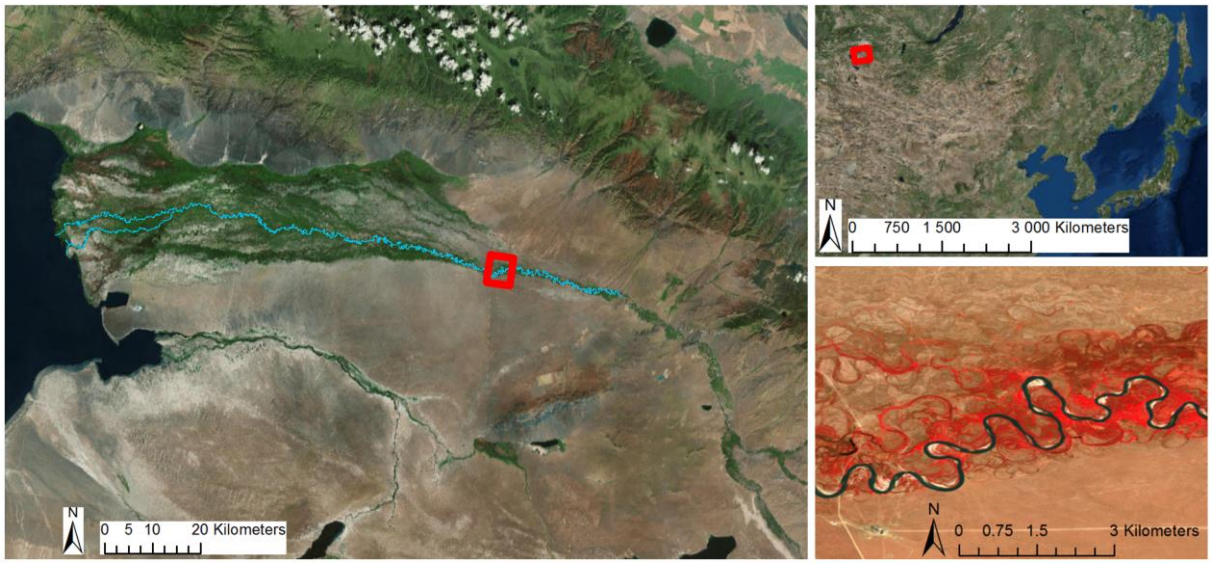


*Figure 3-7 The Uvs fan, Mongolia/Russia*

**Geological setting**

Located in a foreland basin in North Western Mongolia and Russia, the Tes (Tesiyn Gol) river (Figure 3-7) drains into the Uvs Nuur lake. It's a high-altitude area, with mountain ranges from 1000 to 3000 m.a.s.l. There are also large sand dunes to the east, and area with large plains sloping towards the lake. The dunes formed during Pleistocene, and are still active, shaped by dust storms in spring (Paul, 2012).

**Climatic controls**

Situated very far from the nearest ocean (Yellow Sea, Arctic ocean), the climate is continental, with cold winters and hot summers, temperatures ranging from lowest measured at -58°C to 40°C in summer, with an average temperature of -3.6°C Limited precipitation in the basin classifies it as semi-arid to arid, with most of the precipitation in June, July and August although there are strong year to year variations. Vegetation on the plains ranges from grassland steppes to semi-desert (Paul, 2012).

**Water discharge and sediment supply**

The aeolian dunes provides additional sediments, which is transported as bedload. Runoff has been measured as 47.6 $m^3/s$, containing 89 mg/l filterable solids (Paul, 2012).

**Anthropogenic influence**

The area has very low population density, with little industry. People mostly live in small villages or are nomads with sheep, goats, cattle, horses and camels. There were (in 2012), no usage of water

power or damming, and the river was mostly unaffected by human engineering activities. Current trend is reduction in population due to urbanization (Paul, 2012).

## 3.10 Koyukuk, Alaska

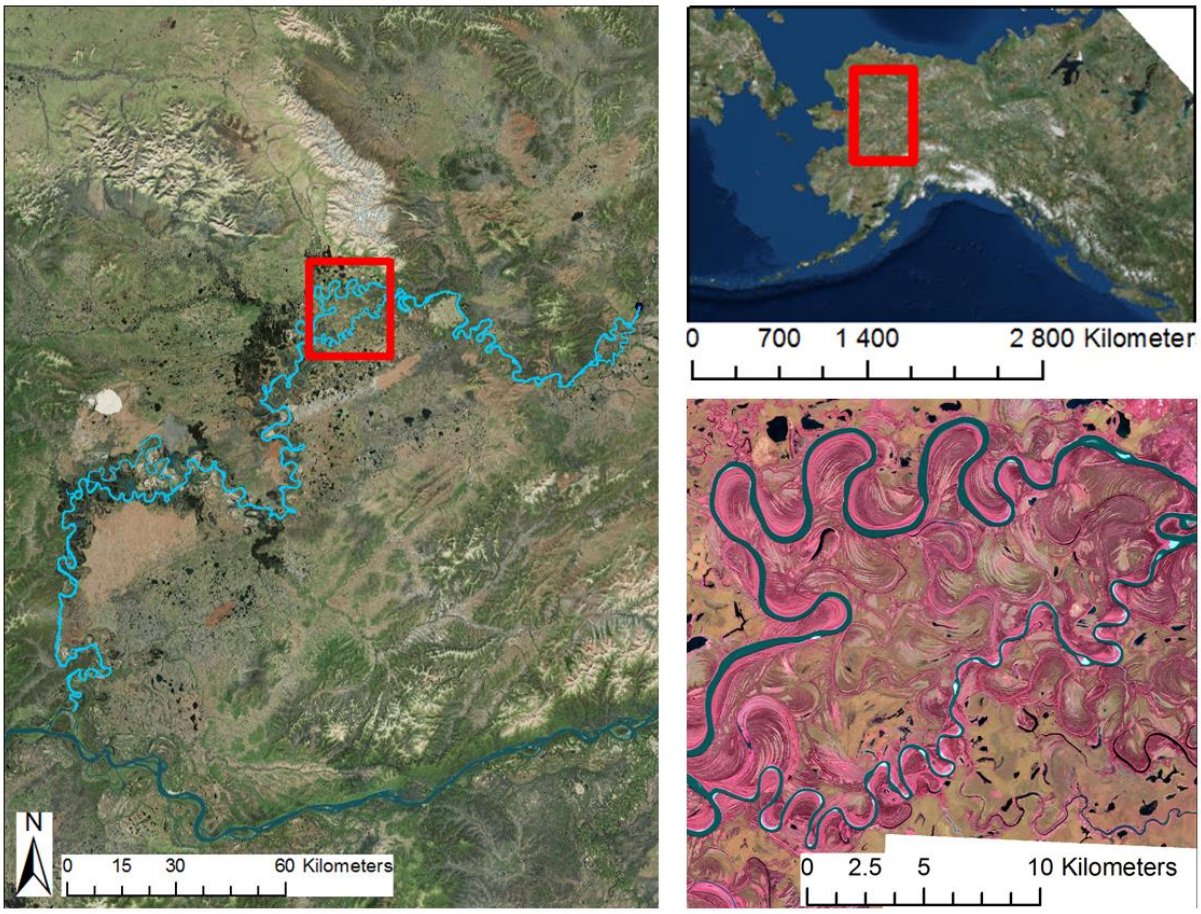


*Figure 3-8 Koyukuk river, Alaska*

**Geological setting**

The Koyukuk river is located in the Yukon-Koyukuk Basin in western Alaska (Figure 3-8). The basin is delineated to the north by the Kobuk fault zone, and the dextral strike-slip Kaltag fault runs WSW-ENE just south of the Koyukuk river. The Youkon-Koukuk basin has been subjected to strong east-west compression (Late Cretaceous), which was replaced by an extensional regime by Early Tertiary, along with widespread vulcanism and movement along the Kaltag fault (Patton and Box, 1989)

Deposits on the Koyukuk Flats have been transported by water and wind, from glaciated areas in the Alaska Range and Brooks Range during the Pleistocene and Holocene (Patton et al., 2009).

**Climatic controls**

Koyukuk has annual snowfall of 191 cm, no glaciation, but permafrost in its catchment area. (Brabets and Walvoord, 2009)

**Water discharge and sediment supply**

Average annual discharge is 6 400$m^3$/s (Brabets and Walvoord, 2009)

**Anthropogenic influence**

The Koyukuk runs largely through the Koyukuk National Wildlife Refuge and is largely undisturbed by human activities and constructions (Patton et al., 2009).

## 3.12 Rio Mamorecillo (Rio Mamoré), Bolivia

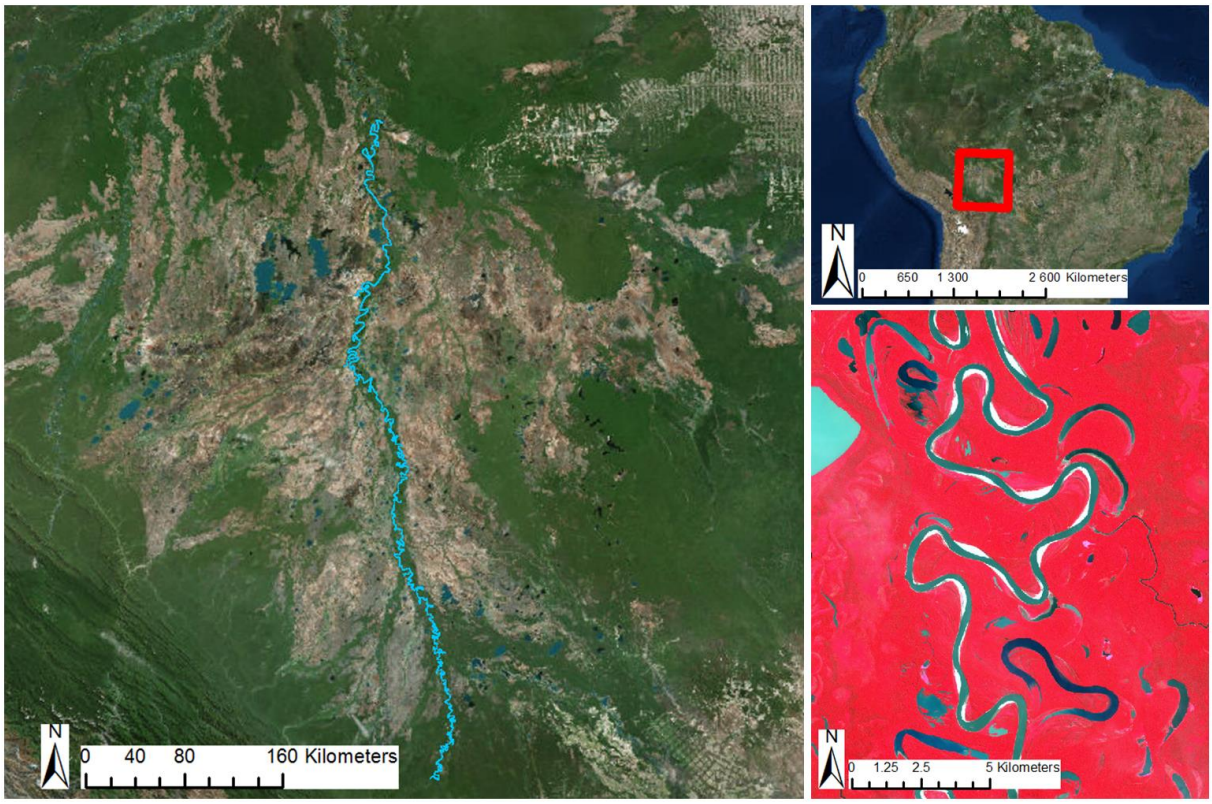


*Figure 3-9 Mamorecillo river, Bolivia*

**Geological setting**

Rio Mamorecillo (Rio Mamorè) is located south west in the Amazon basin, draining the Andean mountains (Figure 3-9). This is an area with high sediment production, due to steep relief, highly erodible rocks and a humid climate (Filizola and Guyot, 2009).

**Climatic controls**

Mamorecillo is in a humid tropical climate, and is directly influenced by the LaNina/ElNinjo cycle, with flooding during LaNina years (Gomes et al., 2018).

**Water discharge and sediment supply**

Mamorecillo has a predominance of suspended sediment (Gomes et al., 2018)

**Anthropogenic influence**

There have been little engineering controls on this river and no large dams constructed (Constantine et al., 2014).

# 4 Methodology and Datasets

## 4.1 Datasets

### 4.1.1 Global Modern Sedimentary Basins (GMSB)

The dataset "Global Modern Sedimentary Basins (GMSB)" was used to identify which sedimentary basins the rivers are located in, and the climatic properties of the same (Nyberg and Howell, 2015).

### 4.1.2 Global Terrestrial Sink Catchment (GTSC)

Used dataset "Global Terrestrial Sink Catchment (GTSC) Database Version 0.1", which contains extensive information about catchment area, such as elevation, whether or not it is in a terrestrial basin, lithology, temperature, water discharge, sediment load, tectonic setting and climate zone (Nyberg et al., 2018a). and "Watershed" (Nyberg et al., 2018b)

### 4.1.3 Hydrosheds

To determine the catchment areas for each river, the dataset for Hydrosheds and Water Flow Direction from WWF were used ("HydroSHEDS").

## 4.2 Temporal variability

### 4.2.1 Global analysis

The datasets Global Terrestrial Sink Catchment (GTSC) and "Global water occurrence" (Pekel et al., 2016) were used for the global analysis. Bodies of water were identified as river systems from the global water occurrence map were extracted based on two criteria. selecting those than have a length to width ratio greater than 10 and a minimum bounding box area Subsequently the GTSC was used to separate source and sink areas and classify regions by climate and tectonic setting.

### 4.2.2 Local analysis - generic workflow

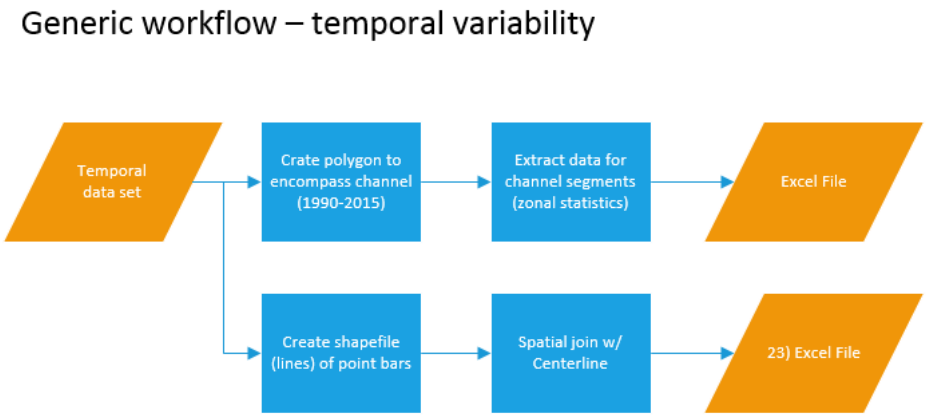


*Figure 4-1 Overview of the workflow used for mapping temporal chnges in the river systems*

Workflow for mapping temporal variability is shown in Figure 4-1. Data on temporal variability since 1990 was obtained from the dataset "Global water occurrence" (Pekel et al., 2016), was, downloaded via Google Earth Engine. This is a raster dataset, and shows which areas were covered by water every year from 1990 to 2015, as shown in Figure 4-2. To highlight total migration of the channel, all the values from the year 1990 to 2014 were classified as abandoned area, which signifies the total area the river has moved away from.

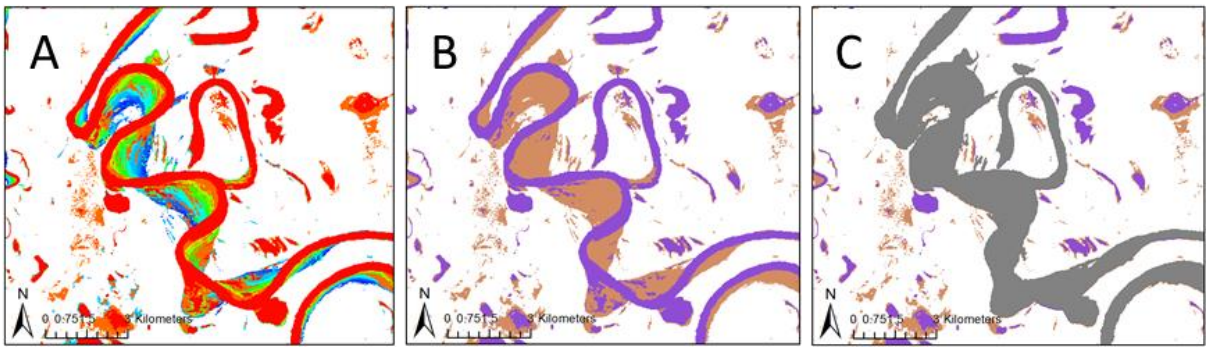


*Figure 4-2 Example from Mamorecillo: A) shows the temporal dataset with different colours for areas covered by water each year. Dark blue is 1984 and red is 2015. B) shows the reclassified data with 1984-2014 values as orange, and the current channel, 2015, as purple. C) shows the grey polygon created to extract raster values from the reclassified dataset in B).This polygon is split in segments, depending on the length of the river, on order to capture trends downstream.*

The values from 2015 were classified as the current channel. A polygon covering the channel was created and split in suitable sections, depending on the length of the river, to obtain enough sections to determine a trend in the data. The polygon was then used to extract values from the temporal data raster file, resulting in a table containing number of pixels from the two raster values for each year. The table was exported to Excel.

### 4.2.3 Point bar migration

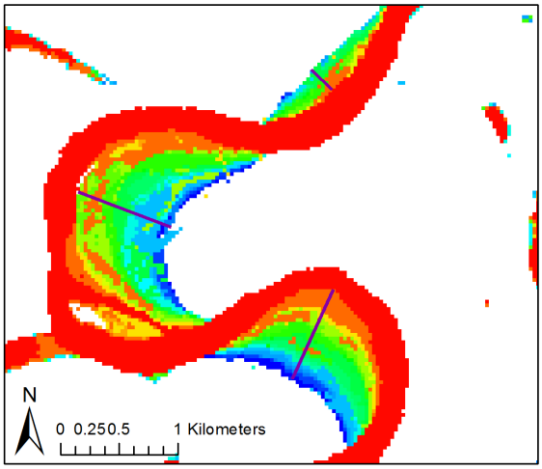


*Figure 4-3 Point bar migration between 1984 and 1990. Each year is represented by a different colour, from dark blue (1984) to red (2015)*

Annual point bar migration was calculated by manually digitising the difference between the edge of the channel in 1984 and 2015. This distance was then divided on number of years to obtain a yearly average.

## 4.3 Spatial variability – generic workflow

### 4.3.1 Channel

Tools have previously been developed to study the geomorphology and arrangement of sand bodies (e.g. Nyberg, Buckley, Howell, & Nanson, 2015)Nyberg et al., 2016?) but they have previously not been applied to answer the above questions.

The quantitative algorithms used have been developed by Nyberg, Buckley, Howell & Nanson (2015), and are available from (source). They can be installed and used as Tools in Esri's ArcGIS software. These were used in conjunction with standard ArcGIS tools, in a work process shown at high level in Figure 4-4 and detailed in Appendix A.

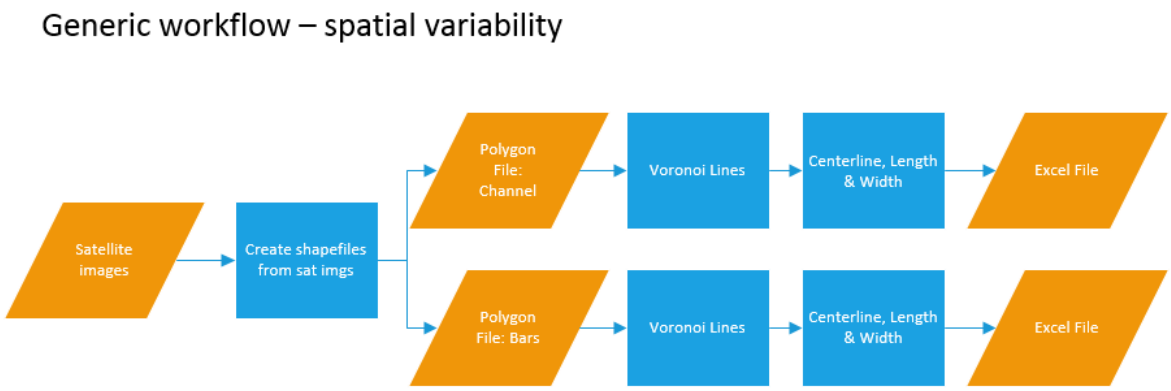


*Figure 4-4 Overview of the workflow used for mapping channels and current sandbars in the river systems*

Several false colour images captured by the Sentinel 2 satellite was imported from SentinelHub. Mostly false colour images consisting of the bands 8,3 and 4 and were chosen because the difference between water and surrounding vegetation shows up very clearly with this combination of bands. It was difficult to distinguish the sandbars from the sediment laden water in the false colour images for the Pilcomayo river, so instead moisture index (bands (B8A-B11)/(B8A+B11)) were used. To distinguish vegetated island from sandbars in the upper reach of the Ili/Bakanas river, NDVI images were used.

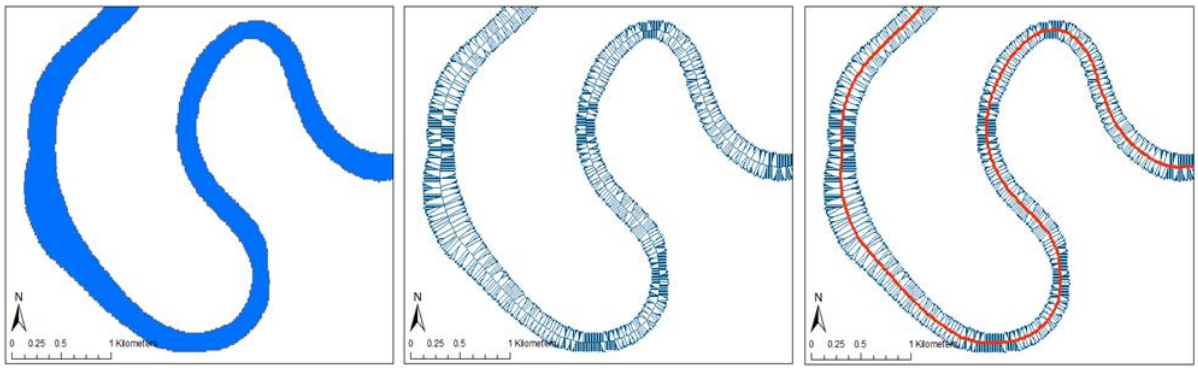

*Figure 4-5 Example of channel (left image), voronoi polylines at even distance along the channel (centre image) and calculated centreline (right image), from Koyukuk river*

Effort was made to find dates with a representative amount of water in the channel, and with no cloud cover. Dates with drought or flooding were avoided. All the images are from 2018.
As the rivers are such long features, it was necessary to import several images to obtain a sufficient resolution. These were mosaicked together to form one raster for further processing. The raster was projected to correct UTM zone, to ensure a correct visualisation of the image and enable further processing.
Some rivers, such as for example Koyukuk, have sections where the shortest path follows anabranched channels much narrower than the main channel. To avoid the centreline going through these unrepresentative channels, the voronoi lines were removed from these channels before the centreline was created, thus forcing it to go through the main channel.
For the floodplain surrounding the Burhi Dihing river in India, a number of paleo ox-bow lakes were digitised manually from a natural colour image.

**Calculated parameters for spatial variability**

Channel length is derived as the furthest distance along the centreline of each mapped river segment from apex to toe.
Aerial distance from apex to end of the mapped channel is obtained from the column “Near” in the table of attributes. This is the distance along the shortest path from apex to the last segment of the centreline.
A measurement for channel width at each centreline segment was plotted. In order to visualise the trend better, a running average of 500 points (sorted by distance from apex) was plotted on top of this. In addition, the average width for each 50km section (25km for the shorter rivers) was calculated and plotted in the same diagram.

### 4.3.2 Sandbar distribution

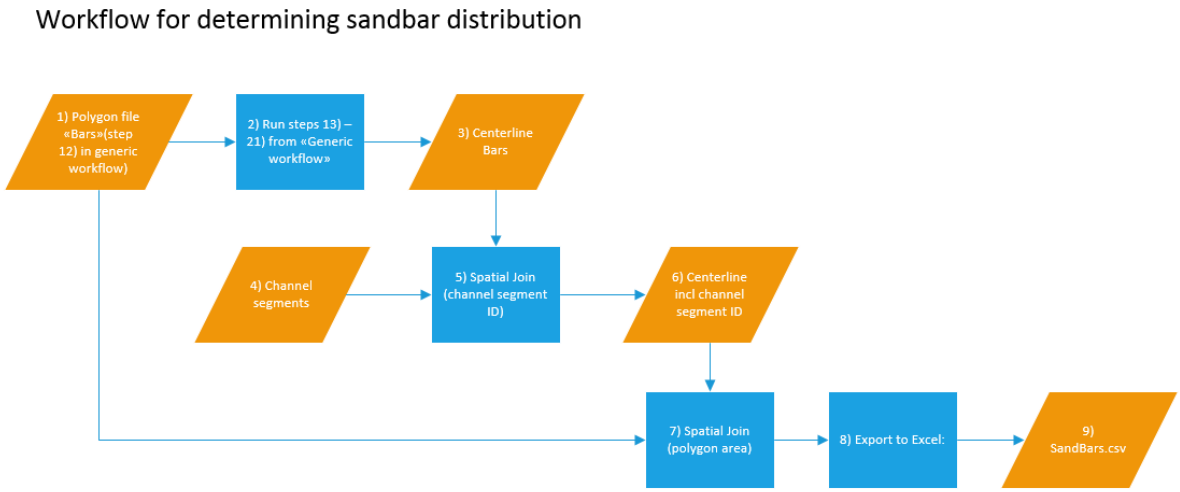


*Figure 4-6 Workflow for sandbar distribution*

## 4.4 Watersheds and discharge

Closely related to the climate is the rivers discharge, which is the volume of water that passes a point in the channel per time unit. It is typically expressed as m3s-1, and calculated by the equation Q=mdv, where m=channel width (m), d=channel depth (m) and v=velocity (ms-1) of the flow (Fryirs and Brierley, 2013). Syvitski Milliman (2007) proposed the following formula for calculating river discharge based on size of catchment area: Qw=kAm, where Qw = water discharge in m3s-1, k = 0,075 and m = 0.8.

This does not however, account for the different climate zones, and how they affect the rivers discharge. To address this, Eide et al (2017) developed differentiated values for k and m as shown in

This does not however, account for the different climate zones, and how they affect the rivers discharge. To address this, Eide et al (2017) developed differentiated values for k and m as shown in Table 4-1, depending on whether the climate is arid, semi-arid, humid or wet.

*Table 4-1 Climate zone affects the constants for calculating discharge (Eide et al. (2017))*

| Model | Class | Runoff (mm·yr$^{-1}$ km$^{-1}$) | $k$ | $m$ | $R^2$ |
|---|---|---|---|---|---|
| Eq. 1, fixed constants | All data | >0 | 0·075 | 0·8 | 0·50 |
| | All data, arid excluded | >100 | 0·075 | 0·8 | 0·74 |
| Proposed method: Eq. 1, constants vary by class | Arid | 0 to 100 | 0·0005 | 1·0633 | 0·72 |
| | Semi-arid | 100 to 250 | 0·0063 | 0·9824 | 0·98 |
| | Humid | 250 to 750 | 0·0161 | 0·9839 | 0·96 |
| | Wet | >750 | 0·0873 | 0·9164 | 0·99 |
| | All data | >0 | Varies | Varies | 0·90 |
| | All data, arid excluded | >100 | Varies | Varies | 0·95 |



The value of these constants considers a rivers runoff efficiency, which is commonly lower in drier catchments due to evapo-transpiration and infiltration, and higher in wetter climates due to water saturation in the soil. A rivers runoff is the rate of annual river discharge to catchment area, whereas runoff efficiency is the ratio of runoff to catchment averaged rainfall (Eide et al., 2018).

Qw is one of the values in the BQART method of determining a rivers sediment supply Qs. Qs can be calculated as Qs=ωBQw0.31 A0.5RT, where ω= , B (Syvitski and Milliman, 2007).

In order to determine the discharge in each river, the datasets Pour points were created at the river's apex. The global flow accumulation dataset was used to determine where to place the pour points, as the waterways are shown in a lighter colour. By exporting a suitable area and changing the display settings, it was possible to clearly see all influx routes of water and place pour points there. Thereafter, these pour points and the global flow direction dataset were used in the ArcGIS "Watershed" tool, to identify and calculate area of above lying land that drains into each pour point.

Constants for calculating $Q_w$ from Eide et al (2018) were used in the formula $Q_w=kA^m$:

| Class | Runoff (mm/yr/km$^2$) | K | m |
|---|---|---|---|
| Arid | 0-100 | 0.0005 | 1.0633 |
| Semi-arid | 100-250 | 0.0063 | 0.9824 |
| Humid | 250-750 | 0.0161 | 0.9839 |
| Wet | >750 | 0.0873 | 0.9164 |

Qs was calculated as $Q_s=\omega BQ_w^{0.31} A^{0.5}RT$ (Syvitski and Milliman, 2007) In this calculation Qw=0.075A0.8 was used.

# 5 Results

This section will summarize the results and observations from the global and regional studies. The eight regional studies are then examined in further detail for relationships between channel length, width, migration rate, point bar migration, gradient, catchment area, water discharge and sediment supply.

*Table 5-1 A short summary of findings, details given in the following sections of chapter 5.*

| | Fluvial systems | Channel migration, % | Rate of point bar migration (m/yr) | Length (km) 1) Channel 2) Aerial distance | Sinuosity (entire river; C/A) | Channel width (rate of change), m/km | Gradient (of mapped channel) | Catchment area (km3) | Discharge Qw ($km^3$/yr) | Sediment supply Qs (MT/yr) |
|---|---|---|---|---|---|---|---|---|---|---|
| 1 | Burhi Dihing, India | 78,44 | 11,35 | 1) 123,3 2) 70,5 | 1,76 | -3,1 | 1:1 231 | 3 071 | 4,32 | 0,36 |
| 2 | Okavango, Botswana | 45,56 | 1,82 | 1) 296,3 2) 140,9 | 2,10 | -0,6 | 1:5 220 | 234 548 | 37,49 | 5,32 |
| 3 | Taquari, Brazil | 42,24 | 6,18 | 1) 403,6 2) 257,3 | 1,57 | -0,8 | 1:2 293 | 28 153 | 32,91 | 1,08 |
| 4 | Pilcomayo, Argentina/ Paraguay | 42,08 | 25,12 | 1) 138,6 2) 84,1 | 1,65 | -2,6 | 1:2 008 | 85 838 | 13,96 | 10,77 |
| 5 | Ili, Kazakhstan | 39,34 | 6,09 | 1) 284,3 2) 195,9 | 1,45 | -1,6 | 1:3 693 | 94 323 | 39,83 | 15,51 |
| 6 | Uvs, Mongolia | 37,97 | 3,37 | 1) 253,4 2) 119,4 | 2,12 | -0,4 | 1:563 | 23 918 | 28,35 | 0,37 |
| 7 | Koyukuk, Alaska | 32,73 | 2,27 | 1) 596,9 2) 190,4 | 3,14 | -0,1 | 1:4 052 | 28 837 | 33,64 | 1,27 |
| 8 | Rio Mamorecillo, Bolivia | 3,96 | 31,51 | 1) 1 172,6 2) 535,6 | 2,19 | 0,4 | 1:6 541 | 11 183 | 14,12 | 0,33 |

## 5.1 Temporal changes - globally

### 5.1.1 Global channel migration

When analysing the global dataset of water distribution the last 30 years, it is clear that there has been as much as three times more lateral migration of the river channels located in the sedimentary basins, than of those in the source regions. Figure 5-1 show the difference from 11.44% in the source regions to 35.33% in the sinks. This is a difference of over 300%, or almost 24 percentage points.

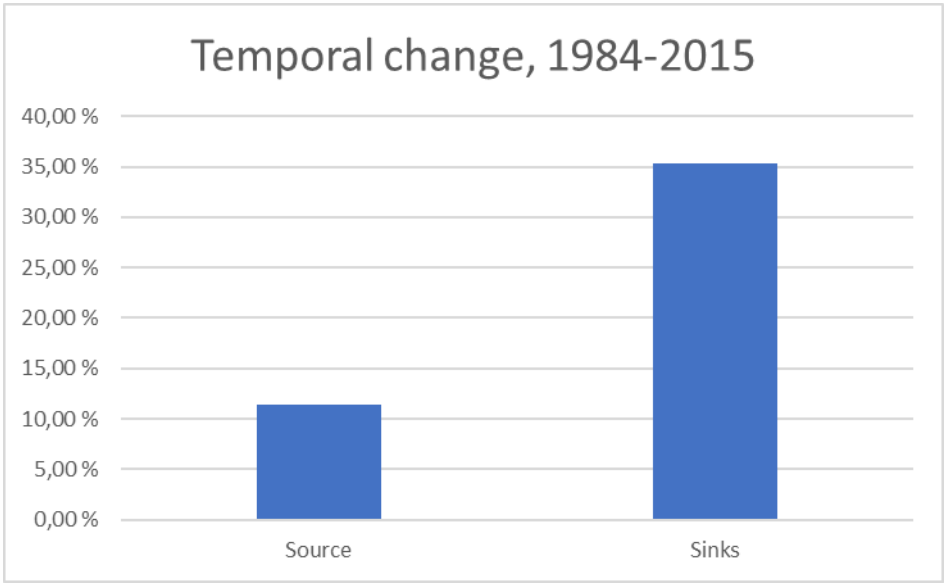


*Figure 5-1 The bars show how many percent of its current area the channel has migrated laterally between 1984 and 2015. In the source regions, the channel has only moved away from 11% of the area it covered 1984-2014, whereas in the sink areas, 35% of the area covered by water previously, is no longer part of the channel in 2015.*

### 5.1.2 Channel migration in different climates

When split into climate zones, it is apparent that the difference seen between source and sink is present in all climates, but not at the same magnitude, as shown in Figure 5-2.

The greatest level of change is found in sedimentary basins in the arid climate zone, followed by those in equatorial and warm temperate zones. These basins all have above 35% change from 1984 to 2015, with the most change found in the arid zone, at above 40%. The coldest environments in the polar and snowy climate zones, both have variability less than 25%.

The larges difference is seen in the warm temperate climate zone, where the difference is 21.07p.p. The equatorial climate zone has a similar figure of 18.71p.p difference, which shows that the two warmest climates have the largest variation in both source and sink.

The two coldest climate zones, snow and polar, have a difference of 15.97p.p. and 13.66p.p respectively, while the driest climate zone has least difference between source and sink.

The greatest change from source to sink occur in snowy climates, with an increase of almost 260%.

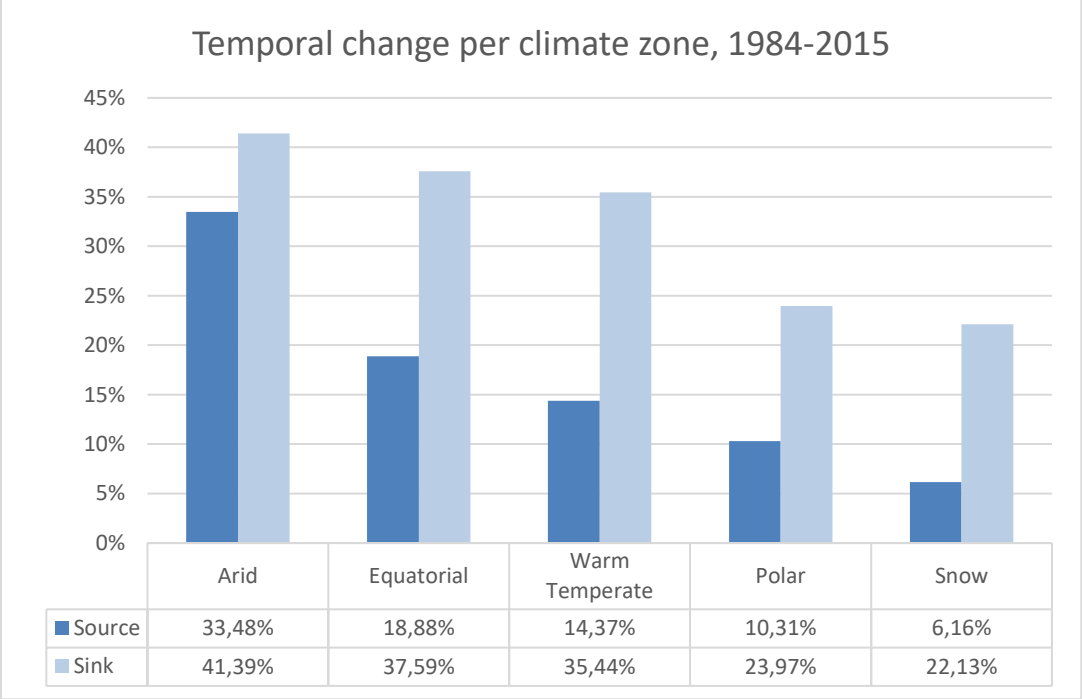


*Figure 5-2 All fluvial systems, both source and sink. Highest level of change is found in warm climates*

*Table 5-2 The different climate zones have different degree of change from source to sink regions*

| Climate zones | Source | Sink | P.p. increase | % increase |
|---|---|---|---|---|
| Arid | 33.48 % | 41.39 % | 7.91 | 23.63 % |
| Equatorial | 18.88 % | 37.59 % | 18.71 | 99.10 % |
| Warm Temperate | 14.37 % | 35.44 % | 21.07 | 146.62 % |
| Polar | 10.31 % | 23.97 % | 13.66 | 132.49 % |
| Snow | 6.16 % | 22.13 % | 15.97 | 259.25 % |

### 5.1.3 Channel migration in different tectonic settings

The greatest change is found in intracratonic basins, with 43.15 change. These systems also have the greatest increase, of almost 400% from source to sink, as they have the lowest change rate in the

sink areas of all the settings. Foreland basins also have a high rate of change, at 35.5%, while strike-slip, fore-arc and passive margin settings are consecutively lower. At the other end of the scale, extensional regimes have the opposite behaviour, where the change is 33.30% less in the basin than in the source region.

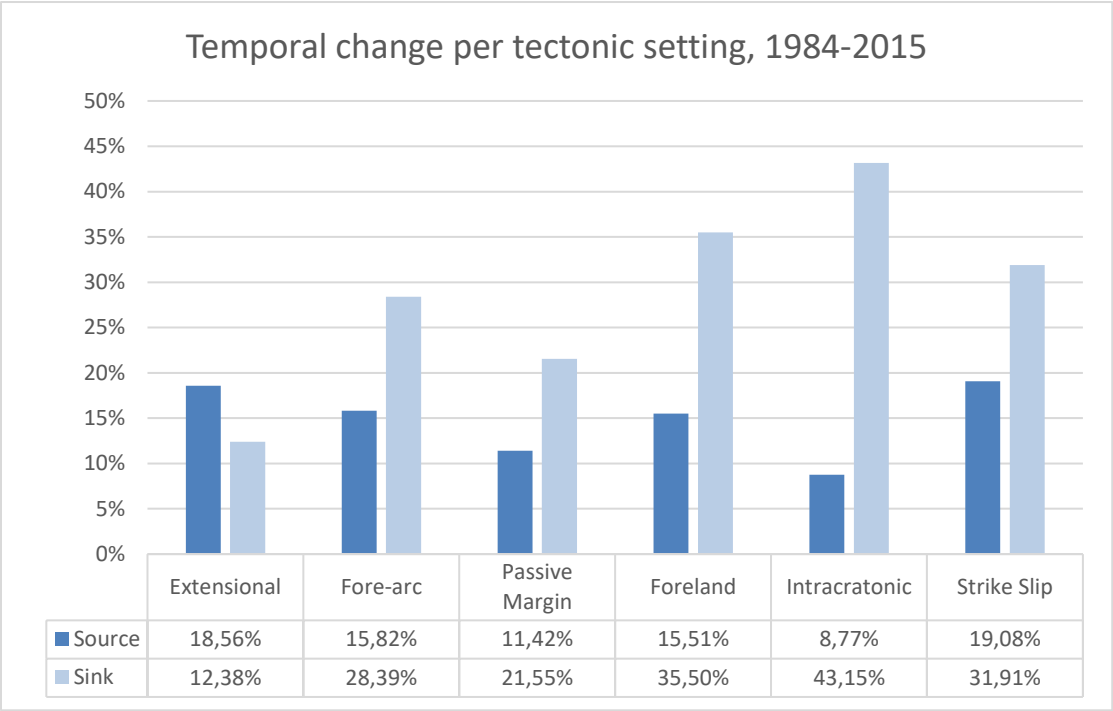


*Figure 5-3 Differences in variability between the different tectonic settings.*

*Table 5-3 Difference in change between the tectonic settings*

| Tectonic settings | Source | Sink | P.p. increase | % increase |
|---|---|---|---|---|
| Extensional | 18.56 % | 12.38 % | -6.18 % | -33.30 % |
| Fore-arc | 15.82 % | 28.39 % | 12.57 % | 79.46 % |
| Passive Margin | 11.42 % | 21.55 % | 10.13 % | 88.70 % |
| Foreland | 15.51 % | 35.50 % | 19.99 % | 128.88 % |
| Intracratonic | 8.77 % | 43.15 % | 34.38 % | 392.02 % |
| Strike Slip | 19.08 % | 31.91 % | 12.83 % | 67.24 % |

When looking at the climate zones and tectonic settings combined, the changes range from 5% in intracratonic snowy source environments, to 72% in arid fore-arc basins. If the arid systems are excluded, the highest level of change (44%) occur in equatorial intracratonic settings.

| SOURCE | Extensional | Fore-Arc | Foreland | Intra-cratonic | Passive Margin | Strike-Slip | All |
|---|---|---|---|---|---|---|---|
| Arid | 21 % | 11 % | 34 % | 40 % | 31 % | 20 % | **33 %** |
| Equatorial | 19 % | 34 % | 25 % | 18 % | 17 % | 25 % | **19 %** |
| Polar | 31 % | 19 % | 19 % | 6 % | 15 % | 23 % | **10 %** |
| Snow | 18 % | 6 % | 9 % | 5 % | 6 % | 26 % | **6 %** |
| Warm Temperate | 15 % | 14 % | 16 % | 14 % | 13 % | 11 % | **14 %** |
| All | **19 %** | **16 %** | **16 %** | **9 %** | **11 %** | **19 %** | |

| SINKS/BASINS | Extensional | Fore-Arc | Foreland | Intra-cratonic | Passive Margin | Strike-Slip | All |
|---|---|---|---|---|---|---|---|
| Arid | 7 % | 72 % | 35 % | 56 % | 28 % | 36 % | **41 %** |
| Equatorial | 22 % | 31 % | 38 % | 44 % | 27 % | 12 % | **38 %** |
| Polar | 20 % | 41 % | 24 % | | 25 % | 19 % | **24 %** |
| Snow | 16 % | 6 % | 29 % | 15 % | 6 % | 29 % | **22 %** |
| Warm Temperate | 27 % | 11 % | 38 % | 34 % | 26 % | 34 % | **35 %** |
| All | **12 %** | **28 %** | **22 %** | **35 %** | **43 %** | **32 %** | |

## 5.2 Local rate of change – temporal variability

Table 5-4 Study areas in tectonic and climatic settings (Table 5-4) below shows where the chosen study areas are placed in climatic and tectonic settings. Five are located in foreland basins, two in intracratonic, and one in an extensional basin. None are in fore-arc, passive margin, or strike-slip settings. Taquari is near the East African Rift zone, which influence the fan (down-fault almost perpendicular to the channel, which separates the upper from the middle and lower parts of the fan). Koyukuk is placed in an extensional setting, but is near a strike-slip zone, and may be influenced by this.

Taquari is placed in the equatorial zone according to the "Global Terrestrial Sink Catchment" dataset, despite megafans being untypical for this climate (Leier 2005), as they require discharge fluctuations to form. Taquari may therefore be on the border between these climate zones and display influence from both.

*Table 5-4 Study areas in tectonic and climatic settings*

| | Extensional | Fore-arc | Foreland | Intracratonic | Passive Margin | Strike-Slip |
|---|---|---|---|---|---|---|
| **Arid** | | | Ili/Bakanas | Okavango (33%) | | |
| **Equatorial** | | | Mamorecillo | Taquari (46%) | | |
| **Polar** | | | | | | |
| **Snow** | Koyukuk | | Uvs | | | |
| **Warm Temperate** | | | Burhi Dihing, Pilcomayo | | | |

### 5.2.1 Channel migration

By far the river with the largest amount of change is the Pilcomayo. At 78% it has changed nearly twice as much as the next six rivers, which all have a similar rate of change, around 40%. At the lower end is Okavango at 33%, and Koyukuk with only 4 (Figure 5-4). The rivers in equatorial and warm temperate climate all have changed more than 40%, while the ones in arid or snowy climates all have changed less than 40%, but between the six middle rivers, the difference is not much.

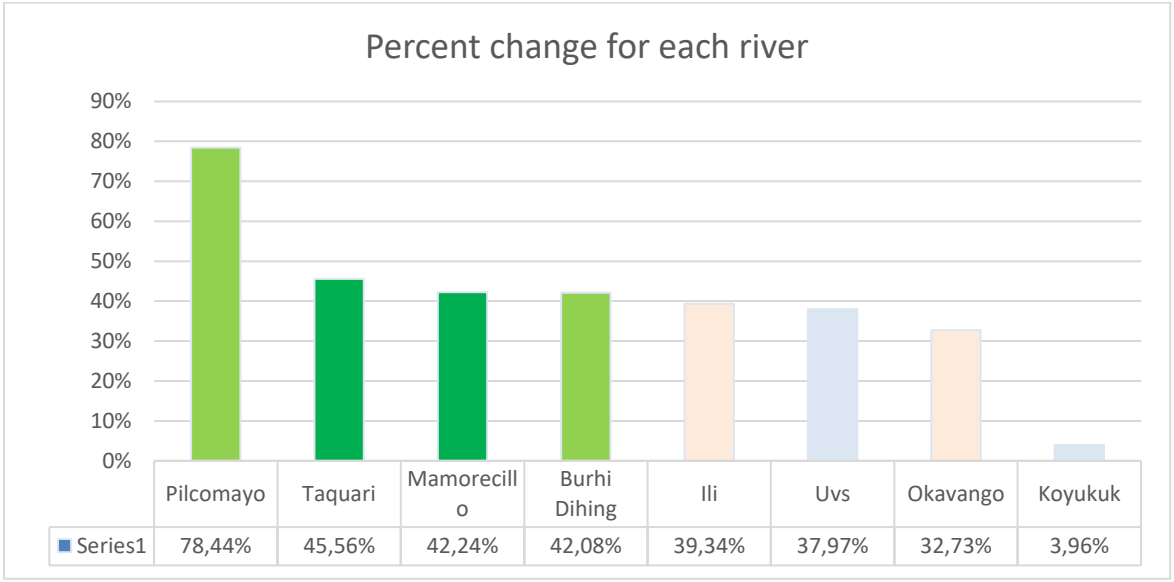


*Figure 5-4 Findings for channel migration show that the change is greatest in the warm and humid climates.*

Equatorial

Warm Temperate

Arid

Snow

Figure 5-5Figure 5-5 shows the amount of change in each river segment, as a percentage of the area occupied by the channel in 2015 in that same segment. This gives a view of where the river has changed the most, in relation to distance from apex. When looking at each river in segments, no clear, common trend is apparent. For Burhi Dihing and Okavango there is a slight upwards trend, showing change increasing with distance from apex. Taquari first shows a rapid decrease in change, followed by an equally rapid increase, with the smallest amount of change appearing in the middle at 100 km from apex. The Pilcomayo and Koyukuk has an even level of change, only slightly increasing downstream. Ili has a slight upward trend for the first 140km, after which it rapidly declines, while Uvs has two sections of increasing change, separated by a rapid decline after 60km.

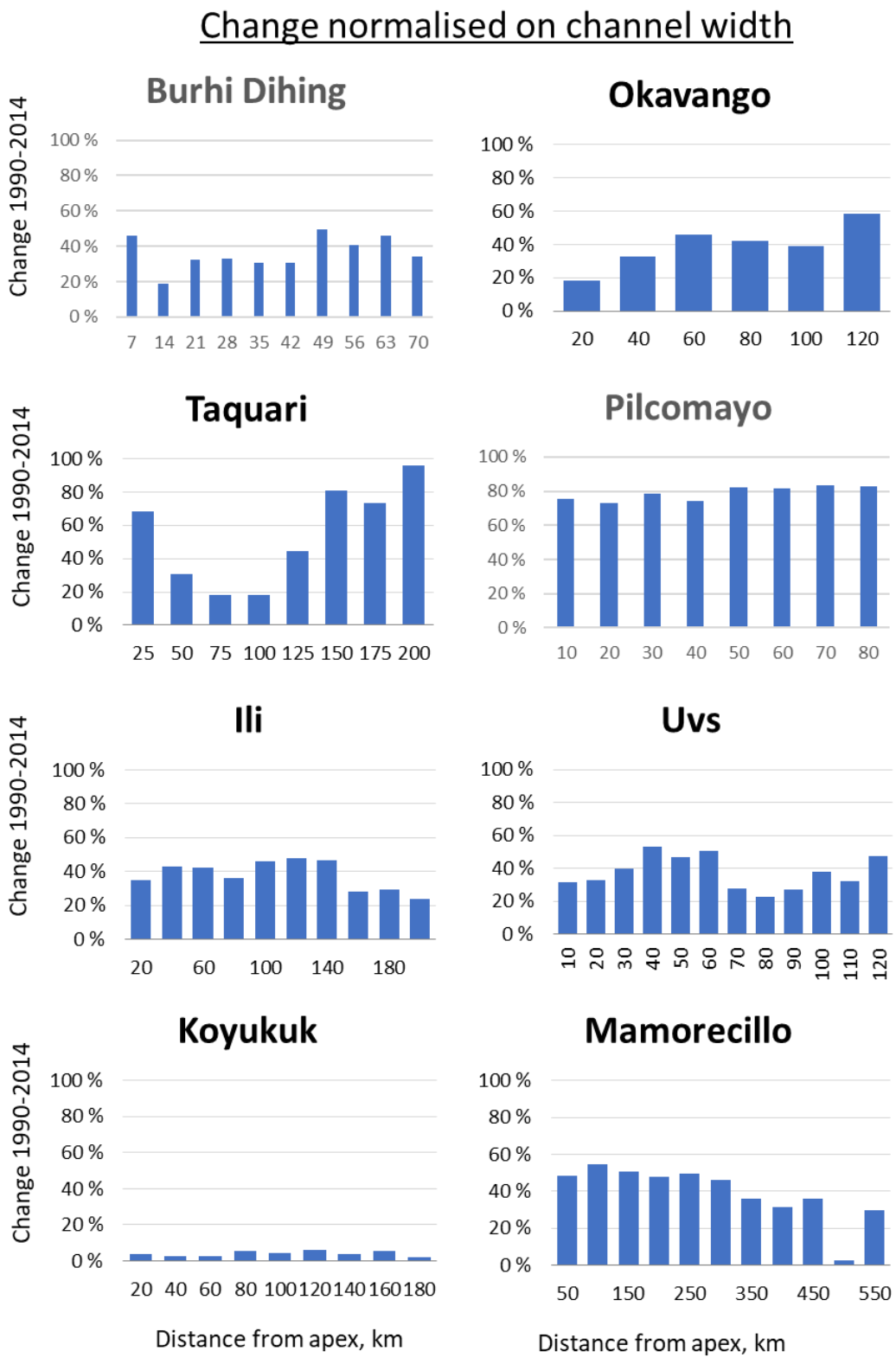


*Figure 5-5 Rivers do not display a strong, common trend in how change varies along the channel*

When looking at the total area of change downstream, several of the systems display a reducing trend. This is most clear in Ili, but can also be seen in in Okavango, Taquari, Pilcomayo, Uvs and Mamorecillo. On the contrary, Burhi Dihing and Koyukuk has an increasing trend.

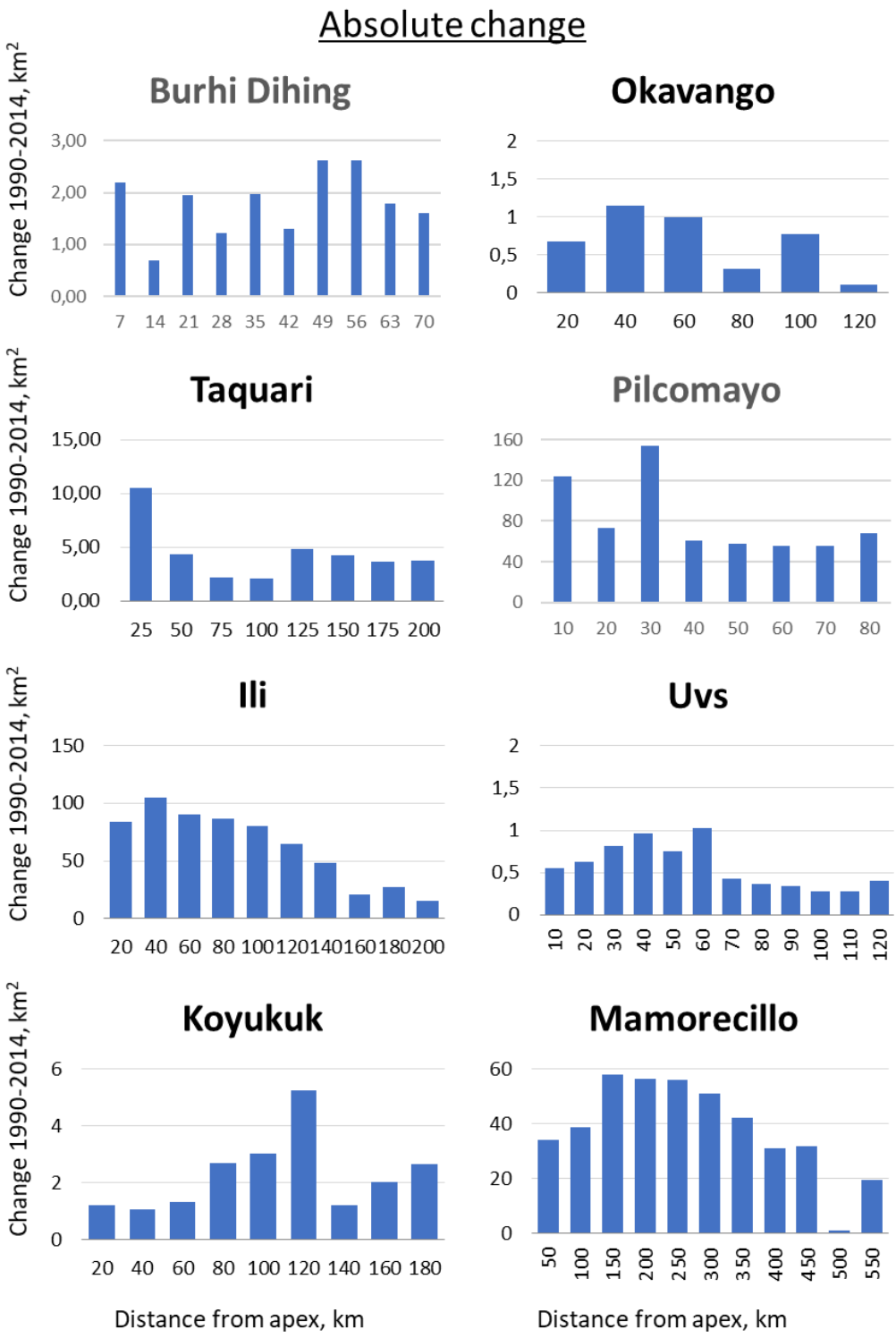


*Figure 5-6 Shows the absolute change in each river segment*

### 5.2.2 Point bar migration

Four of the eight rivers show an increasing trend, where the pointbars grow faster downstream than closer to the apex. Two rivers, Uvs and Koyukuk, have an almost flat rate of change, and two show a declining rate. Thus, no clear common trend can be observed.

Burhi Dihing is alone in showing a clear increasing trend, with an R2 value of over 0.8. For the others, the variability is much more, and the R2 values all below 0,4. Okavango lacks data after approximately 100 km, where the river exits the panhandle and spreads out, the temporal dataset shows very little data, and it cannot be interpreted any further. For this section, higher resolution images would be required.

Burhi Dihing, Pilcomayo and Ili have much fewer pointbars than the others.

The point bars in Taquari migrate at an even rate for the first 120km, after which the migration rate appears to increase markedly, and also the difference between each sandbar becomes larger. The change occurs at the point of an ongoing avulsion.

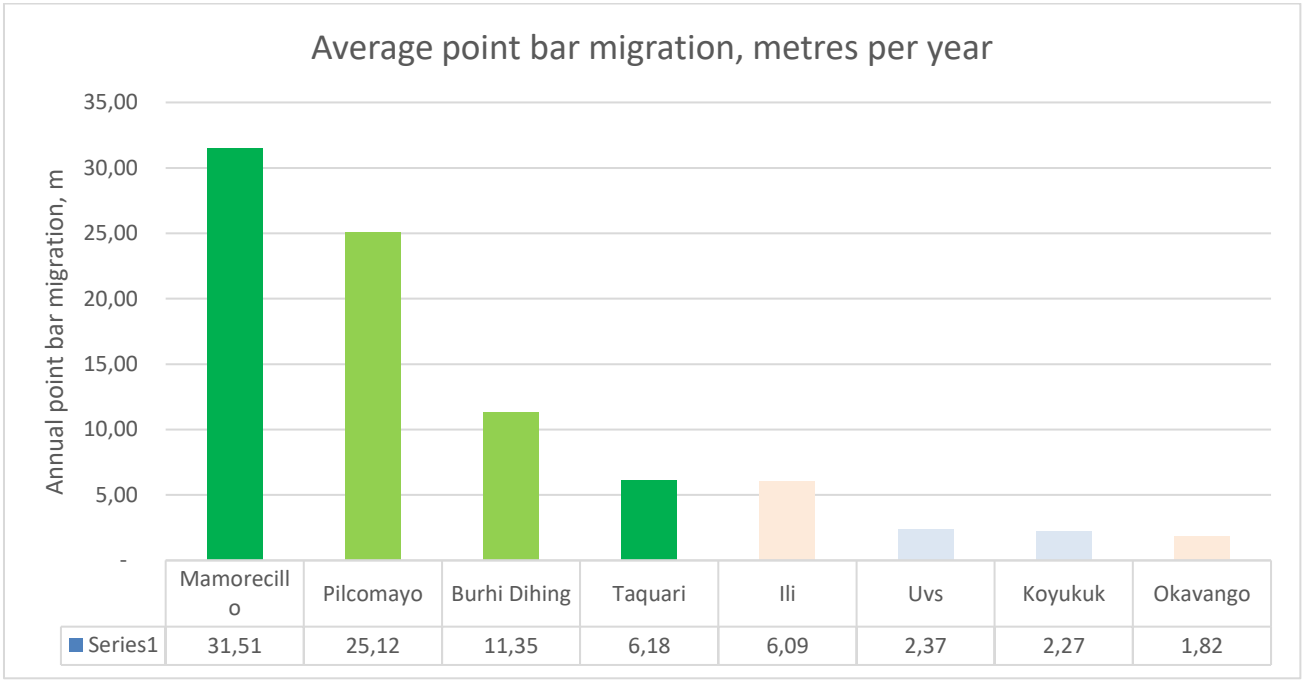


*Figure 5-7 Average point bar migration show clearly that systems in warmer and more humid climates migrate faster than those in colder and drier climates*

Equatorial
Warm Temperate
Arid
Snow

When looking along each river, there are no clear trends as to how the sandbars are distributed. Some of the rivers show that sandbars grow faster further from the apex, but not all. Okavango and

Mamorecillo show a slight decline downstream, whereas Uvs and Koyukuk have a nearly even growth along the whole channel.

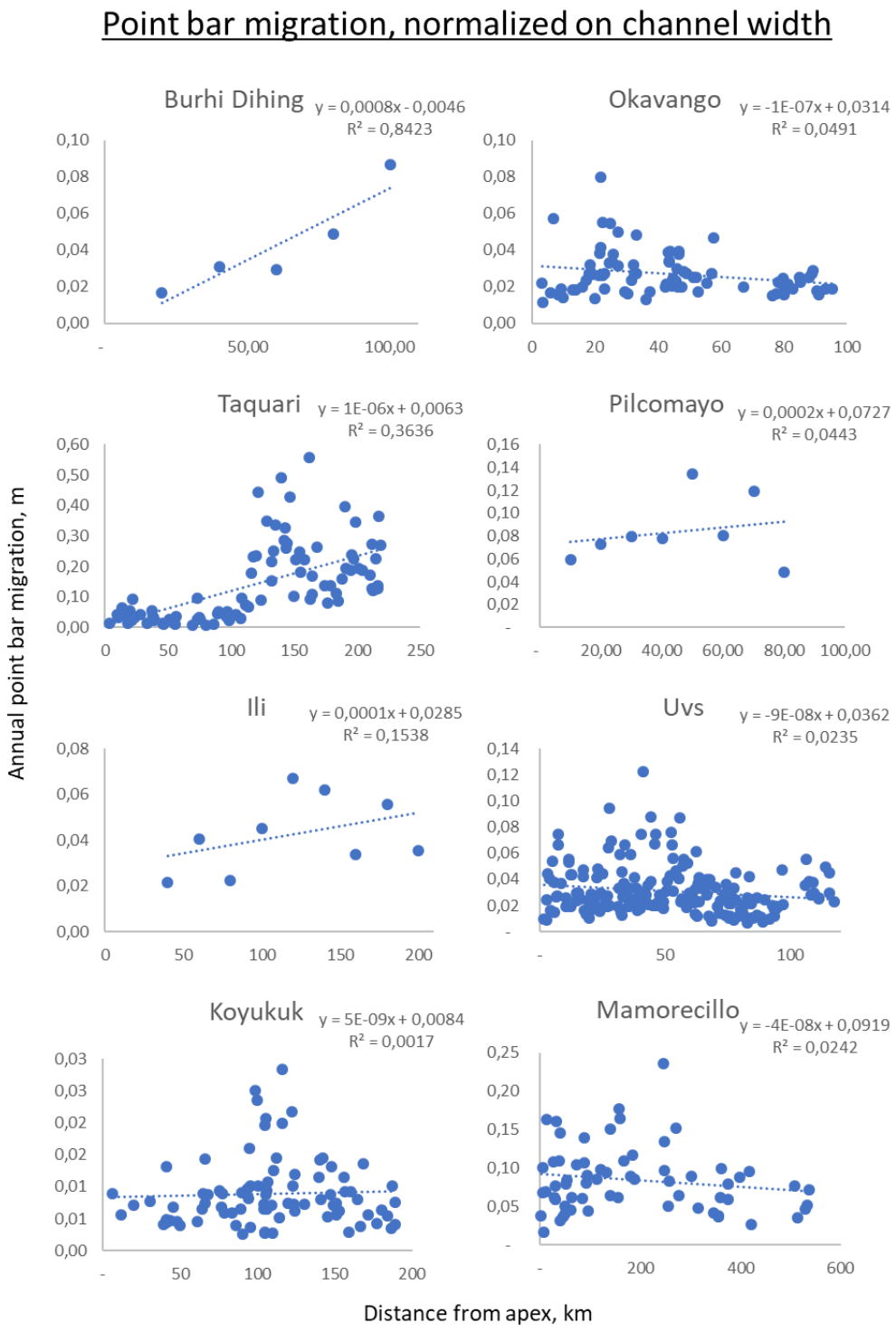


*Figure 5-8 The rate of point bar migration downstream shows great variability and no common clear trends when adjusted for channel width.*

## 5.3 Spatial variability

### 5.3.1 Source to sink - Catchment areas and sedimentary basins

Identified catchment areas:

| | |
|---|---|
| Burhi Dhing: 3 071 km$^3$ | Okavango: 234 548 km$^3$ |
| 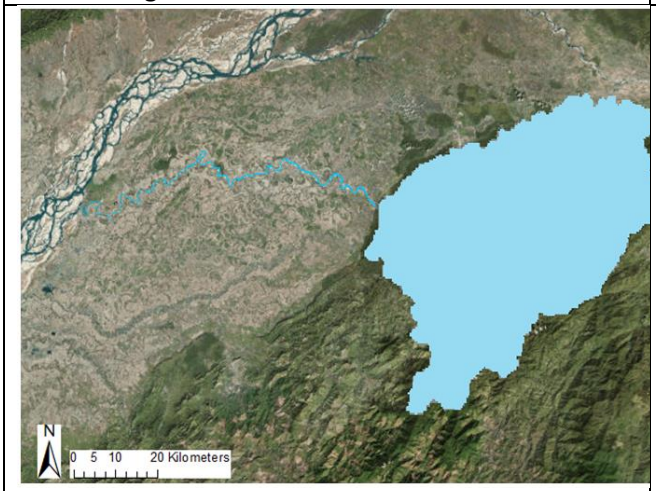 |  |
| Taquari: 28 153 km$^3$ | Pilcomayo: 85 838 km$^3$ |
| 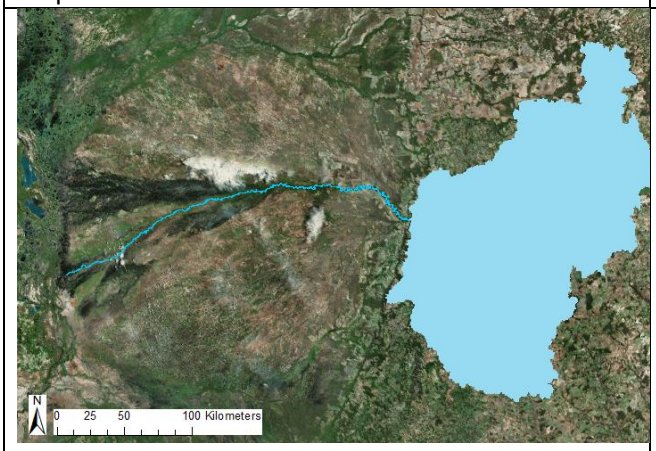 | 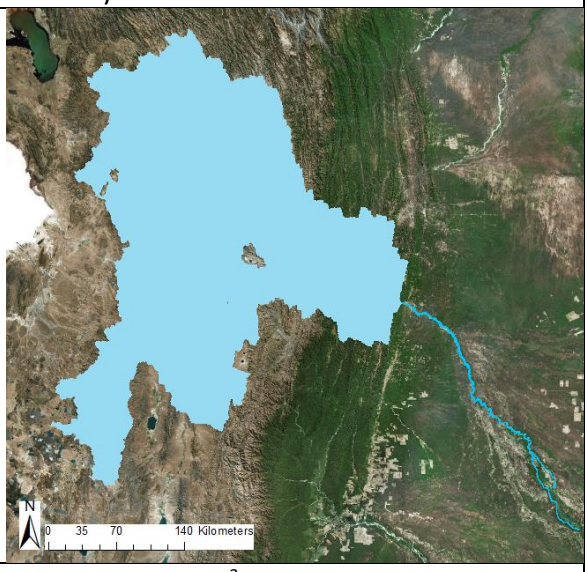 |
| Ili: 94 323 km$^3$ | Uvs: 23 918 km$^3$ |

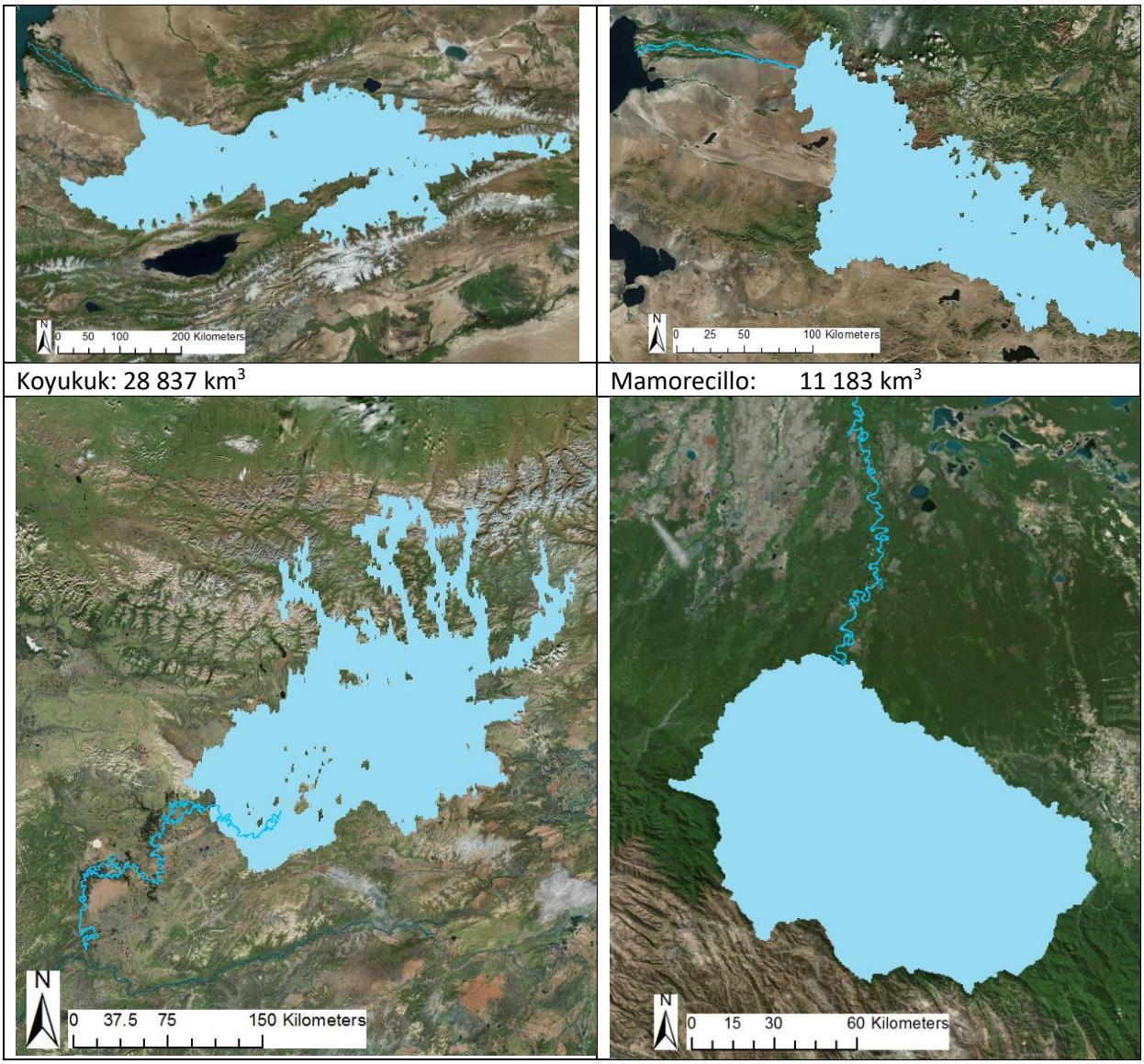


*Table 5-5 Calculated catchment areas. Note that catchment area for all rivers, including Mamorecillo is calculated at apex.*

### 5.3.2 Channel slope

*Table 5-6 Calculated channel slope for all rivers, based on the entire channel.*

| | Apex, m.a.s.l | End of channel, m.a.s.l | Diff, m | Aerial distance, m | Change in elevation, m/m | Gradient |
|---|---|---|---|---|---|---|
| Burhi Dihing | 156 | 99 | 57 | 70173 | 0,000812 | 1:1 231 |
| Okavango | 997 | 970 | 27 | 140948 | 0,000192 | 1:5 220 |
| Taquari | 202 | 90 | 112 | 256784 | 0,000436 | 1:2 293 |
| Pilcomayo | 273 | 231 | 42 | 84341 | 0,000498 | 1:2 008 |
| Ili | 394 | 341 | 53 | 195737 | 0,000271 | 1:3 693 |

| | | | | | | |
|---|---|---|---|---|---|---|
| Uvs | 971 | 760 | 211 | 118948 | 0,001774 | 1:563 |
| Koyukuk | 83 | 36 | 47 | 190422 | 0,000247 | 1:4 052 |
| Mamorecillo | 211 | 132 | 79 | 516710 | 0,000153 | 1:6 541 |

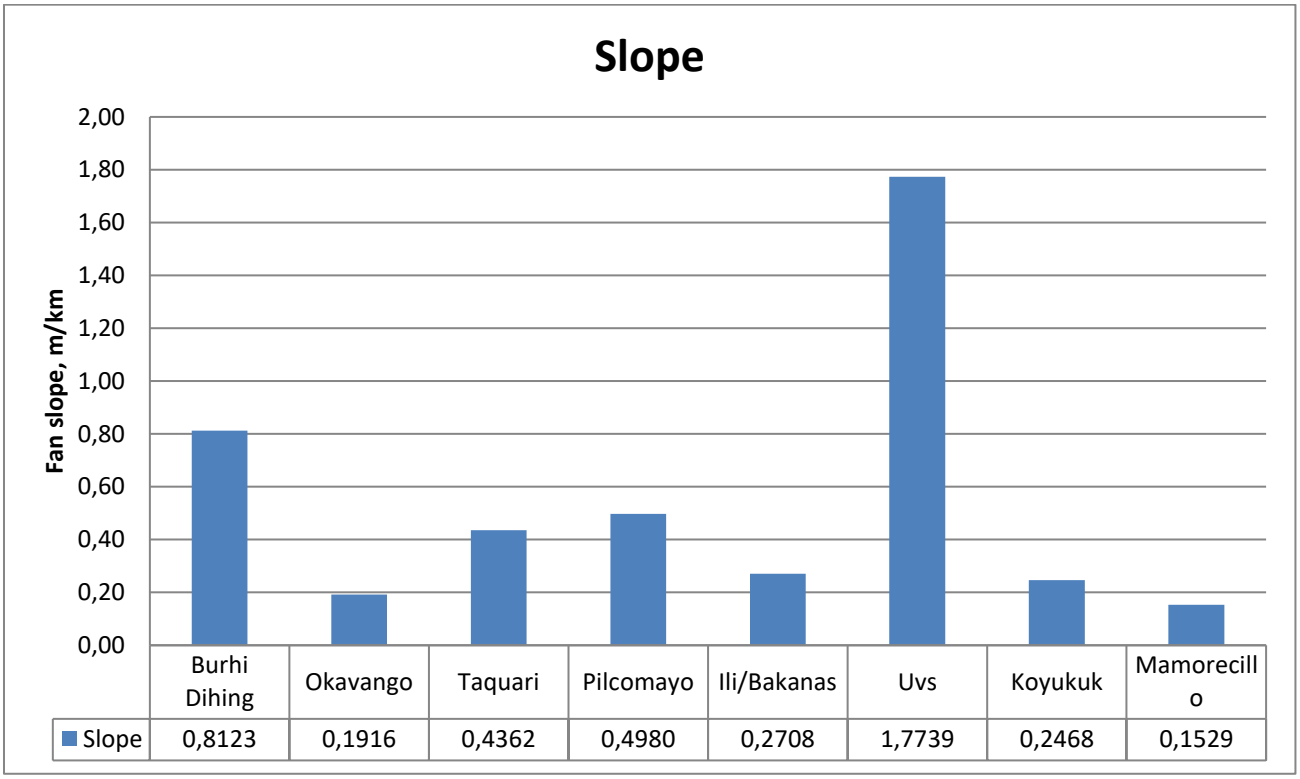


*Figure 5-9 Calculations of slope for all systems show similar gradient, except Uvs which is more than twice as steep as any of the others.*

The Uvs fan has by far the steepest gradient at 1:565, which is twice that of the Burhi Dihing which is second at 1:1 235.

### 5.3.3 Sinuosity

Burhi Dihing, Taquari, Pilcomayo and Ili can be classified as sinuous/meandering, with a sinuosity below 1.8, while Okavango, Uvs, Koyukuk and Mamorecillo are tortuous and show a sinuosity above 2 (Fryirs and Brierley, 2013).

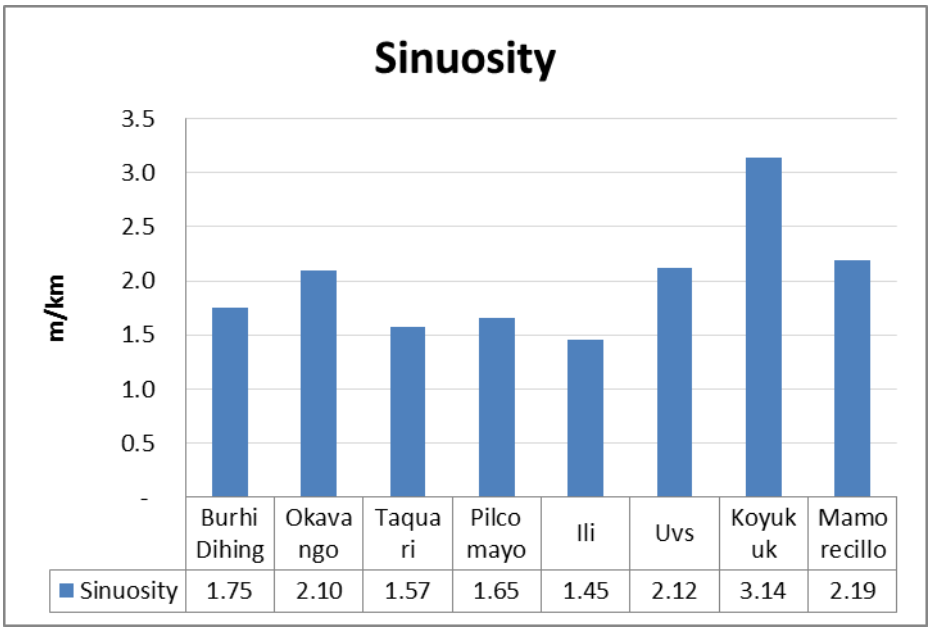


*Figure 5-10 Sinuosity for each river, calculated as channel length divided by aerial distance from apex to end of channel.*

### 5.3.4 Channel width

The Burhi Dihing is the river with the fastest reducing channel width, at a rate of just above 3m per km. When it first enters the basin, the variability in channel width is high, before it drops markedly at approximately 50km from apex.

Okavango shows a steady decline in channel width downstream, before reaching a plateau between 60 and 80km, after which it increases again for the next 20km. This coincides with where the channel anabranches into two channels before re-merging into one.

The Koyukuk also has two sections where the channel anabranches, shown as less channel width and less variability at 80km and 150km.

Mamorecillo differs from the other systems, in that it receives influx from tributaries after it enters the basin. In this chapter, the analysis is carried out on the entire channel, from it enters the basin, until it joins the larger Madeira river. The largest individual tributary along the basin is the Rio Grande, which joins the main channel 105 km from apex. This gives an additional catchment area of 95 164km$^2$. Towards the end, Mamorecillo has a sudden reduction in channel width.

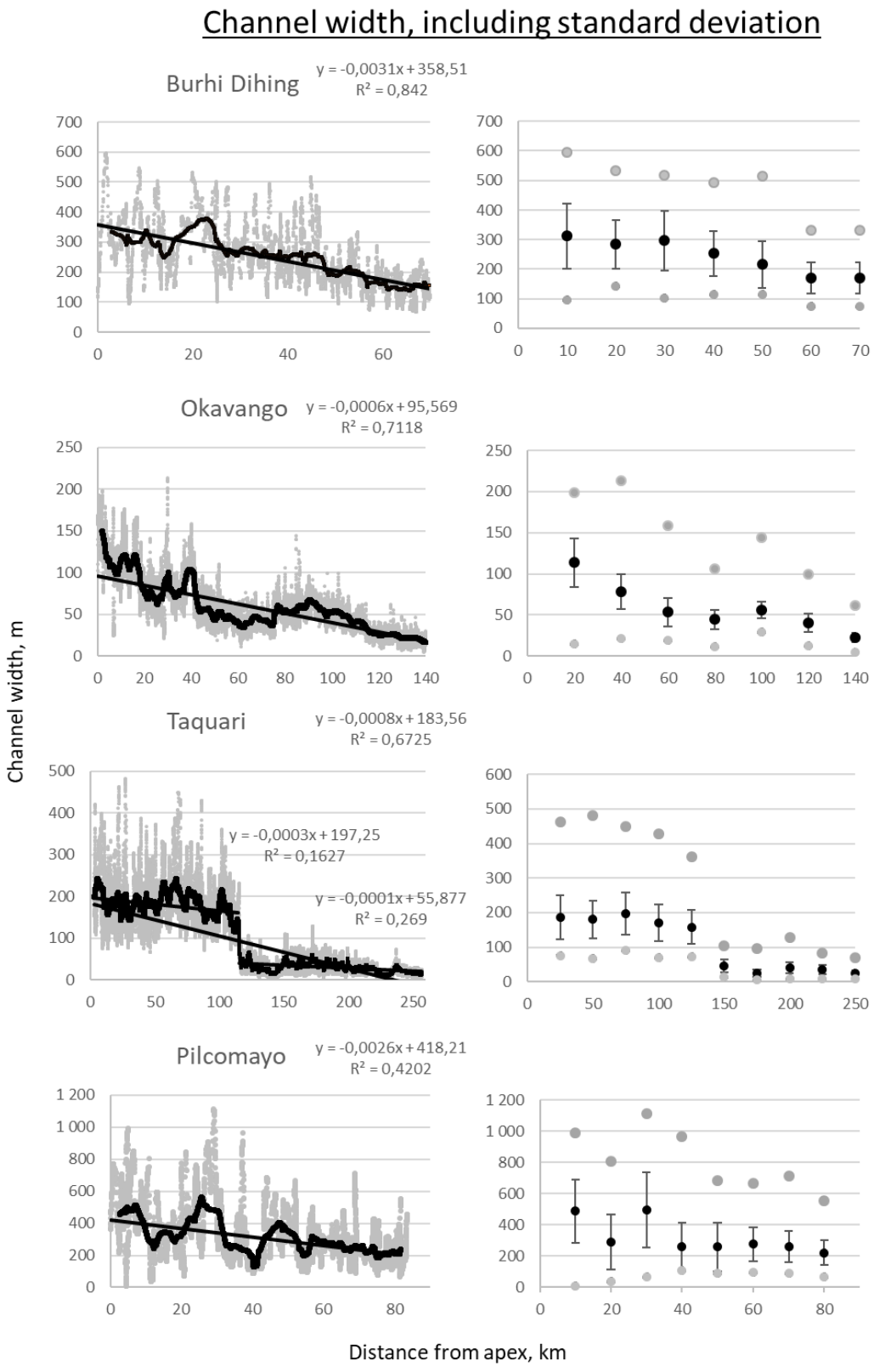
Channel width, including standard deviation
Burhi Dihing
y = -0,0031x + 358,51
R² = 0,842
Okavango
y = -0,0006x + 95,569
R² = 0,7118
Taquari
y = -0,0008x + 183,56
R² = 0,6725
y = -0,0003x + 197,25
R² = 0,1627
y = -0,0001x + 55,877
R² = 0,269
Pilcomayo
y = -0,0026x + 418,21
R² = 0,4202
Channel width, m
Distance from apex, km

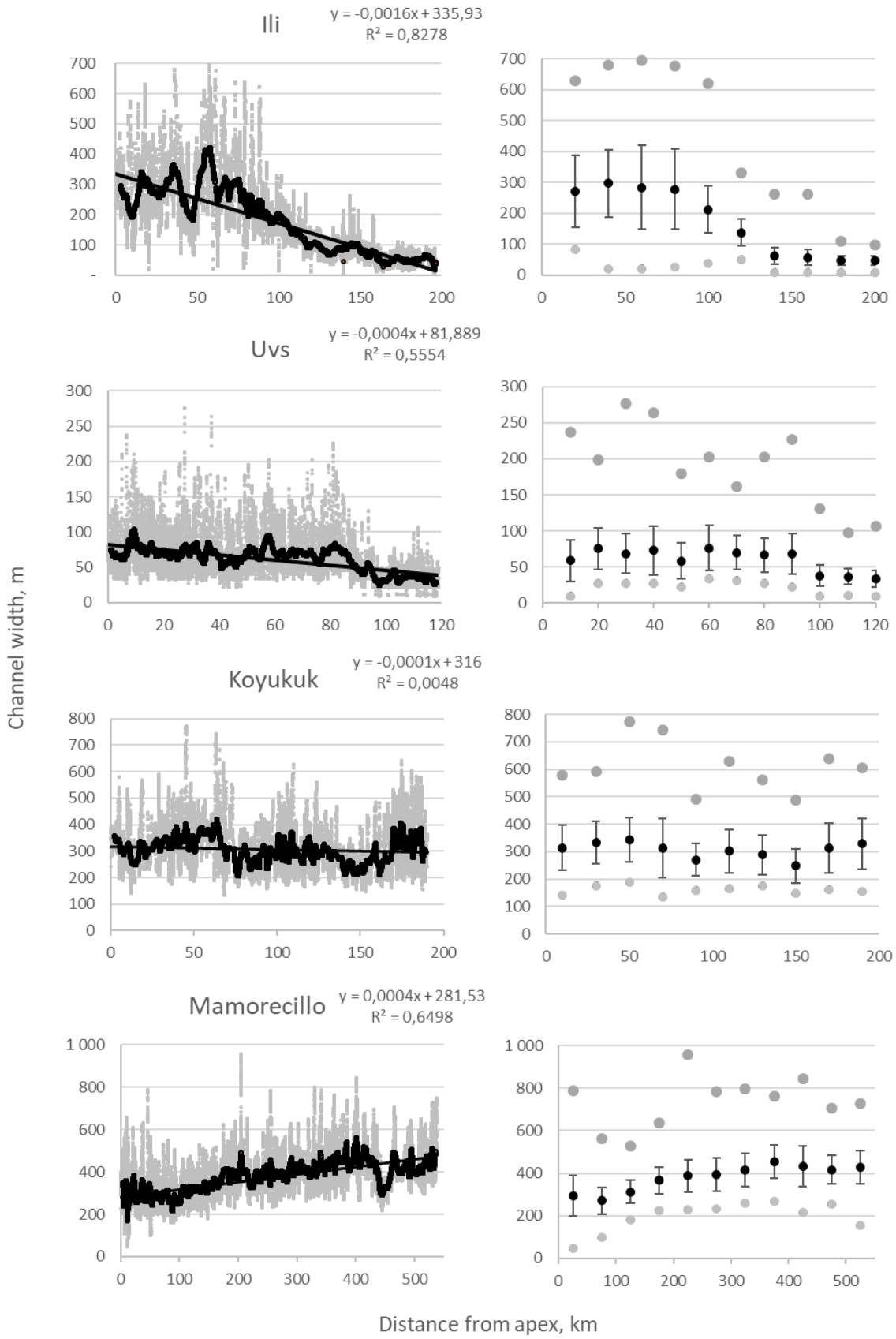


*Figure 5-11 Six of the eight systems analysed show a declining trend in channel width in relation to distance from apex. The graphs to the left show all measuring points, while the plots on the right include standard deviation around the mean for each section of river*

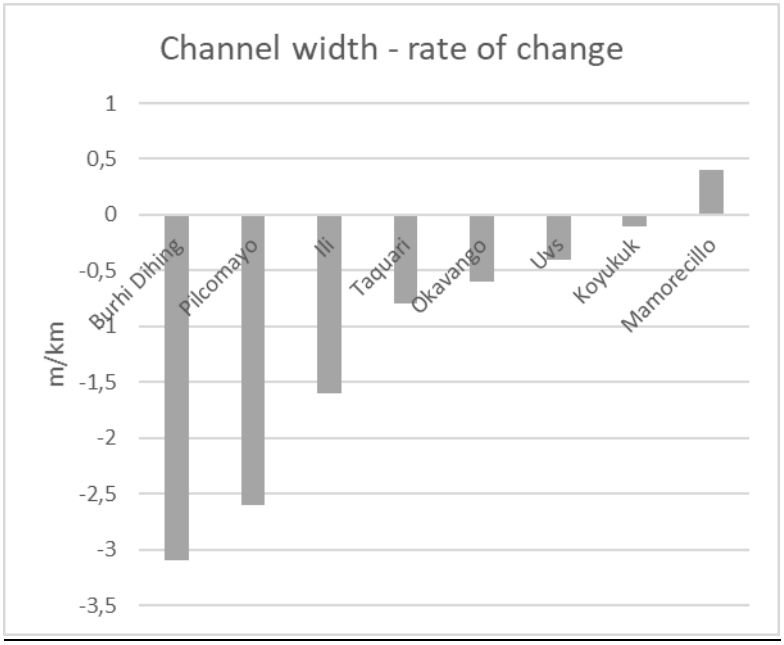


*Figure 5-12 The rate at which the channel gets narrower varies from over three metres reduction in Burhi Dihing, to almost 0,5 m increase per km in Mamorecillo*

### 5.3.5 Sandbar distribution

Most of the systems show a decline in total area of sandbars downstream. For Okavango, no sandbars were visible in the satellite images. Mamorecillo shows an increasing trend, with more sandbars further from apex. Pilcomayo and Ili show a sudden decline in sandbars along the channel, but whereas Pilcomayo has most sandbars 30km from the apex, Ili has most 80km downstream. Uvs also has most sandbars at 30km from apex, but this system shows a gradual decline from then on, not sudden like the Pilcomayo and Ili. Burhi Dihing shows a varying trend in sandbar area, with peaks at 14,28 and 49 km from apex, before it becomes markedly less for the last km of the channel. For both Ili and Taquari, no sandbars are visible in the satellite resolution for the last sections of the channel Figure 5-13.

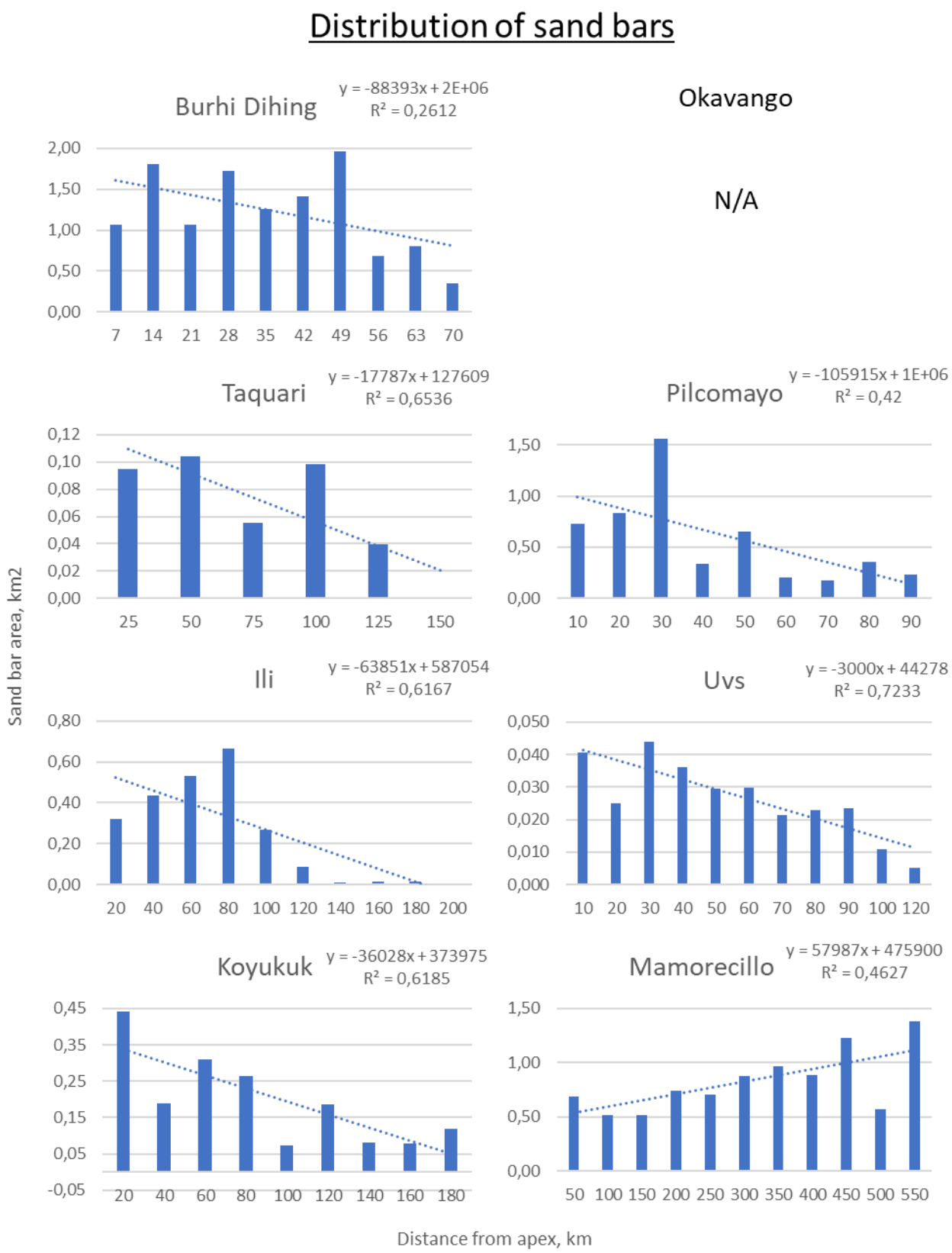


*Figure 5-13 Sandbar distribution down-stream show the same trend as channel width for most of the systems. Okavango has no visible unvegetated sandbars in the satellite images.*

*Table 5-7 Rate of change from apex to end of channel for each of the systems*

| River | Rate of change, $km^2/km$ |
|---|---|
| Burhi Dihing | -0,088 |
| Taquari | -0,018 |
| Pilcomayo | -0,106 |
| Ili | -0,064 |
| Uvs | -0,003 |
| Koyukuk | -0,036 |
| Mamorecillo | 0,058 |

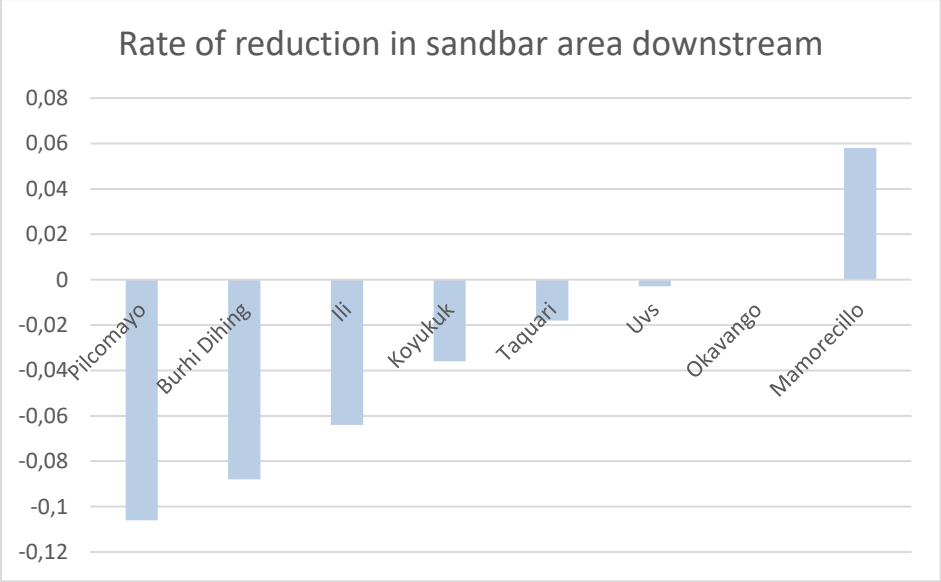


### 5.3.6 Discharge

The categories in Eide et al. (2018) classification is not 1:1 with the climate zones from the global datasets used. On this scale, based on annual run-off, both Okavango and Ili were classified as humid, although otherwise classified as being in arid climates.

*Table 5-8 * Based on precipitation, classified according to Eide et al (2018)*

| River system | Catchment, $km^2$ | Precipitation, $mm/yr/km^2$ | Class* | $Q_{w,(Eide)}$ ($km^3/yr$) | Climate |
|---|---|---|---|---|---|
| Burhi Dihing | 3 071 | 1 563 | Wet | 4,32 | Warm Temp |
| Okavango | 234 548 | 656 | Humid | 37,49 | Arid |
| Taquari | 28 153 | 1 477 | Wet | 32,91 | Equatorial |
| Pilcomayo | 85 838 | 1 477 | Humid | 13,96 | Warm Temp |
| Ili | 94 323 | 474 | Humid | 39,83 | Arid |
| Uvs | 23 918 | 933 | Wet | 28,35 | Snow |
| Koyukuk | 28 836 | 850 | Wet | 33,64 | Snow |
| Mamorecillo | 15487 | 2 542 | Wet | 14,12 | Equatorial |

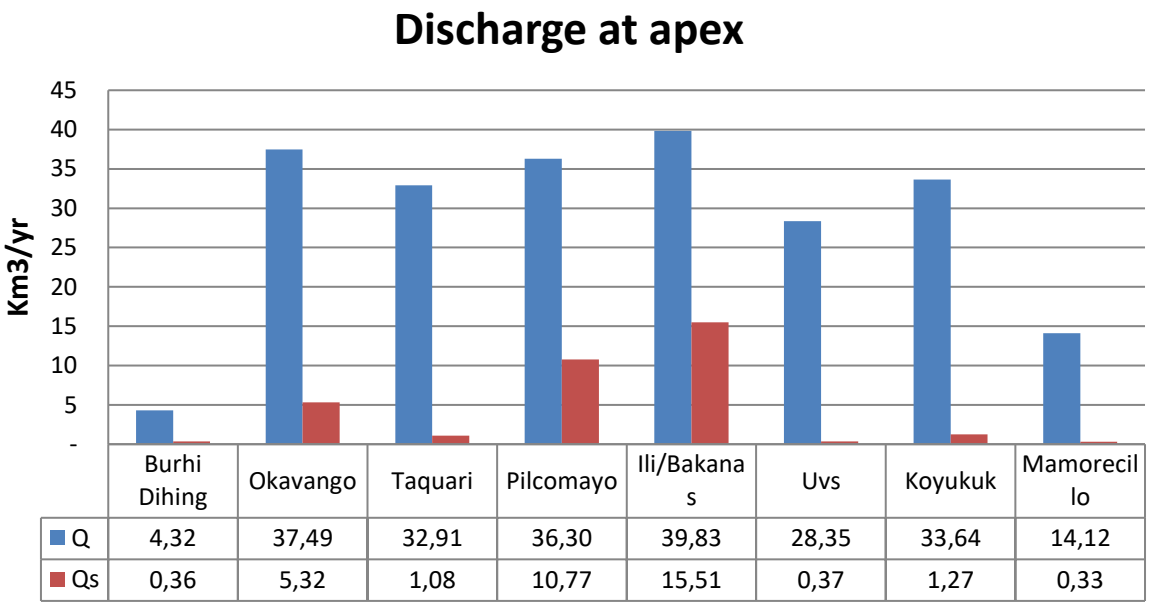


| | Burhi Dihing | Okavango | Taquari | Pilcomayo | Ili/Bakanas | Uvs | Koyukuk | Mamorecillo |
|---|---|---|---|---|---|---|---|---|
| Q | 4,32 | 37,49 | 32,91 | 36,30 | 39,83 | 28,35 | 33,64 | 14,12 |
| Qs | 0,36 | 5,32 | 1,08 | 10,77 | 15,51 | 0,37 | 1,27 | 0,33 |

*Figure 5-14 Discharge calculated using the constants from K and m calculated by Eide et al (2018). Blue bars are water discharge, red bars are sediment supply.*

Figure 5-15 shows the relationship between precipitation, catchment area, discharge and climate zones, where colours represent the same climate zones as in Table 5-8 Discharge is represented by the size of the bubbles, numbers are also given in Table 5-8

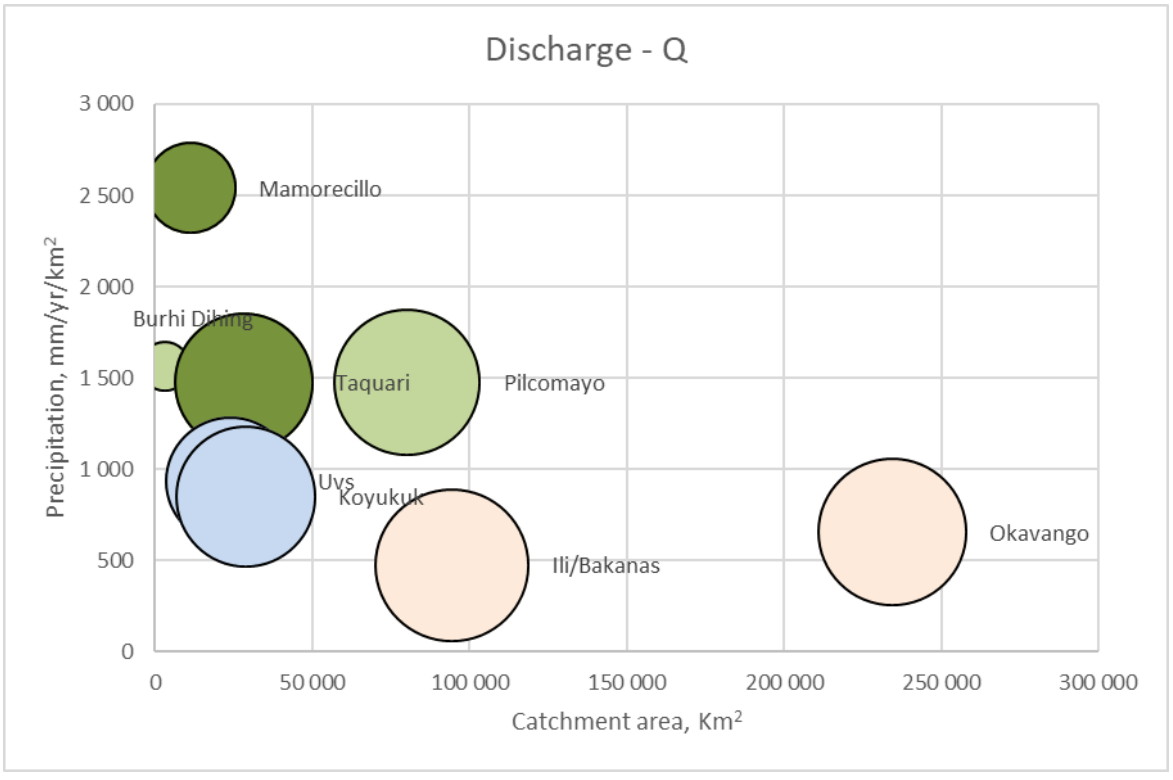


*Figure 5-15 The size of the bubbles represents the discharge for each system. Colour signify climate zone*

### 5.3.7 Sediment supply

| | B | A Catchment ($km^3$) | Q ($km^3$/yr) (Syvitski) | w | R elevation (km) | T temperature | Qs (MT/yr) (Syvitski) |
|---|---|---|---|---|---|---|---|
| Burhi Dihing | 3.8 | 3 071 | 1.46 | 0.0006 | 2.521 | 19.07 | 0.36 |
| Okavango | 0.2 | 234 548 | 46.78 | 0.0006 | 1.105 | 25.15 | 5.32 |
| Taquari | 0.3 | 28 153 | 8.58 | 0.0006 | 0.715 | 25.60 | 1.08 |
| Pilcomayo | 0.3 | 85 838 | 20.93 | 0.0006 | 5.131 | 16.32 | 11.34 |
| Ili/Bakanas | 1.5 | 94 323 | 22.57 | 0.0006 | 4.191 | 5.09 | 15.51 |
| Uvs | 0.5 | 23 918 | 7.53 | 0.0012 | 2.121 | -11.28 | 0.39 |
| Koyukuk | 1.7 | 28 837 | 8.75 | 0.0012 | 1.869 | -14.30 | 1.23 |
| Mamorecillo | 0.9 | 11 183 | 4.10 | 0.0006 | 3.710 | 24.92 | 0.33 |

### 5.3.8 Planforms

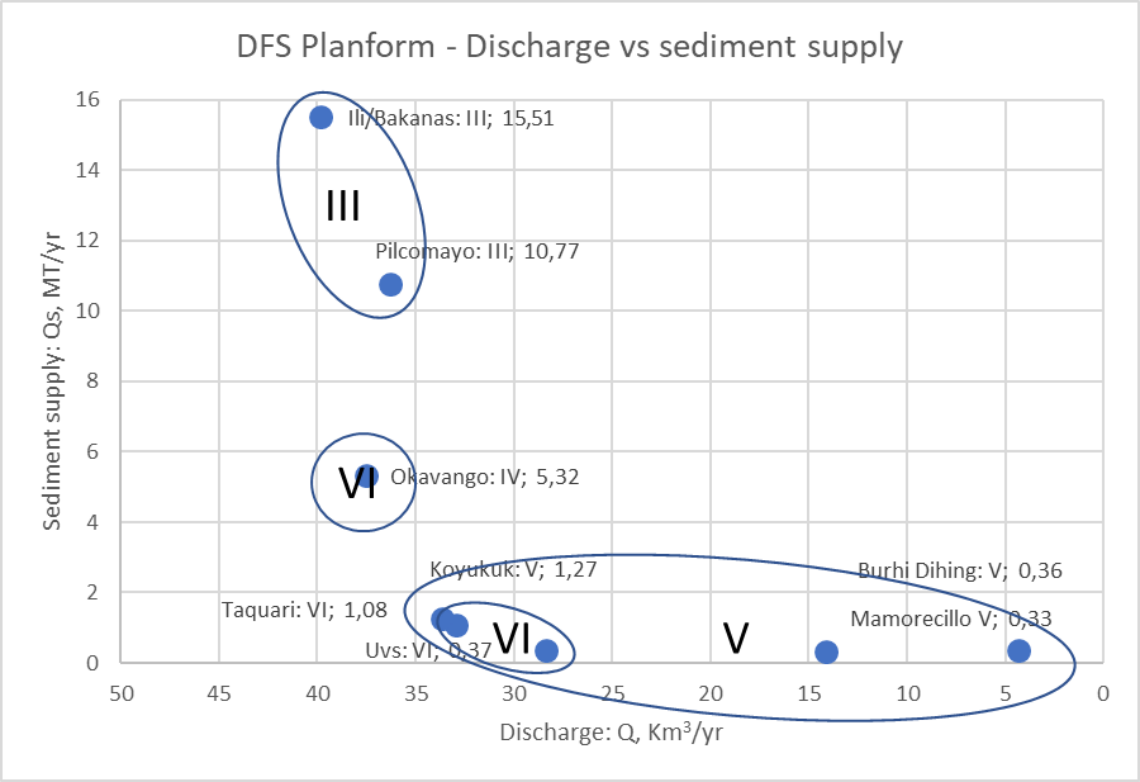


*Figure 5-16 When looking at sediment supply vs discharge, most of the systems follow the planform model, although Koyukuk (V) plots below Uvs and Taquari (VI) on the discharge axis*

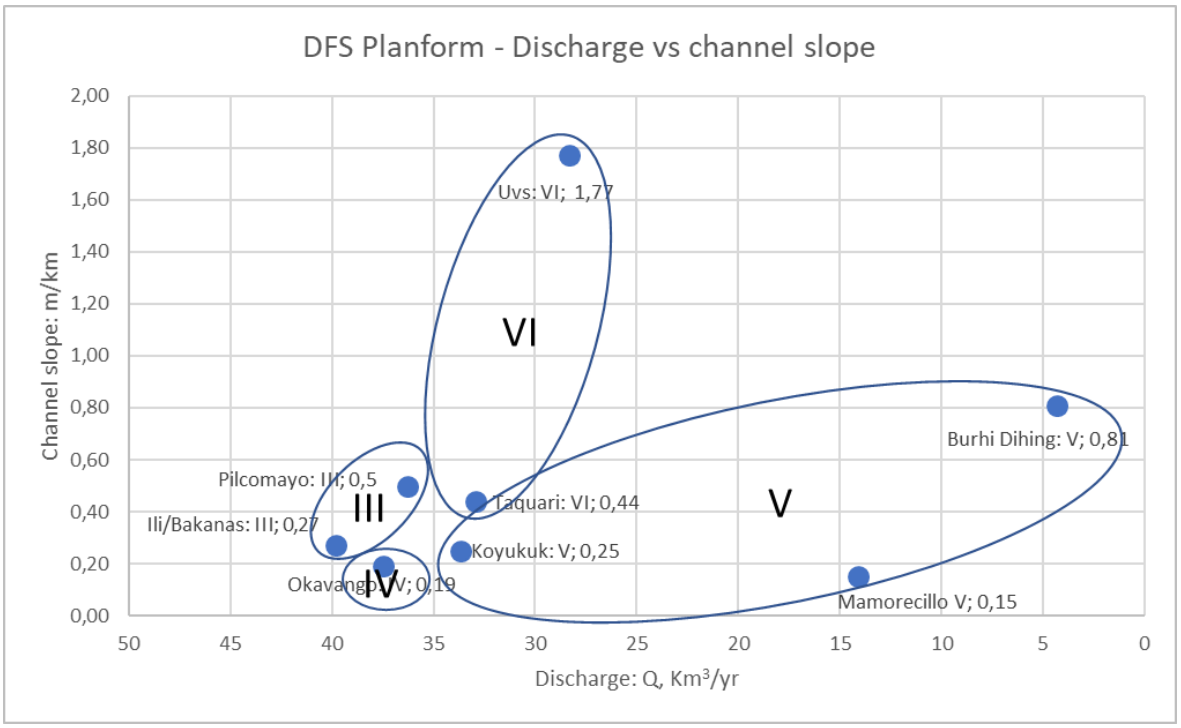


*Figure 5-17 Uvs stand out as having the steepest channel slope when plotting slope against discharge*

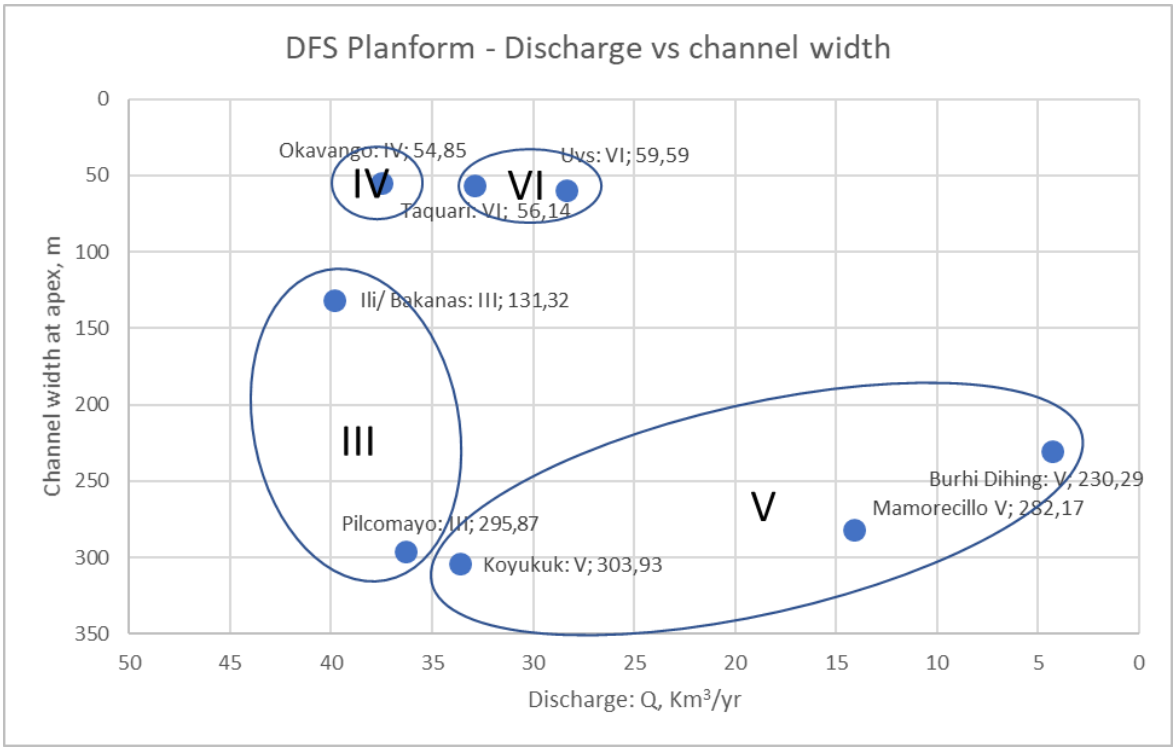


*Figure 5-18 When looking at channel width, Koyukuk do not plot in the same area as the VI systems*

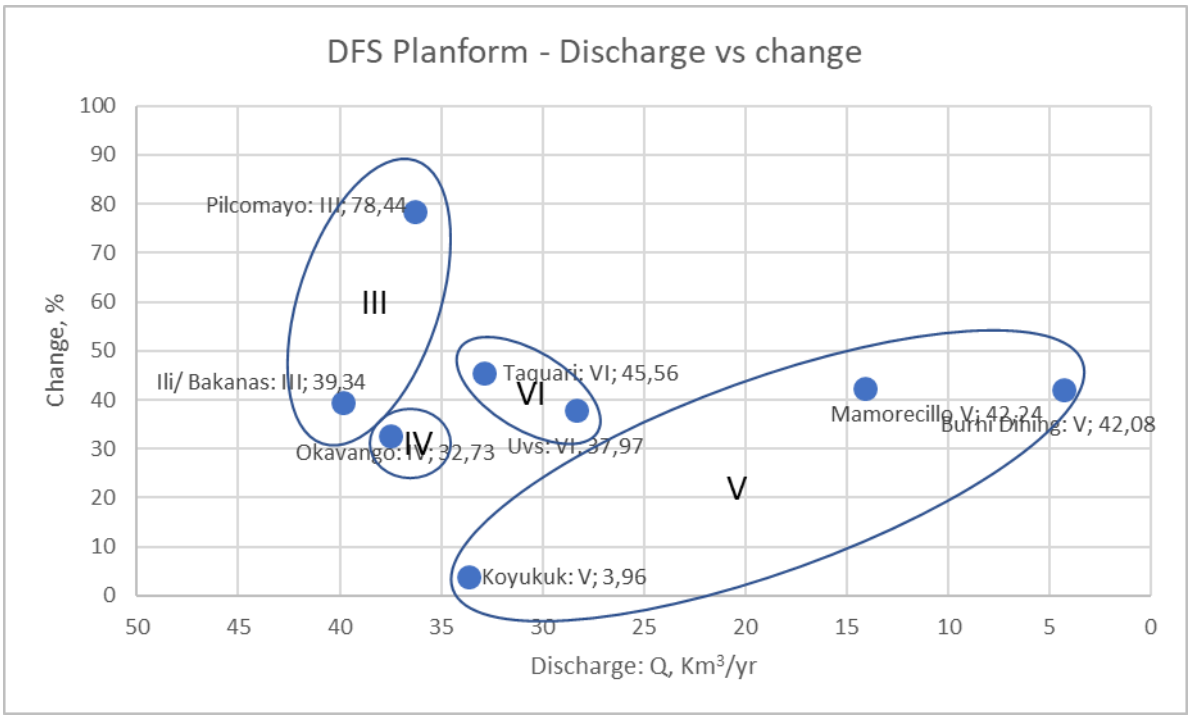


*Figure 5-19 Temporal change adds a new aspect to the existing planform model. The figure shows absolute change*

When comparing the channels and fan shape of the study areas to the model (Figure 2-2), Burhi Dihing, Koyukuk and Mamorecillo classified as planform V, with one single sinuous channel, and abandoned ox-bow lakes on the surrounding floodplain. In two stretches, Koyukuk has anabranching channels, and as such has elements of planform VI as well. Okavango's single channel in the panhandle bifurcates at the edge of the basin into several channels further down the fan and is classified as planform IV.

This study does not include any rivers with braided channels (planform I and II). Taquari and Uvs are classified as planform VI, with multiple sinuous channels

According to the model, type III fans; braided to meandering channels, should form when sediment supply is relatively low, and the discharge relatively large. Pilcomayo and Ili have been classified as type III, but plot high on sediment supply, and Pilcomayo also plots high on discharge, compared to the model for planform III.

# 6 Discussion

The discussion section will look at the differences of fluvial meandering rivers in sedimentary basins versus source regions, the temporal and spatial characteristics of meandering river systems across tectonic and climatic zones and the context of those results to our previous understanding of distributive fluvial systems (DFS). The data in this study can be used to improve our conceptual models, and to constrain numerical models in understanding the development and evolution of fluvial meandering systems. The section will further highlight an improved objective and semi-automated methodology can increase our capacity to study the temporal and spatial evolution of modern depositional environments for analogue studies.

## 6.1 The Temporal and Spatial Evolution of Meandering Fluvial Systems

### 6.1.1 Difference between source and sink

The findings in this study show distinct differences in the meandering river geomorphology between hinterland and sedimentary basin meandering river geomorphology. This supports recent work (Hartley et al., 2010; Weissmann et al., 2010; Nyberg and Howell, 2015; Helland-Hansen et al., 2016) which highlights the differences in sedimentary environments between source and sink areas (Figure 5-1), and the importance of choosing the correct analogues and models for reservoir modelling and prediction.

The variation found is attributed to the channel being more confined in the source areas, which are erosive environments, where the channel cuts through source rock to create valleys and canyons. As it enters the distributive environment in the sedimentary basin, it becomes unconfined, and channels can migrate laterally over large areas (Weissmann et al., 2010).

As the channel will spreads out and thereby loses velocity, sediments are deposited in the channel, which leads to avulsions and increased meandering (Davidson et al., 2013). In this study, the sedimentary basin is found to show a 300% increase in variability as compared to its source region.

### 6.1.2 Spatial-temporal variability in relation to climate

A higher degree of change occurs in the warmer climate zones (equatorial and warm temperate), than in the colder (snow and polar), as shown in Figure 5-2. This is because climate is an important control on discharge and sediment supply, which again affect temporal variability, as systems with more energy in form of higher discharge and more sediment supply display more lateral movement.

Warm temperate climates have more seasonal precipitation with drier seasons that have less effect on the channel migration. Peak flooding can create cutoffs and avulsions, which cause sudden shifts in the channel.

An example of this is the Pilcomayo river, which has the highest amount of change of the systems analysed. The satellite images show that the channel shifts a lot from year to year, depositing and eroding sandbars in an irregular pattern. The Koyukuk river, in the cold Alaskan climate, constitutes the opposite end member of these eight systems. This river is frozen over, and its banks remain immobilised during winter, so despite its catchment area being three times as large as that draining into Mamorecillo's apex, its lateral change is approximately one tenth of that of Mamorecillo.

Equatorial climates experience an even and high rate of precipitation, which means the channel is continuously reshaped by the water flow. Mamorecillo has the third highest level of overall change, and the fastest growing point bars of all, also when normalised on channel width.

Unexpectedly, the highest temporal variability found in arid climates, but this can be accounted for by the ephemeral nature of many of these rivers. They are dry for extended periods, and then experience heavy flash flooding some years. In the dataset used, these floods will show up as large water covered areas the wet years, and represent a large difference to the 2015 channel, which may be a dry year in many arid locations.

This is concordant with the findings for individual rivers, where those in warmer climate zones, Pilcomayo, Taquari, Mamorecillo and Burhi Dihing, all show more than 40% change, while the others all show less than 40%. The same trend can be seen for migration of point bars, the same river systems, in the warm, humid climates show a higher average migration than those in colder and drier climates (Figure 5-7).

Hartley et al (2010) has associated large DFSs with compressional settings. The uplift in continental collision zones, create a high relief catchment area with ample erosion, and the scale and subsidence in the foreland basins can accommodate large fans. Three of five foreland basin rivers in this study are parts of large systems; Burhi Dihing in the Assam basin to the south of the Himalayas, and Pilcomayo (Pantanal basin) and Mamorecillo (Amazon basin) created to the east of the Andes.

### 6.1.3 Changes within each system

The reduction in absolute change downstream found in most of the systems shows that the lateral change of the channel covers less area downstream. This is in keeping with existing and well-established theory that the channel to mud plain ratio decreases further down the fan.

When the data is adjusted for changes in channel width, it becomes clear that the two are closely related, as the trend for relative change normalised on channel width is nearly flat for most of the systems. This has implications for prediction of channel deposits, as when the channel becomes narrower, the temporal variability also reduces accordingly. In an unconfined sedimentary basin, a decrease in channel width and migration trends (Figure 5-11) will result in a higher proportion of floodplain facies. The observed trends can be used as a method to predict trends in other basins based on similar climates and tectonics settings of the study.

Examining point bar migration, no clear change can be seen between distance from apex and point bar migration (Figure 5-8). Pilcomayo has the largest overall change in channel migration, and second in point bar migration (Figure 5-7). This could be explained by the large shifts in the channel, which erode parts of the point bars at times, rather than continuously add to them. On the other hand, point bar migration along the Okavango is slow as the channels are confined by vegetation in the panhandle region, and so movement is restricted. This has been observed by other authors including (Mccarthy and Cairncross, 2000). In summary, the variability in meandering river systems show that from proximal to distal portion of the DFS system, the absolute proportion of change in terms of point bar and channel migration may vary but the relative change may not. This could indicate that a majority of the studied systems are self-similar in geomorphology from apex to toe as explained by a steady-state between uplift, erosion and deposition.

One of the defining characteristics of DFS fans, as described by Hartley et al. (2010), is the reduction of channel width downstream. This trend is as expected seen in nearly all the systems analysed. The Mamorecillo River stands out as the only one with increasing channel width downstream. This is caused ty an influx of water, as it receives several tributaries along its course.

All systems show greater variability in width closer to the apex, but the reduction does not occur in a recognizable and similar pattern between the systems. Burhi Dihing has a marked change in channel variability later in its course than Okavango, and Koyukuk has three separate stretches with high variability. Sections after bifurcations have less variability, as the channel becomes narrower, but bifurcations occur at different stages along the fan. Koyukuk has three anabranching sections, the first very close to the apex, while Uvs bifurcate only once, 25 km from the end of the channel.

The reduction in channel width and sandbar distribution is closely related. The decreasing trend of sandbar area downstream in most of the systems can be attributed to the loss of velocity as the river enters the basins reduces the rivers ability to transport sediments. Most sediment will be deposited in sandbars near apex, and thus less and finer sediments are transported and deposited further downstream.

From a reservoir perspective, sandbars have good reservoir properties with regards to porosity, but interconnectivity between bars can be an issue. It is therefore of interest to predict both total area and distribution of sandbars in a river system.

The downstream increase in sandbar area in Mamorecillo can be explained by influx of water and sediments from several tributaries along the channel. The sudden reduction of sandbars in Ili corresponds to a reduction in channel width, at the same place (approximately 100 km from apex). This trend is described by Fryirs and Brierley (2013) as occurring when the sediment load of silt and sand has been deposited, and only suspended load of silt and clay remains. The deposits then change from bank attached point bars, to lateral bars, which can be observed in Ili. Okavango's lack of visible sandbars can be due to vegetation (papyrus) on the riverbanks obscuring the sandbars from view or growing so fast that the sandbars get covered. It can also be due to the sand being deposited further upstream, as the discharge is low, and there are no silt and clay in suspension due to the aeolian provenance of the sediment.

For example, the Taquari, which is experiencing an ongoing avulsion after 100km, where since 1988 large parts of the flow has been diverted into a more northern channel, leaving the existing channel with much less water. This accounts for much of the rapid increase in change in the lower part of the channel (Assine, 2005).

## 6.2 DFS Model

As described by Weissmann et al (2010), a DFS has certain distinct features, such as a clear apex where the river enters the basin, from where channels pivot laterally and create a radial pattern.

All the systems analysed in this study conform to this definition, although some of the features are easier to recognise in some than others. Okavango and Taquari are classical examples of such fans, while some features are not so clear in other systems. Burhi Dihing and Mamorecillo do not display this radial fan shape, despite both being depositional systems. These both terminate in larger rivers, and as such are not able to fully develop the radial shape seen in fans that terminate by eventually

losing all their water to percolation and evaporation. The frequent cut-offs and ox-bow lakes show that these channels currently migrate by cut-offs rather than nodal avulsions closer to the apex. This is contrary to Weissmann et al. (2010), who observe that rivers primarily migrate over DFS fans by nodal avulsions. There is however evidence of nodal avulsions on the Burhi Dihing floodplain in form of numerous ox-bow lakes as well as longer sections of abandoned paleo-channels showing that the rivers course has changed over a longer time frame. This indicates that the model holds for this system as well.

As DFS systems occur at different temporal and spatial scales, location of apex is sometimes ambiguous. as some systems have more than one basin along the channel, for example the Burhi Dihing, which passes through one smaller basin before becoming confined in a hinterland again, before it reaches the edge of the Assam basin. According to the model, this would constitute two apexes along the same channel. This may make it difficult to assess and correlate trends and requires a strong paleogeographic reconstruction to constrain sediment fairway inputs. Another example is the Mamorecillo, which receives several tributaries along its way, each junction representing a new apex from there the trends, such as channel width, starts again, changing both spatial and temporal morphology of the system. This can make it difficult to recognise the idealized DFS model from other fluvial amalgamated sandbodies in the rock record.

Previous geomorphologic observations along the DFS model from Davidson et al, (2013) based on a limited number of manual measurements identifies three distinguished parts of a DFS system from proximal, medial to distal. These general trends are observed in this study as well. In addition, the current study notes that the temporal change decreases downstream with decreasing channel width, although relative to channel width remains relatively constant. However, the study does highlight that there exists significant variability within each system that needs to be taken in consideration in studying ancient counterparts. For example, fluvial discharge input, individual point bar migration and channel width may change significantly. Hence, it is important to consider these factors in outcrop or subsurface studies when limited amount of data is preserved in order to make an informed decision.

The different types of DFS characteristics proposed by Hartley et al. (2010) and Davidson et al. (2013), based on relative assumptions for sediment supply, water discharge, channel slope and width match well to many of the quantitative data of similar systems in this study (Figure 5-16 - Figure 5-18). Koyukuk has higher discharge than the other planform V rivers (single sinuous channel), which also can be seen in its planform, as it has three sections with anabranching channels, and as such has elements of planform IV (more than one active sinuous channel) as well, which explains why

it plots close to Uvs and Taquari. Ili and Pilcomayo, which both have planform III with braided to meandering channels plot close together, but higher on the sediment supply than the model seem to indicate. They do for example plot higher than Okavango, which has planform IV, which should have been relatively higher then III. In terms of temporal change (Figure 5-19), the data shows that DFS type III generally has a higher variability than type IV and higher than type V. In summary, the quantitative data in this study show that the different platform rivers types plot reasonably well on the original DFS model Figure 2-2 but may vary slightly in order of occurrence for the various geomorphic parameters.

## 6.3 Implications to subsurface prediction and numerical models

While we recognize the preserved amalgamated sandbodies represent the channel belt - the trends show characteristics that provide a powerful predictive tool. Caineville in Utah is a characteristic example of a DFS system that developed in a foreland basin, which in planview display similarities to the paleo oxbows found on the southern floodplain of Burhi Dihing (Hartley et al., 2015)

The trend in the Mamorecillo river systems shows that it may be difficult to find proximal to distal DFS trends in a system with multiple inputs. This may explain at time the lack of downstream trends observed in the Palaeocene–Eocene Bighorn Foreland Basin in Wyoming, USA by Owen et al., (2018). Additional information about provenance and source regions, for example by detrital zircon analyses as carried out in Canada and Gulf of Mexico, can help to constrain the observed trends by suggesting multiple source regions (Blum and Pecha, 2014).

Current work to develop basin scale predictive models of alluvial architecture highlights the importance of recognising and quantifying these trends in current trends, to be able to improve subsurface models (Owen et al., 2019).

Combined with the relationships of system size and channel width in this study as shown in Figure 5-11, this can provide a powerful tool to estimate the potential size of the source region contributions.

Quantitative data gathered in this study provide an observable database to test and condition numerical process-based models to the real world.

The data can also be catalogued in the SAFARI database for modern analogue finder, where it adds content in form of numerical data for the eight modern fluvial systems from the proximal to distal

parts. This will help reservoir modelers to extract useful information for a particular reservoir model and use those statistical relationships to develop a subsurface model.

## 6.4 Remote Sensing Workflows

The methodologies developed in this study have shown that the temporal and spatial analysis of modern meandering fluvial systems can be objectively and efficiently analysed based on a semi-automated approach. This has the benefit of reducing uncertainty in biased sampling of the river reach and analysing the intra-variability in the geomorphology of the system.

For example, the Mamorecillo river reach, has been measured by almost 70 000 samples along 915 km of its river length for width, and the temporal data for the whole river is available for each year between 1985 and 2015. In comparison, previous methods for remotely sensing information of the same river systems, for example by Constantine et al. (2014) looked at the geomorphology of 3 measuring points along the channel, measured 3-5 times during between 195 and 2013. This enables very detailed studies of large systems, at a scale not previously possible. Depending on the channel length, each river has between 8 700 and 101 500 measuring points for width. This means that the temporal and spatial variability can be captured at a point bar migration resolution for regional to global based studies.

The methods can be used on images with a wide spectre of resolutions. Satellite images are limited by the satellite's resolution, but airplanes or drones do not have the same limitation. This makes possible very detailed analysis of high-resolution images. It and can be utilised in many different fields, for example engineering a driver surveillance. Likewise, if there is access to images with high temporal resolution, it can be used for monitoring and analysis of flood areas to better understand patterns and predict changes.

## 6.5 Limitations/Possible sources of errors

Although efforts were made to choose images that show bank-full discharge in the rivers, it must be considered that cloud cover and satellite orbits lead to images from different dates being used, both within the same river system, and certainly between each river. For example, for the Pilcomayo river, the first set of images downloaded was subsequently discarded, as the discharge was disproportionately high, and not representative for the channel forming. This was done by visual inspection as several crevasse splays were visible and under water, and the channel was not clearly

defined. On the opposite, it is possible that images from for example Burhi Dihing show sandbars that would not have been visible on a day with higher discharge. When comparing the rivers to each other, these sources of error might be considerable, although trends within each river will be less affected. For long rivers, the entire length of the channel was not covered in one satellite image, and images from several different dates had to be mosaicked together. If there had been a rainfall in-between, it would affect both the channel width and area of sandbars visible.

Some of the systems go through multiple climate zones. For example, the lower section of the Ili/Bakanas channel is in an arid climate zone, while the upper section has a warm temperate climate whereas parts of the watershed area are in snow/polar climate zones.

Some of the rivers analysed are in densely populated areas, such as the Burhi Dihing in Northern India, whereas for example the Okavango is partly a nature reserve and much less influenced by humans. Some of the river engineering efforts can be easily identified from the satellite images, such as large dams and straight canals, for example the Ili/Bakanas which has a large impoundment upstream from its apex. Other modifications, such as dredging, channel widening and straightening, is harder to see, and might not be identified. One example is the very straight section of the Mamorecillo river, which stand out from the rest of the channel. This may or may not be anthropogenic influence. Likewise, river engineering upstream may affect water discharge, but be so far from the study area visible in the satellite image, and not sufficiently considered. Added sediments from anthropogenic activities, such as open cast coal mining upstream in the Burhi Dihing are also impossible to see from the images analysed but may be sufficient quantity to affect the deposition downstream.

One of the characteristics of DFS system is that the grain size reduces with distance from apex. This is not directly identifiable with this method. Assumptions can be made due to different sediments ability to retain moisture, for example, so that fine grain mud and silt will appear with more humidity than courser and more permeable sand, but to be sure, on site samples must be gathered.

The global datasets include a margin of error that although acceptable on a global scale, may have a large effect when used on a local scale. These could be determining where the basin edge is, especially when adjacent to mountains and alluvial fans with a greater gradient (Nyberg and Howell, 2015). Inaccuracies can also occur when using some of the parameters included in this dataset, such as for example precipitation, which for the large basins will have one value despite the actual precipitation patterns differing over the area.

The BQART model is based on measurements of suspended loads over less than 30 years, and it does not take into consideration rare events with large magnitude, which may have large effects on the system. Large flooding events and storm induced landslides can have a large impact on the sediment load and hence evolution of the channel migration (Helland-Hansen et al., 2016). Likewise, would anthropogenic activities like open cast mining increase the influx of sediments, such as in Pilcomayo and Burhi Dihing (Syvitski and Milliman, 2007).

# 7 Conclusions and further work

## 7.1 Conclusions

This study has developed a workflow to quantitively analyse the temporal and spatial geomorphology of large river systems at a scale previously not feasible. The main findings of this study have shown that:

- Trends and variability within each system has been found to comply with current models of DFS, but with considerable variability within and between systems.
- Channel width, gradient, sediment load and water discharge characteristics of meandering river systems within DFS environments have been quantified and agree with previous trends and models.
- Changes in lateral channel migration has been documented and quantified as three times more in the basins compared to the source areas. Temporal variability is more significant in warmer climates compared to colder associated with higher water discharge rates.
- Temporal variability has been added to the DFS model showing the absolute temporal variability decreases downstream similar to channel width trends. Hence, relative to channel width, there is no observable trend from apex to toe suggesting a higher proportion of floodplain environment downstream.
- The application of DFS facies models to ancient sedimentary systems should be applied with recognition that trends may break if there are multiple fluvial apexes as a river system enters in and out of a sedimentary basin. In addition, any additional water input, from for example coalesced DFS systems, will likely increase channel width and thickness downstream as opposed to the models suggested decrease.
- Remote sensing workflows applied in this study can be used to gather detailed information about large systems in an accessible and cost-efficient way. The workflows developed can be important tools in improving current predictive facies models for sedimentary basin, as the results document, they can quantify system wide trends in current fluvial settings.

## 7.2 Further work

- In order to provide more data for analogue databases, it would be useful to perform similar analysis on systems in other tectonic settings, especially passive margin, as these are areas with large deposits and reservoir potential.

- Study other types of fluvial systems, for example braided rivers, both perennial and ephemeral
- The large amount of measuring points available enables more detailed study of river. geomorphology, such as for example meander classification (type, symmetry), sinuosity, crevasse splays (distribution from apex) and different types of sand (distribution from apex).

# References:

Assine, M., 2003, Quaternary of the Pantanal, west-central Brazil: Quaternary International, v. 114, p. 23–34, doi:10.1016/s1040-6182(03)00039-9.

Assine, M.L., 2005, River avulsions on the Taquari megafan, Pantanal wetland, Brazil: Geomorphology, doi:10.1016/j.geomorph.2005.02.013.

Blum, M., and Pecha, M., 2014, Mid-cretaceous to paleocene North American drainage reorganization from detrital zircons: Geology, v. 42, p. 607–610, doi:10.1130/G35513.1.

Blum, M.D., and Törnqvist, T.E., 2000, Fluvial responses to climate and sea-level change: A review and look forward: Sedimentology, v. 47, p. 2–48, doi:10.1046/j.1365-3091.2000.00008.x.

Brabets, T.P., and Walvoord, M.A., 2009, Trends in streamflow in the Yukon River Basin from 1944 to 2005 and the influence of the Pacific Decadal Oscillation: Journal of Hydrology, v. 371, p. 108–119, doi:10.1016/j.jhydrol.2009.03.018.

Bridge, J.S., 2003, Rivers and Floodplains: Bodmin, Blackwell Publishing Ltd, 491 p.

Buehler, H.A., Weissmann, G.S., Scuderi, L.A., and Hartley, A.J., 2011, Spatial and Temporal Evolution of an Avulsion on the Taquari River Distributive Fluvial System from Satellite Image Analysis: Journal of Sedimentary Research, v. 81, p. 630–640, doi:10.2110/jsr.2011.040.

Constantine, J.A., Dunne, T., Ahmed, J., Legleiter, C., and Lazarus, E.D., 2014, Sediment supply as a driver of river meandering and floodplain evolution in the Amazon Basin: Nature Geoscience, v. 7, p. 899–903, doi:10.1038/ngeo2282.

Davidson, S.K., Hartley, A.J., Weissmann, G.S., Nichols, G.J., and Scuderi, L.A., 2013, Geomorphic elements on modern distributive fluvial systems: Geomorphology, v. 180–181, p. 82–95, doi:10.1016/j.geomorph.2012.09.008.

Dostay, Z., Alimkulov, S., Tursunova, A., and Myrzakhmetov, A., 2013, Modern hydrological status estuary of Ili River: Arabian Journal of Geosciences, v. 6, p. 3041–3047, doi:10.1007/s12517-012-0561-2.

Eide, C.H., Müller, R., and Helland-Hansen, W., 2018, Using climate to relate water discharge and area in modern and ancient catchments: Sedimentology, v. 65, p. 1378–1389, doi:10.1111/sed.12426.

Fernandes, A.M., Törnqvist, T.E., Straub, K.M., and Mohrig, D., 2016, Connecting the backwater hydraulics of coastal rivers to fluviodeltaic sedimentology and stratigraphy: v. 44, 979–982 p., doi:10.1130/G37965.1.

Filizola, N., and Guyot, J.L., 2009, Suspended sediment yields in the Amazon basin: An assessment using the Brazilian national data set: Hydrological Processes, v. 23, p. 3207–3215, doi:10.1002/hyp.7394.

Fryirs, K.A., and Brierley, G.J., 2013, Geomorphic analysis of river systems: An approach to reading the landscape: Chichester, Wiley-Blackwell, 345 p.

Gilvear, D., and Bryant, R., 2016, Analysis of remotely sensed data for fluvial geomorphology and river science: , p. 103–132.

Gomes, C.H., Sperandio, D.G., and Dessart, R.L., 2018, Remote Sensing analysis of the meanders

migration in the Mamorecillo River between 1985 and 2012, Bolivia: International Journal of Advanced Engineering Research and Science, doi:10.22161/ijaers.5.4.32.

Gorelick, N., Hancher, M., Dixon, M., Ilyushchenko, S., Thau, D., & Moore, R. (2017). Google Earth Engine: Planetary-scale geospatial analysis for everyone. Remote Sensing of Environment.

Das Gupta, A.B., and Biswas, A.K., 2000, Geology of Assam: Bangalore, Geological Society of India, 169 p.

Hartley, A.J., Owen, A., Swan, A., Weissmann, G.S., Holzweber, B.I., Howell, J., Nichols, G., and Scuderi, L., 2015, Recognition and importance of amalgamated sandy meander belts in the continental rock record: Geology, v. 43, p. 679–682, doi:10.1130/G36743.1.

Hartley, A.J., Weissmann, G.S., Nichols, G.J., and Warwick, G.L., 2010, Large distributive fluvial systems: characteristics, distribution, and controls on development: , p. 167–183, doi:10.2110/jsr.2010.016.

Helland-Hansen, W., Sømme, T.O., Martinsen, O.J., Lunt, I., and Thurmond, J., 2016, Deciphering Earth's Natural Hourglasses: Perspectives On Source-To-Sink Analysis: Journal of Sedimentary Research, v. 86, p. 1008–1033, doi:10.2110/jsr.2016.56.

Heywood, I., Cornelius, S., and Carver, steve, 2011, An Introduction to Geographical Information Systems: Harlow, Pearson Education Limited, 446 p.

HydroSHEDS World Wildlife Fund, Inc., https://hydrosheds.org/ (accessed June 2019).

Immerzeel, W., 2008, Historical trends and future predictions of climate variability: v. 254, p. 243–254, doi:10.1002/joc.

Ingersoll, R. V., 2012, Tectonics of Sedimentary Basins, with Revised Nomenclature: 1–43 p., doi:10.1002/9781444347166.ch1.

Ioris, A.A.R., 2016, Tropical Wetland Management: The South-American Pantanal and the International Experience: Routledge, 376 p.

Iriondo, M., 1993, Geomorphology and late Quaternary of the Chaco (South America): Geomorphology, v. 7, p. 289–303, doi:10.1016/0169-555X(93)90059-B.

J.N. Sarma, 1986, Sediment transport in the Burhi Dihing river, India: Hydrologie.org, p. 199–215.

Jervey, M.T., 1988, QUANTITATIVE GEOLOGICAL MODELING OF SILICICLASTIC ROCK SEQUENCES AND THEIR SEISMIC EXPRESSION: Sea-Level Changes, p. 47–69, doi:10.2110/pec.88.01.0047.

Latrubesse, E.M., 2015, Large rivers, megafans and other Quaternary avulsive fluvial systems: A potential "who's who" in the geological record: Earth-Science Reviews, doi:10.1016/j.earscirev.2015.03.004.

Makaske, B., Maathuis, B.H.P., Padovani, C.R., Stolker, C., Mosselman, E., and Jongman, R.H.G., 2012, Upstream and downstream controls of recent avulsions on the Taquari megafan, Pantanal, south-western Brazil: Earth Surface Processes and Landforms, v. 37, p. 1313–1326, doi:10.1002/esp.3278.

Mandal, K., and Dasgupta, R., 2011, Upper Assam Basin and its basinal depositional history:

Mccarthy, T.S., and Cairncross, B., 2000, Incremental aggradation on the okavango delta- fan, botswana: v. 1, p. 267–278.

McCarthy, T.S., and Ellery, W.N., 1998, The okavango delta: Transactions of the Royal Society of South Africa, v. 53, p. 157–182, doi:10.1080/00359199809520384.

Nyberg, B., Buckley, S.J., Howell, J.A., and Nanson, R.A., 2015, Geometric attribute and shape characterization of modern depositional elements: A quantitative GIS method for empirical analysis: Computers and Geosciences, v. 82, p. 191–204, doi:10.1016/j.cageo.2015.06.003.

Nyberg, B., Gawthorpe, R.L., and Helland-Hansen, W., 2018a, The distribution of rivers to terrestrial sinks: Implications for sediment routing systems: Geomorphology, doi:10.1016/j.geomorph.2018.05.007.

Nyberg, B., Helland-Hansen, W., Gawthorpe, R.L., Sandbakken, P., Eide, C.H., Sømme, T., Hadler-Jacobsen, F., and Leiknes, S., 2018b, Revisiting morphological relationships of modern source-to-sink segments as a first-order approach to scale ancient sedimentary systems: Sedimentary Geology, v. 373, p. 111–133, doi:10.1016/j.sedgeo.2018.06.007.

Nyberg, B., and Howell, J.A., 2015, Is the present the key to the past? A global characterization of modern sedimentary basins: Geology, v. 43, p. 643–646, doi:10.1130/G36669.1.

Owen, A., Hartley, A.J., Ebinghaus, A., Weissmann, G.S., and Santos, M.G.M., 2019, Basin-scale predictive models of alluvial architecture: Constraints from the Palaeocene–Eocene, Bighorn Basin, Wyoming, USA: Sedimentology, v. 66, p. 736–763, doi:10.1111/sed.12515.

Patton, W.W., and Box, S.E., 1989, Tectonic setting of the Yukon-Koyukuk Basin and its borderlands, Western Alaska: v. 94, p. 15807–15820.

Patton, B.W.W., Wilson, F.H., Labay, K.A., and Shew, N., 2009, Geologic Map of the Yukon-Koyukuk Basin , Alaska: : U.S. Geological Survey Scientific Investigations Map 2909, scale 1:500,000, 2 sheets and pamphlet [https://pubs.usgs.gov/sim/2909/].: USGS Pamphlet,.

Paul, M., 2012, Limnological aspects of the Uvs Nuur Basin in northwest: Technishce Unviersitat Dresden.

Pekel, J.F., Cottam, A., Gorelick, N., and Belward, A.S., 2016, High-resolution mapping of global surface water and its long-term changes: Nature, v. 540, p. 418–422, doi:10.1038/nature20584.

Pott, A., and Pott, V.J., 2005, Features and conservation of the Brazilian Pantanal wetland: Wetlands Ecology and Management, doi:10.1007/s11273-005-1754-1.

Sahoo, M., and Gogoi, K.D., 2009, Depositional History, Processes and Mechanisms of Early Miocene Sediments ofUpper Assam Basin: Journal of the Geological Society of India, v. 73, p. 575–585, papers2://publication/uuid/AB42A557-C617-4D90-B14A-84808E6E0853.

Sarma, J.N., Borah, D., and Goswami, U., 2007, Change of river channel and bank erosion of the burhi dihing river (assam), assessed using remote sensing data and gis: Journal of the Indian Society of Remote Sensing, v. 35, p. 93–100, doi:10.1007/BF02991837.

Singh, P., and Bengtsson, L., 2005, Impact of warmer climate on melt and evaporation for the rainfed, snowfed and glacierfed basins in the Himalayan region: Journal of Hydrology, v. 300, p. 140–154, doi:10.1016/j.jhydrol.2004.06.005.

Smith, N.D., McCarthy, T.S., Ellery, W.N., Merry, C.L., and Rüther, H., 1997, Avulsion and anastomosis in the panhandle region of the Okavango Fan, Botswana: Geomorphology, v. 20, p. 49–65, doi:10.1016/S0169-555X(96)00051-7.

Smolders, A.J.P., Guerrero Hiza, M.A., Van Der Velde, G., and Roelofs, J.G.M., 2002, Dynamics of discharge, sediment transport, heavy metal pollution and Sábalo (Prochilodus lineatus) catches in the lower Pilcomayo river (Bolivia): River Research and Applications, v. 18, p. 415–427, doi:10.1002/rra.690.

Syvitski, J.P.M., and Milliman, J.D., 2007, Geology, Geography, and Humans Battle for Dominance over the Delivery of Fluvial Sediment to the Coastal Ocean: The Journal of Geology, v. 115, p. 1–19, doi:10.1086/509246.

Tandon, S.K., and Sinha, R., 2008, Geology of Large River Systems, *in* Gupta, A. ed., Large rivers: geomorphology and management, Chichester, John Wiley & Sons, Ltd, p. 689.

Van Wagoner, J.C., Mitchum, R.M., Campion, K.M., and Rahmanian, V.D., 1990, Siliciclastic Sequence Stratigraphy in Well Logs, Cores, and Outcrops: Concepts for High-Resolution Correlation of Time and Facies, *in* ME 7: Siliciclastic Sequence Stratigraphy in Well Logs, Cores, and Outcrops: Concepts for High-Resolution Correlation of Time and Facies, p. III–55, http://archives.datapages.com/data/specpubs/seismic2/data/a174/a174/0001/0000/iii.htm[31.05.201909:55:31].

Weissmann, G.S. et al., 2013, PROGRADING DISTRIBUTIVE FLUVIAL SYSTEMS — GEOMORPHIC MODELS AND ANCIENT EXAMPLES Baylor University , Department of Geology , One Bear Place # 97354 , Waco , Texas 76798 , USA: , p. 131–147, doi:10.2110/sepmsp.104.16.

Weissmann, G.S., Hartley, A.J., Nichols, G.J., Sciences, E., Holloway, R., Scuderi, L.A., Olson, M.E., Buehler, H.A., and Massengill, L.C., 2011, ALLUVIAL FACIES DISTRIBUTIONS IN CONTINENTAL SEDIMENTARY BASINS — DISTRIBUTIVE FLUVIAL SYSTEMS: , p. 327–355.

Weissmann, G.S., Hartley, A.J., Nichols, G.J., Scuderi, L.A., Olson, M., Buehler, H., and Banteah, R., 2010, Fluvial form in modern continental sedimentary basins : Distributive fl uvial systems: , p. 39–42, doi:10.1130/G30242.1.

Xie, X., and Heller, P.L., 2009, Plate tectonics and basin subsidence history: Bulletin of the Geological Society of America, v. 121, p. 55–64, doi:10.1130/B26398.1.

Zani, H., Assine, M.L., and McGlue, M.M., 2012, Remote sensing analysis of depositional landforms in alluvial settings: Method development and application to the Taquari megafan, Pantanal (Brazil): Geomorphology, v. 161–162, p. 82–92, doi:10.1016/j.geomorph.2012.04.003.

# Appendix

## Detailed workflows

**Generic workflow for mapping channels and sand bars**

To map, calculate parametres, and analyse the results, a generic workflow as described below was used for each river. For some of the rivers adjustments had to be made, these are detailed in the sections below.

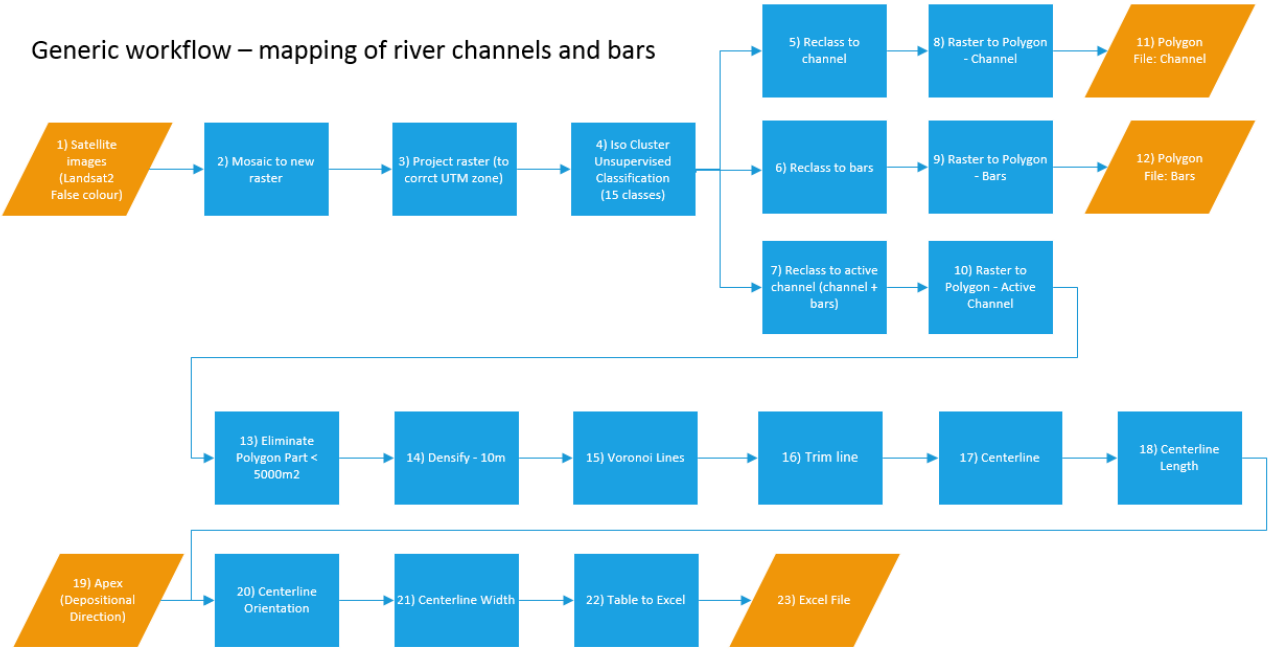


1) **Satellite images**

Several false colour images captured by the Sentinel 2 satellite was imported from SentinelHub. This consisted of the bands 8,3 and 4 and was chosen because the difference between water and surrounding vegetation shows up very clearly with this combination of bands. Effort was made to find dates with no cloud cover, and with a representative amount of water in the channel. Times with drought or flooding was avoided.

2) **Mosaic to new raster**

As this is a long river, it was necessary to import several images to obtain a sufficient resolution. These were mosaiced together to form one raster for further processing.

Input: Satellite images

Output: Raster file covering entire river length

3) **Project raster**

The raster was projected to correct UTM zone, to ensure a correct visualisation of the image and enable further processing.

Input: Raster mosaic covering the entire area

Output: Projected raster mosaic of the same area

**4) ISO Cluster Unsupervised Classification**

Unsupervised classification is available as a standard tool in ArcMap. It assigns values to pixels based on their spectral values, and groups similar values into groups. The pixels in the false colour image were grouped into 20 classes, and because of the unique signature of water, the river channel was clearly delineated. The sand bars along, and in the middle, of the river were also identified as one group, as the clean sand also has an identifiable signature. Separating the values into 15 classes gave good results for most of the areas, where insufficient 20 was used.

Input: Raster file of entire river

Output: Raster file with 15 classes

**5) Reclassify to channel**

The class corresponding to the water filled channel was retained; all other classes were reclassified as NoData

Input: Raster file with 15 classes

Output: Raster file with 1 class: Channel

**6) Reclassify to bars**

The class corresponding to clean sand was retained; all other classes were reclassified as NoData

Input: Raster file with 15 classes

Output: Raster file with 1 class: Bars

**7) Reclassify to active channel**

The classes corresponding to water and clean sand were given the same value, all other classes were reclassified as NoData. This gives the entire surface area of the active river channel.

Input: Raster file with 15 classes

Output: Raster file with 1 class: Active channel

**8) Raster to Polygon - Channel**

To perform the geometric characterization, the raster was converted to polygons using the Raster to Polygon tool.

Input: Raster – Channel

Output: Polygon - Channel

**9) Raster to Polygon – Bars**

To perform the geometric characterization, the raster was converted to polygons using the Raster to Polygon tool.

Input: Raster – Bars

Output: Polygon - Bars

**10) Raster to Polygon – Active Channel**

To perform the geometric characterization, the raster was converted to polygons using the Raster to Polygon tool.

Input: Raster – Active Channel

Output: Polygon – Active Channel

**11) Polygon file: Channel, for later use**

**12) Polygon file: Bars, for later use**

**13) Eliminate polygon part**

Polygon parts less than 5000$m^2$ were removed to 'tidy up' pixels that were given the wrong classification initially, and thereby appear as holes in the polygon. This could be due to areas with very shallow water, small sandbars near the surface, floating vegetation or objects such as boats and bridges.

**14) Densify**

To ensure even distances between the vertices in the polygon, the densify tool was used to insert vertices every 10 m along the outline of the polygon. This enables the creation Voronoi Polylines at equal and suitable intervals.

Input: Polygon file - Active channel

Output: Polygon file with evenly spaced vertices

**15) Voronoi Polylines** (Nyberg et al., 2015)

The Voronoi Polylines tool was used to creates Thiessen lines around each of the vertices in the polygon.

Input: Polygon file (densified)

Output: Voronoi Polylines

**16) Trim line**

To reduce the number of lines in the dataset and speed up subsequent calculations, the lines with one dangling end were trimmed off. This operation was re-run several times until most of the "fish bone" lines were eliminated

Input: Voronoi Polylines

Output: Voronoi Polylines

**17) Centreline (Nyberg et al., 2015)**

The Centreline tool creates the longest centreline by distance within each polygon in the input file. A desired threshold can be determined, where the option "0" creates the single, longest centreline possible. Any other number enables a branched centreline to be created and determines how many segments will be cropped from each branch.

Input: Voronoi Polylines

Output: Centreline

**18) Centreline Length (Nyberg et al., 2015)**

This tool calculates the total length of the centreline segments in each polygon, as well as identifies the points along the centrelines where the width and deviation will be calculated. This does not produce a new file, but adds the following parameters to the attribute table of the existing file:

Distance, Reverse Distance, Distance Coordinate X, Distance Coordinate Y, Reverse Distance Coordinate X and Reverse Distance Coordinate Y.

Input: Centreline

Output: Centreline

19) Create Features – Point

In order to define the apex for the river, a point feature is created at the end of the centre line.

Output: Point feature – Apex

20) Centreline Orientation (Nyberg et al., 2015)

To determine the direction of the river, the distance from apex to each centreline segment is calculated using the Centreline Orientation tool. This does not produce a new file, but adds fields to the existing:

Input: Centreline and Apex

Output: Centreline

21) Centreline Width (Nyberg et al., 2015)

The centreline width tool calculates the distance between each of the vertices along the centreline, and the polygon that was used to create the centreline. Again, this adds fields to the existing attribute table rather than create a new file.

Input: Centreline and Channel polygon

Output: Centreline

22) Table to Excel/Export data a

If the number of rows in the attribute table is less than 65 000, the tool Table to Excel can be used, which creates a .xlsx file which then can be opened analysed using Excel. If the number of rows exceeded this, the attribute table was exported as a .csv file which was imported from Excel and saved as a new .xlsx file.

Input: Centreline or Table of attributes

Output: Excel file

**Assam – Paleo-Oxbows**

Ox-bows Assam

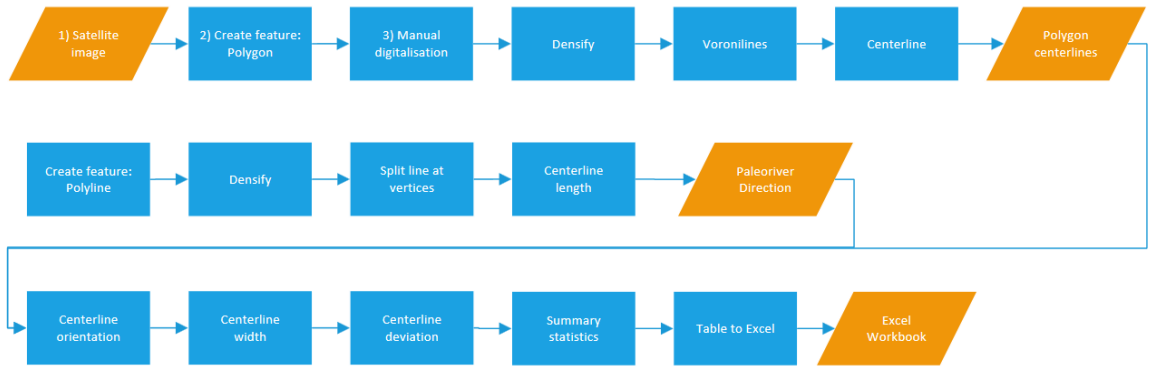


1) Satellite Image

A natural colour image captured by the Sentinel 2 satellite 04.04.2018 was obtained from SentinelHub (apps.sentinel-hub.com) and imported into ArcMap 10.6 software from Esri, as it showed clearly the paleo oxbow-lakes on the plains to the south of the Burhi Dihing river. They appear as grey/brown crescent shapes against the darker green surroundings. A false colour version of the same image was also imported for visual assistance.

2) Create feature: Polygon

A new polygon feature was created in the chosen geodatabase

3) Manual digitising of ox-bow lakes

The ox-bow lakes were digitised manually by tracing the line boarder between the grey colour and the green colour in the images, where the shapes had the typical crescent shape of oxbow lakes and river meanders. Areas with similar colour but different shapes were not included. Each paleo ox-bow or channel segment was digitised as a separate polygon.

Input: Satellite image

Output: Polygon shapefile showing each paleo oxbow lake as a unique polygon

The Centreline tool creates the longest centreline by distance within each polygon in the input file.

4) Create feature: Polyline

Later in the workflow, a feature defining the depositional direction is required. In this workflow, a new polyline feature was created, that runs along the estimated flow of the paleo river, i.e. roughly along the middle of the area covered by the paleo oxbow lakes.

Output: Polyline feature; Paleoriver Direction

5) Densify

The densify tool was used to insert vertices every 1000m along the polyline.

Input: Polyline; Paleoriver Direction

Output: Polyline with evenly spaced vertices

6) Split line at vertices

This tool was used to split the long polyline into many segments.

Input: Densified polyline; Paleoriver Direction

Output: Line segments; Paleoriver Direction

7) Centreline Length (Nyberg et al., 2015)

The Centreline length tool was used to assign the parameter "Distance" to the attribute table. This is required for calculating "Along Distance" in the next step.

8) Centreline Orientation (Nyberg et al., 2015)

In order to determine the distance of each oxbow lake from the rivers apex, the Centreline Orientation tool is used. This calculates the distance from each centreline in relation to a selected object. This also does not generate a new file but adds the parameter "Along Distance" to the attribute table.

Input: Paleo River Direction

Centreline

9) Centreline Width (Nyberg et al., 2015)

For each end coordinate (DCoordx, DCoordy) along the centreline, the distance to the side of the polygon is calculated. This gives a measure of the width of the polygon and adds it as "Width" to the attribute table.

Input: Centreline

Polygon file

10) Centreline Deviation (Nyberg et al., 2015)

Like for the centreline width calculation, the centreline deviation is calculated for each coordinate along the centreline as a new attribute field named "Deviation". The value for each point is the distance between the centreline and the shortest path between the start and end of each centreline.

11) Summary statistics

This was used to reduce the number of rows in table, so that each row now corresponds to one paleo oxbow lake.

12) Table to Excel

The last step in the ArcGIS workflow is to export the attribute table to excel for further analysis.

1) **Burhi Dihing**

13) – 22) Same steps as in the workflow for the paleo-oxbows were used, with the exception of Depositional Direction for this river only a short line representing the location of the apex was used, instead of the long polyline following the direction of the river.

**2) Okavango Delta**

1) – 5) Same as for Assam

6) Buffer Polygon

The active channel in this river is very narrow in some places, especially far from the apex. The pixel resolution is 10 metres, and in the narrows stretches, the channel is depicted in single pixels. It also means the raster is converted into a number of single pixel polygons. In order to make the channel a continuous polygon, a 2m buffer was added to enable the creation of one continuous centre line later in the process. Where segments were still missing, this was corrected by manual editing.

7) Merge Polygon

All the overlapping segments of the channel polygon were merged into one continuous polygon covering the entire channel of the river.

8) Smooth Polygon

The single pixel channel width also affects the accuracy of the river bed and gives a jigsaw line. To counter this, the Smooth polygon tool was used. As both step 6) and 8) might compromise the accuracy of the digitisation, the resulting polygon was compared to the original mosaic for quality assurance.

**4) Pilcomayo**

It was difficult to distinguish the sandbars from the sediment laden water in the false colour images for this river, so instead moisture index (bands (B8A-B11)/(B8A+B11)) was used.

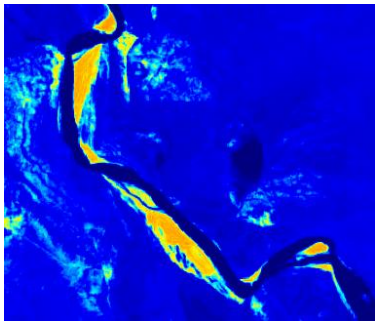

**5) Ili/Bakanas**

Especially the upper part of this river has numerous sandbars and small island, which were difficult to digitise from the false colour image. Instead a NDVI image, also obtained from SentinelHub, was used to separate sandbars from intrachannel islands with vegetation.

**6) Uvs**

**7) Koyukuk**

This river has sections where the shortest path follows anabranched channels much narrower than the main channel. To avoid the centreline going through these unrepresentative channels, the voronoi lines were removed from these channels before the centreline was created, thus forcing it to go through the main channel.

## Temporal variability

Temporal changes – mapping of river migration

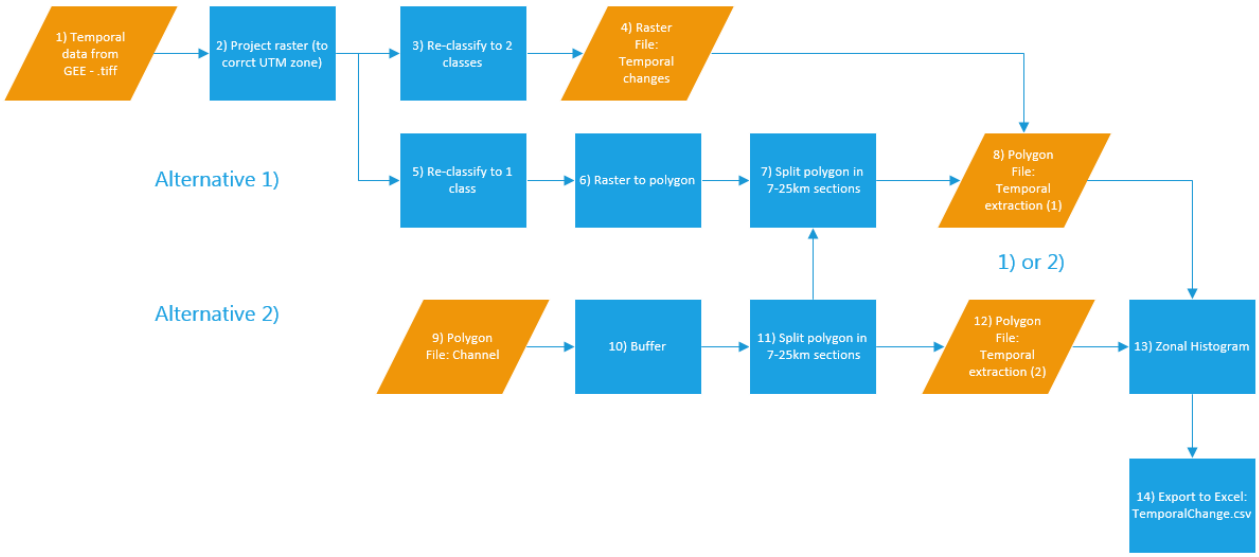


1) **Dataset from GEE**
   Data on temporal variability since 1990 was obtained from the dataset"Global water occurrence" (Pekel et al., 2016), downloaded via Google Earth Engine. This is a raster dataset, and shows which areas were covered by water every year from 1984 to 2015.

2) **Project raster**
   The raster dataset was projected to the correct UTM zone

3) **Re-classify**
   To highlight total migration of the channel, all the values from the year 1990 to 2014 were classified as abandoned area, which signifies the total area the river has moved away from. The values from 2015 were classified as the current channel.

4) **Raster file:** Temporal changes, for later use.

5) **Re-classify**
   Where the channel was clearly delineated (for example Mamorecillo and Kuyukuk), all the temporal data was merged into one class, which then represents all areas that have been occupied by the river at some point since 1990.

6) **Raster to polygon**
   This was then converted to polygons, which resulted in one continuous polygon representing the channel as it has ever been. The surrounding polygons were deleted.

7) **Split polygon**
   Split the polygon in suitable sections, depending on the length of the river, to obtain enough sections to determine a trend in the data.

8) **Polygon file:** Temporal extraction, for later use

9) **Polygon file: "Channel"**

   The file created in the previous workflow for spatial data analysis was used for input as alternative 2, when the channel in the temporal dataset was not clearly delineated from the surrounding wet area

10) **Buffer**

    10-100m wide buffer zones were created around the channel polygon, to encompass meandering, and excluding surrounding wetland.

11) **Split polygon**

    Split the polygon in suitable sections, depending on the length of the river, to obtain enough sections to determine a trend in the data.

12) **Polygon file:** Temporal extraction (2), for later use

13) **Zonal histogram**

    One of the polygon files was used to extract values from the temporal data raster file, resulting in a table containing number of pixles from the two raster values for each year.

14) **Export to excel**

    The table was exported to excel as a .csv file

    Further analysis and plotting were carried out in Excel

Workflow for determining sandbar distribution